University of Alberta

Self-Tuned Indirect Field Oriented Controlled IM Drive

by

Mavungu Masiala

A thesis submitted to the Faculty of Graduate Studies and Research
in partial fulfillment of the requirements for the degree of

Doctor of Philosophy
in
Power Engineering and Power Electronics

Electrical and Computer Engineering

Fall 2010
Edmonton, Alberta

Examining Committee

Andy Knight, Electrical and Computer Engineering

John Salmon, Electrical and Computer Engineering

Petr Musilek, Electrical and Computer Engineering

Brian Fleck, Mechanical Engineering

Peter Lehn, University of Toronto

Abstract

The simplest form of induction motors, known as AC squirrel cage motor, is the universal workhorse of industrial and commercial premises. For many years it was restricted to constant speed applications while DC motors were preferred for high-performance variable speed and servo drives. With modern advances in semiconductor and digital signal processing technologies, it is now possible to operate induction motors in high-performance drives at a reasonable cost with *Field Oriented Control* methods. The latter have made induction motor drives equivalent to DC drives in terms of independent control of flux and torque; and superior to them in terms of dynamic performance.

In developing *Field Oriented Control* for induction motors engineers are faced with two major challenges: (1) the estimation of rotor data to compute for the slip gain, and (2) the compensation of changes in drive operating conditions and parameters in order to maintain the drive performance high at all time. This thesis addresses these issues by introducing two independent control systems.

The first system is designed to estimate online the value of the slip gain in the entire torque-speed plane in order to maintain decoupled control of torque and flux despite the so-called detuning effects. It is based on evaluating the operating condition of the drive in terms frequency and load torque, and selecting the appropriate estimation method

accordingly. A fuzzy controller is used to generate the distribution factor for the methods.

The second system is a fuzzy self-tuning speed controller, with reduced sensitivity to motor parameters and operating condition changes. It has the ability to adjust its gains in real time according to the current trend of the drive system. It is designed to maintain tight control of speed and torque for high-performance applications.

The performances of the two controllers are validated through a series of simulation and experimental tests using a 2HP 3-phase induction motor with an ADMC21992 160-MHz DSP microprocessor.

Acknowledgments

I wish to thank my supervisor, Dr. Andy Knight, for his support, advice, and encouragement throughout the course of this work. Your constructive criticism, respect, and faith in your students always motivated me to reach for the best. Thank you very much.

I would also like to acknowledge the collaboration of all my colleagues and friends at the Power Lab/U of A. It was a wonderful journey, guys; but I've got to go! I'll miss you all. Special thanks to Behzad Vafakhah (sorry, Dr. Vafakhah) and Albert Terhiede for their help in implementing the theories developed in this thesis.

To my supervisory committee (Dr. J. Salmon, Dr. P. Musilek, Dr. B. Fleck, Dr. P. Lehn (U of T), & Dr. D. Barlage), I am very grateful for your constructive inputs. Dr. John Salmon, thanks for reviewing my papers.

To all my family, thank you very much for your prayers. There is a "doctor" in the family now. Mum, I know you don't understand a thing about this "electrical engineering", let alone the "fuzzy control" logic. It's ok, I'm done!

Finally, to the Masialas, My Didi, Iva, & Kiese Masiala, thank you so much to all of you for keeping me awake at nights when I had a chapter to submit the following day. I am kidding! I love you all. You can have me now; well… kind of.

Dedication

A mon père

Edmond Vangu Masiala

Table of Contents

List of Abbreviations

AI	—	Artificial Intelligence
ANN	—	Artificial Neural Network
CAV	—	Center of Average
COG	—	Centre of Gravity
CSI	—	Current-Sourced Inverter
DFOC	—	Direct Field Oriented Control
DSP	—	Digital Signal Processor/Processing
EKF	—	Extended Kalman Filter
ELO	—	Extended Luenberger Observer
EMF	—	Electromagnetic Force
FL	—	Fuzzy Logic
FLC	—	Fuzzy Logic Control/Controller
FOC	—	Field Oriented Control
GA	—	Genetic Algorithm
GTO	—	Gate Turnoff Rectifier
IFOC	—	Indirect Field Oriented Control
IGBT	—	Insulated Gate Bipolar Transistor
IM	—	Induction Motor
MF	—	Membership Function
MRAS	—	Model Reference Adaptive System
PI	—	Proportional-Integral
PWM	—	Pulse Width Modulation
RMS	—	Rout Mean Square
SCR	—	Silicon Controlled Rectifier
SFC	—	Sectorial Fuzzy Controller
SMC	—	Sliding Mode Control/Controller
STFC	—	Self-Tuning Fuzzy Controller
SV	—	Space Vector
TSK	—	Takagi-Sugeno-Kang
VC	—	Vector Control
VSD	—	Variable Speed Drive
VSI	—	Voltage-Sourced Inverter

List of Key Symbols

$\widehat{K}_s$ — Estimated slip gain

$\hat{\lambda}_r$ — Peak rotor flux linkage

Φ_{m} — Peak air-gap flux

B_m — Peak value of the air-gap density

E_1 — Per-phase induced EMF in the stator winding, H

F_r — Peak value of the Magneto-Motive Force (MMF)

I_2 — Rotor current, A

I_a — Armature current, A

I_f — Field current, A

I_m — Magnetizing current, A

I_r — Rotor current (referred to the stator), A

I_s — Stator current, A

I_{s1} — Stator current at fundamental frequency, A

K_I — Integral gain of PI controller

K_P — Proportional gain of PI controller

K_a — Constant coefficient of DC developed torque

K_s — Slip gain

K_t — Torque constant (IM)

L_{l2} — Per-phase rotor leakage inductance, H

L_{lr} — Per-phase rotor leakage inductance (referred to the stator), H

L_{ls} — Per-phase stator leakage inductance, H

L_m — Per-phase magnetizing leakage inductance, H

L_r — Rotor inductance, H

L_s — Stator inductance, H

L_σ — Leakage inductance, H

N_1 — Total number of stator turns per phase

P_{FW} — Friction and windage losses

P_d — Developed power

P_g — Air-gap power

P_{lr} — Rotor copper loss

P_{sh} — Shaft output power

T_e — Electromagnetic developed torque, in N.m

T_r — Rotor time constant

V_o — Boost voltage, V

V_s — Supply voltage, V

V_s^* — Reference phase voltage, V

a_{eff} — Effective rotor-to-stator turns ratio

e_{dq} — Voltage vector error

$e_\omega^{'}$ — Variable “speed tracking error”

e_ω — Variable “tuning error”

f_s — Stator frequency, Hz

f_s^* — Reference frequency, Hz

i_{ds}^* — Flux component current command, A

i_{ds}^e — Flux-producing component current, A

i_{qs}^* — Torque component current command, A

i_{qs}^e — Torque-producing component current, A

k_u — Ultimate gain (of Ziegler-Nichols method)

k_{w1} — Stator winding factor

n_{ce} — Input scaling gain of variable “ce”

n_e — Input scaling gain of variable “e”

n_{sl} — Slip speed, rpm

n_u — Output scaling gain of variable “u”

r_2 — Per-phase rotor resistance, Ω

r_c — Per-phase stator core loss resistance, Ω

r_r — Per-phase rotor resistance (referred to the stator), Ω

r_s — Per-phase stator resistance, Ω

s_L — Laplace operator

t_u — Ultimate frequency (of Ziegler-Nichols method)

w_{ce} — Online updating factor of input scaling gain (n_{ce})

w_e — Online updating factor of input scaling gain (n_e)

w_f — Weight factor (for slip gain estimation method)

w_u — Online updating factor of output scaling gain (n_u)

θ_e — Rotor flux (field) angle/position

θ_r — Rotor angle/position

λ_{dr}^e — d-axis rotor flux, in synchronous reference frame

λ_{qr}^e — q-axis rotor flux, in synchronous reference frame

ω_b — Base speed/frequency, rad/s

ω_m — Mechanical rotor speed/frequency, rad/s

ω_r — Electrical rotor speed/frequency, rad/s

ω_r^* — Rotor speed/frequency reference (command), rad/s

ω_r^r — Reference model output frequency, rad/s

ω_s — Synchronous speed/frequency, rad/s

ω_s^* — Reference stator speed/frequency, rad/s

ω_{sl} — Slip speed/frequency, rad/s

K_t — Torque constant

n_r — Rotor speed, in rpm

n_s — Synchronous speed, in rpm

P — Number of poles of an IM

B — Viscous friction coefficient

J — Motor inertia

l — Axial length of the IM, m

r — Radius of the IM, m

s — Slip

$u(t)$ — Fuzzy output

$\Phi(I_f)$ — Field flux (DC motor)

α — Weight factor for input variable "e"

β — Weight factor for input variable "ce"

γ — Weight factor for output variable (u)

δ — Torque angle

σ — Distribution factor for MFs

List of Figures

List of Tables

Epigraph

"[4]One generation passeth away, and another generation cometh: but the earth abideth for ever. [6]The wind goeth toward the south, and turneth about unto the north; it whirleth about continually, and the wind returneth again according to his circuits. [9]The thing that hath been, it is that which shall be; and that which shall be done: and there is no new thing under the sun. [10]Is there any thing whereof it may be said, See, this is new? It hath been already of old time, which was before us."

King Solomon, Ecclesiastes 1:4-10, KJV

Introduction

Electric machine applications include electric vehicles, oil and gas exploration, conveyors, liquid pumping, paper machines, textile mills, servo and robotics, and many more. The flexibility of energy conversion that was introduced by electric machines has been harnessed and controlled by the application of torque, speed and position controllers. Such controllers are often referred to as Variable Speed Drives (VSDs). For applications where high level of precision of torque and speed is required, VSDs are often referred to as servo drives [1]. Nowadays it is estimated that more than 75% of all electric machines applications require variable speed or the torque to be increased or both [2][3]. Hence, VSDs and servo drives have become very important interferences for proper operation and use of electric machines in industry.

In general, VSDs are used to match the speed and/or torque of the drive to the system requirements, to improve its efficiency, and to save energy (for applications such as centrifugal pumps and fans). For example, modern VSDs can be used to accurately control the speed of an IM within ±0.1% independent of load, compared to a direct online IM, where the speed can vary up to 3% from no-load to full load [1].

The interplay of technical, economic, and environmental issues in today's commercialized industry requires such advanced control approaches to electric machines. Hence, there is a significant research effort in directions such as machine tool axis control, glass engraving, precision polishing machines, electric cars in the automotive industry, and more electric aircraft in the aviation industry [3][4]. This ability to effectively control the speed and torque of motors to achieve the system requirements continues to be a major stimulus to growth in the VSD and

servo drive market. It has also opened up more research opportunities and improved the performance of electric machines in general.

Among all types of machines, the simplest form of AC Induction Motor (IM); also known as the squirrel-cage IM, is the universal workhorse of modern industry [5][6]. Its popularity is due to high reliability, low maintenance, and low cost. However, for many years IMs have been restricted to constant-speed applications while DC motors were preferred for high-performance VSDs requiring very accurate speed and torque control. The main changes over the years for DC VSDs were concerned with different methods of generating variable DC voltage from 3–phase AC supplies. Since the 1970s, the controlled DC voltage has been easily produced from static power electronic AC/DC converters, especially the thyristor-controlled rectifiers [1].

One of the main problems with thyristor-controlled DC drives is the cost of maintenance related to mechanical commutators and brushes of DC motors. This limits significantly their industrial applications; especially in areas where high reliability is required [7]. As a consequence, since the 1980s, the popularity of IM VSDs has grown rapidly due to advances in power electronics and Digital Signal Processor (DSP) technologies [1][5][6]. It is now possible to provide the necessary variable voltage and frequency that an IM requires for efficient, dynamic, and stable speed/torque control. As a result, IM drives are successfully and progressively replacing DC motor drives in many modern applications [5][7].

Advances in electronic control technology of electric machines have not only made the use of IMs possible for many applications but have also enabled users to take advantage of their low cost and low maintenance. The practical effect is the possibility to drive an IM in such a way as to obtain a dynamic performance similar to a phase-controlled separately-

excited DC motor drive. However, despite these efforts, improved IM drive technologies remain an ongoing engineering challenge.

In General, IM drives are considered high-performance when the rotor speed and torque can be made to follow closely a predefined trajectory at all time. Traditionally, the well known scalar *Volt per Hertz* methods with standard Proportional-Integral (PI) controller have been used to ensure proper control of speed and torque [2]. In order to design the PI controller, the IM drive system is linearized using a small-signal perturbation at a steady-state operating point. A transfer function is then derived between a pair of input and output signals. By doing so, the dynamic model of the IM can be described by a 5^{th}-order multi-variable system.

Research has shown that this control system design approach often results in poor dynamic and steady-state responses; especially if the drive is required to operate in a very wide range of operating conditions and parameter changes [5][8]. Moreover, as far as IMs are concerned, the PI controller response is also affected by the motor nonlinear characteristics and disturbances, and the coupling of flux and torque. Therefore, an effective and high-performance closed-loop speed control of an IM drive should include: (1) an advanced nonlinear control approach, and (2) a method to reduce or eliminate the coupling effect between the flux and torque.

When operated at constant flux, a separately-excited DC motor behaves like a 2^{nd}-order linear system. Its flux (produced by the field current) is decoupled from torque (produced by the armature current). This decoupling characteristic results in high control flexibility and fast torque response. Many conventional linear methods have been successfully applied to control such systems [13]. In order to effectively deal with the coupling effect of flux and torque in IMs, they are often operated like

separately-excited DC drives to benefit from their inherent decoupling characteristic of flux and torque. This manner of operating IMs is referred to as *Vector Control* (VC) or *Field Oriented Control* (FOC) [9].

Invented in the early 1970's [9], FOC methods have made AC drives equivalent to DC drives in terms of independent control of flux and torque, and superior to them in dynamic performances. Hence, with FOC schemes higher dynamic and steady-state performances of IMs (or AC motors in general) can possibly be achieved. Approximately 13 years after the invention of FOC, another technique, also based on decoupled control of torque and flux was introduced as Direct Torque Control (DTC) or Direct Torque and Flux Control (DTFC) [10][11]. Despite the pros and cons of DTC and FOC presented in many research studies such as [12][5], only the technique of FOC is considered in this thesis.

Several types of FOC schemes are available [5]: rotor flux, stator flux, and magnetizing oriented FOCs. However, only the rotor flux oriented control yields complete decoupling [5][6][7]. In this thesis, only the rotor flux oriented type of control, also termed FOC, is considered.

In developing FOC IM for high-performance drives, engineers are faced with two major challenges:

(1) Measurement of motor data to compute for the IM rotor time constant or slip gain, and;
(2) Compensation of the drive operating condition and parameter disturbances.

These two challenges are systematically addressed in this thesis as follows.

- Slip Gain Estimation

FOC is achieved by creating decoupled channels of flux and torque control. If the rotor flux position is known, the stator current is resolved along and in quadrature to it. In this case, the in-phase component of the flux represents the field current component and the quadrature component represents the torque current component, similarly to the field and armature currents of a separately-excited DC motor, respectively.

The resolution of the stator current requires the rotor flux position, also known as field angle. The latter can either be measured directly (Direct FOC or DFOC) or estimated online (Indirect FOC or IFOC) [5][8][14]. The absence of field angle sensors and the ease of operation at low speeds have favoured the use of IFOC schemes [6]. The main drawback of the standard IFOC scheme is the rotor time constant or slip gain dependency since it relies on the IM model or its parameters for rotor flux position estimation.

The rotor time constant is defined as the ratio of rotor inductance over rotor resistance. The slip gain is the inverse of the product of the rotor time constant and the reference field current component. Any deviation between the instrumented and the actual rotor time constant is said to *detune* the drive. This mismatch results in deterioration of drive performance in terms of steady-state and dynamic oscillations of rotor flux and torque. Consequently, the overall performance of the drive will be affected.

The effects of mismatch can be reduced by adapting the rotor time constant in the IFOC at all times. If field is kept constant, which is the case in this thesis, this task is shifted to the adaptation of the slip gain. Without online adaptation, the output torque capability of the drive can be reduced up to 29% or more. In this case, for applications where IFOCs

are used to save energy the motor must still be oversized. However, if an online adaptation is applied, it is possible to limit the torque degradation between 3 and 7%, which is acceptable in most high-performance applications [15]. As a result, recent literature has included a significant effort toward the development of accurate online estimation schemes for the rotor time constant or slip gain [8][14]–[19]. These methods are broadly discussed in chapter 3.

- Parameter and Operating Condition Changes

If an *ideal* FOC is achieved and applied to an IM, the overall drive can be viewed as a linear system (like a DC drive system). Under this condition, a linear control system can be used with classic (linear) design approaches, such as Nyquist and Bode plots [5][13]. However, in industrial environments the electrical and mechanical parameters of the drive system hardly remain constant. In addition, the system may also be affected by other perturbations, such as load torque and uncertain power electronics dynamics [20]. For example, in subway drives and electric vehicles, the inertia of the system will change depending on passenger load. The inertia of a robot arm drive, on the other hand, varies according to the length of the arm and the load it carries [5]. These examples indicate that linear and fixed-gain controllers such as PI controllers may be insufficient to deal with many IM drive issues.

In order to achieve and/or to maintain high-performance under the above conditions, the gains of a fixed-gain controller must be continuously updated according to the actual trend of the system. Many advanced adaptive techniques, such as *Model Reference Adaptive System* (MRAS), *Sliding Mode Control* (SMC), and *Artificial Intelligence* (AI) have been theoretically developed to fulfill this requirement. Unfortunately, due to their complexity and poor performances only a few have been implemented on FOC IM drives [20][21][22].

The difficulty related to the implementation of conventional advanced adaptive techniques on IM drives indicates that it can be difficult to effectively deal with machines problems through strict mathematical formulations. Alternatively, AI-based techniques, in particular *Fuzzy Logic* (FL), have emerged as a powerful complement to conventional methods. Design objectives that are mathematically hard to express can be incorporated into a Fuzzy Logic Controller (FLC) using simple linguistic terms.

The merit of FLC relies on its ability to express the amount of ambiguity in human reasoning. When the mathematical model of a process does not exist or exists with uncertainties, FLC has proven to be one of the best alternatives to move with unknown process. Even when the process model is well-known, there may still be parameter variation issues and power electronic systems, which are known to be often ill-defined.

Recent literature has also paid significant attention to the potentials of FLCs for modern IM drives [5][17][20]–[33]. Many approaches have been developed. They can be classified as non-adaptive and adaptive FLCs. A section of chapter 4 is dedicated to the analysis of these methods, their merits and applications.

▪ Objectives

The literature reviews conducted and provided in chapters 3 and 4 for the slip gain estimation methods and speed/torque control of IFOC IM drives, respectively will clearly indicate that:

(1) None of the slip gain estimation methods can solve the tuning problem in the entire torque-speed plane. In many cases, in order to expand the torque-speed plane of an algorithm one of the following is required:

- Addition of sensors such as flux search coils, Hall sensors.
- Use of very powerful processors to handle complex algorithms.

(2) There is relatively little experimental validation of advanced adaptive schemes suitable for FOC IM drives.

Motivated by the challenges of FOC IM drives, the objective of this thesis consists of:

(1) Using FLC and MRAS approaches to develop a real-time estimation scheme for the slip gain capable of operating in the entire torque-speed plane.
(2) Combining the advantages of FLC and conventional methods to effectively deal with the two motion control objectives, namely (i) performance tracking, and (ii) disturbance rejection.

The first objective is achieved by the proposed slip gain estimation scheme [17]. It consists in combining three distinctive MRAS quantities in a single controller in order to expand the torque-speed operating region of the algorithm. A FLC is used to ensure the switching between the three adaptive quantities based on the drive's operating speed and load torque. The mechanism behind the approach is outlined in chapter 3.

A *Self-Tuning Fuzzy Controller* (STFC) is designed and implemented to deal with the second objective [33]. As it will be shown, the proposed STFC has the ability to intelligently synthesize a conventional (non-adaptive) FLC for the process and tune its parameters in real time. It is suitable for applications, where the system must operate under severe parameter changes and uncertain conditions, and when the available a priori information about the system is limited. Under such conditions, it is difficult to design a fixed-parameter FLC or PI controller that performs sufficiently well.

The STFC is derived from the design of a non-adaptive FLC specifically calibrated for FOC IM drives. Initial tuning of a non-adaptive FLC can be very challenging and time consuming due to the coupling effects of its parameters. In order to deal with this issue, a new method is introduced to reduce the design time of FLCs. The proposed method is based on the available nameplate information of the IM, its operation in FOC mode, and the mathematical formulation of the drive operation and dynamics. Simulation and experimental results are provided to validate this design methodology. Finally, the stability analysis (based on the passivity approach) of the STFC is verified from that of the proposed non-adaptive FLC. Chapter 4 is dedicated to the design and implementation of this STFC.

▪ Thesis Structure

The remaining of the thesis is structured as follows. Chapter 1 outlines the basic principles of IM drives and the concept of FOC as applied in IM drives. The two major issues of IFOC IM drives, namely the slip gain online estimation and the speed control system design are also briefly introduced in chapter 1.

Since the proposed slip gain estimation method and STFC are based on the principles of FLC, a brief introduction and description of fundamental theories and concepts of FL and FLC is provided in chapter 2.

In chapter 3, the proposed slip gain online estimation approach is explained. The coupling effects of flux and torque on the drive are investigated. The various slip gain estimation methods are also discussed and compared in order to derive the proposed scheme.

The proposed systematic design methodology of non-adaptive FLCs and the STFC are introduced in Chapter 4. Sufficient simulation and DSP-

based experimental tests are provided to validate the approaches. The effect of detuned slip gain on the drive performance will also be investigated in the last section of this chapter.

Finally, conclusions and recommendations for future works can be found in the final section of the thesis.

Chapter 1

Induction Motor Drives

There are two types of IM rotors (with identical stator structure): (1) the wound-rotor winding IM, and (2) the squirrel-cage IM. The latter is made of short-circuited bars. It is the most commonly used type of IM due its rigidity. The theories of speed control and slip gain estimation developed in this thesis can be applied to both types of IM even though only the squirrel-cage type is considered.

1.1. Fundamental Concepts of IM

Consider a 3-phase squirrel-cage IM. Feeding its stator windings with a 3-phase sinusoidal voltage system will result in rotating magnetic field in the air-gap. The speed of this magnetic field, also known as *synchronous speed*, is given in [rpm] by

$$n_s = \frac{120 f_s}{P} \tag{1.1}$$

where f_s is the stator frequency in [Hz] and P is the number of poles of the IM.

If the rotor is stationary, its conductors will be subjected to a sweeping magnetic (air-gap) field, inducing an air-gap voltage known as *Electromagnetic Force* (EMF) in the rotor bars at synchronous speed (n_s). Since the rotor bars form a closed path (for squirrel-cage IMs), the induced EMF will generate current in the rotor, which in turn will also produce rotor magnetic field. The interaction between the air-gap and the rotor fluxes results in electromagnetic developed torque (T_e), which can be defined as [5]:

$$T_e = \pi \left(\frac{P}{2}\right) lrB_m F_r \sin\delta \tag{1.2}$$

where l is the axial length of the IM, r is the radius of the IM, B_m is the peak value of the air-gap flux density, F_r is the peak value of rotor Magneto-Motive Force (MMF), $\delta = \pi/2 + \theta_r$ is the torque angle between the magnetizing current (which produces the air-gap flux) and the rotor current (which represents the rotor flux), and θ_r is rotor angle between the induced EMF and rotor current. Other expressions of developed torque will be given later.

The developed torque, according to Lenz's law, will force the rotor to move in the direction of rotating field such that the relative speed between the rotating magnetic field and the rotor decreases. Depending on the shaft load, the rotor will eventually settle at a rotor speed (n_r) that is less than the synchronous speed (n_s). Obviously at $n_r = n_s$, there is no induced EMF and current in the rotor circuit and, consequently no T_e. Note that the developed torque (if present) and the rotor acceleration will follow the direction of the air-gap flux rotation.

The difference between n_s and n_r is referred to as *slip speed* (n_{sl}). Therefore, the *slip* (s) of an IM can be defined as:

$$s = \frac{(n_s - n_r)}{n_s} = \frac{n_{sl}}{n_s} \tag{1.3}$$

A practical per-phase equivalent circuit that is normally used to analyse and predict the steady-state performances of IMs with sufficient accuracy is represented in Figure 1-1 [34]: V_s is the per-phase stator terminal voltage, r_s is the per-phase stator winding resistance; r_r is the per-phase rotor winding resistance referred to the stator; L_{ls} and L_m are the per-phase stator and magnetizing leakage inductances, respectively; L_{lr} is the per-phase rotor leakage inductance referred to the stator; r_c is the per-

phase stator core loss resistance, and E_1 is the per-phase induced EMF in the stator winding.

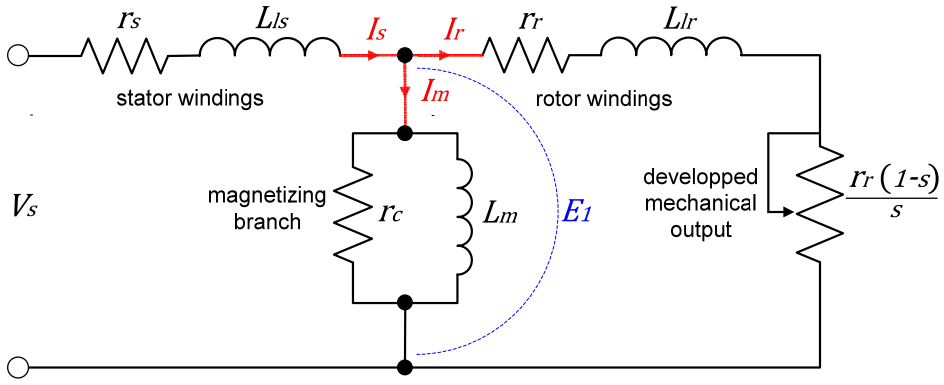

Figure 1-1: Steady-state per-phase equivalent circuit of an IM with respect to the stator

The magnetizing current (I_m) consists of a core loss component (E_1/r_c) and a magnetizing component ($E_1/\omega_s L_m$), where $\omega_s = 2\pi f_s$ is the synchronous frequency in [rad/s]. The stator current (I_s) consists of magnetizing current (I_m) and the rotor current referred to the stator (I_r).

In reality, the rotor induced EMF (E_2) causes rotor (induced) current (I_2) at slip speed (ω_{sl}). The induced current is limited by the rotor resistance (r_2) and rotor leakage reactance ($\omega_{sl} L_{l2}$), where L_{l2} is the rotor leakage inductance (not referred to the stator). Therefore, the rotor parameters referred to the stator in Figure 1-1 can be defined as [34]:

$$I_r = \frac{I_2}{a_{eff}} \qquad r_r = a_{eff}^2 r_2 \qquad L_{lr} = a_{eff}^2 L_{l2} \tag{1.4}$$

where a_{eff} is the effective rotor-to-stator turns ratio. The rotor resistance, rotor leakage reactance, and the effective turns ratio are very difficult to obtain for squirrel-cage IMs. Fortunately, there exist available self-commissioning methods capable of estimating directly I_r, r_r, and L_{lr} even

though r_2, L_{l2} and a_{eff} are not known separately. Such methods are discussed briefly in Section 1.3.5.

In terms of induced EMF, the supply voltage can be expressed as (Figure 1-1):

$$V_s = E_1 + (r_s + jx_{ls})I_s \tag{1.5}$$

where $x_{ls} = \omega_s L_{ls}$ is the stator leakage reactance. For a distributed phase winding, the RMS value of E_1 can be defined as [35]:

$$E_1 = 4.44 f_s N_1 k_{w1} \Phi_m \tag{1.6}$$

where N_1 is the total number of stator turns per phase, k_{w1} is the stator winding factor, and Φ_m is the peak air-gap flux. For most 3-phase machine windings k_{w1} is about 0.85 to 0.95 [35].

For simplicity, the equivalent circuit described in Figure 1-1 is usually approximated to that shown in Figure 1-2, where the core loss resistance is dropped and the magnetizing inductance is shifted to the input. Performance predictions using this approximate model vary only within ±5% from that of the actual IM model (Figure 1-1) [5][8][34][35].

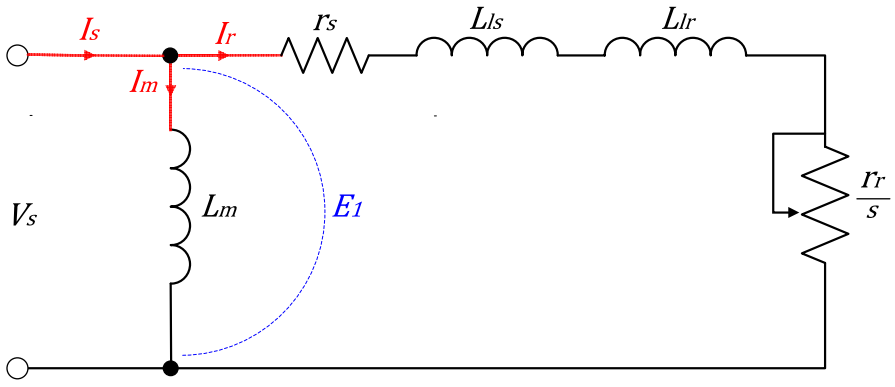

Figure 1-2: Approximate steady-state per-phase equivalent circuit model of an IM with respect to the stator

Using Figure 1-2, the magnitude of I_r can be expressed as:

$$I_r \approx \frac{V_s}{\sqrt{(r_s + r_r/s)^2 + \omega_s^2 (L_{ls} + L_{lr})^2}} \tag{1.7}$$

The developed torque can be defined as the ratio of the developed power (P_d) and the mechanical rotor frequency (ω_m) as:

$$T_e = \frac{P_d}{\omega_m} = \frac{(P_g - P_{lr})}{\omega_m} = \frac{\left(\frac{3I_r^2 r_r}{s} - 3I_r^2 r_r\right)}{\omega_m} = 3\left(\frac{P}{2}\right) I_r^2 \frac{r_r}{s\omega_s} \tag{1.8}$$

where P_g is the air-gap power, P_{lr} is the rotor copper loss, and $\omega_s = \omega_m/(P/2)$. Substituting (1.7) in (1.8) yields

$$T_e \approx 3\left(\frac{P}{2}\right) \frac{r_r}{s\omega_s} \frac{V_s^2}{\left[\left(r_s + \frac{r_r}{s}\right)^2 + \omega_s^2 (L_{ls} + L_{lr})^2\right]} \tag{1.9}$$

The shaft output power of the machine can be defined as

$$P_{sh} = P_d - P_{FW} \tag{1.10}$$

where P_{FW} is the friction and windage losses of the machine, proportional to the speed and the square of the speed, respectively [8]. Equation (1.10) indicates that the developed torque in (1.9), which is generated by the internal electric-to-mechanical power conversion, differs from the torque available at the shaft of the motor by the amount equal to the friction and windage torques in the machine [34].

Equation (1.9) indicates that if stator frequency and voltage are kept constant, the developed torque is a function of the slip and internal circuitry elements representing the IM. It should also be noted that I_r depends on the slip at constant frequency, according to (1.7). These special features of IMs play a fundamental role in their speed and torque control characteristics.

1.2. Basic IM Drive Concepts

Traditionally IMs were designed for constant-speed applications for the following reason. At constant supply voltage and frequency, based on the torque-speed characteristics of equation (1.9), IMs are essentially constant-speed motors: the operating speed is very close (less than 5%) to the synchronous speed [4]. If the load torque is increased, the speed drops by only a very small amount; making them very suitable for constant-drive systems.

However, many industrial applications require variable speeds or a continuous variable range of speeds. With modern power electronics and VSD technologies it is possible to provide the necessary variable voltage and frequency that an IM requires for efficient and dynamic variable speed control. Modern power electronics, although more complex that those used for DC drives, have not only made IMs suitable for many drive applications but also extended their applications and enabled users to take advantage of their low capital and maintenance costs. The practical effect is the possibility to drive an IM to achieve a dynamic performance higher than that of a phase-controlled separately-excited DC drive. In order to understand how power electronics schemes are used to achieve such performances, it is important to analyze the fundamental concepts behind IM drives in general.

A careful analysis of equations (1.1) and (1.9) indicates that in general the speed and/or torque of an IM can be controlled by one of the following methods [4][5][7][8]:

(1) Stator voltage,
(2) Frequency,
(3) Voltage and frequency, and
(4) Voltage (or current) and frequency.

Depending on how the measured variables (current, voltage, and frequency) of the motor are manipulated in the controller, these methods can also be broadly divided into (1) Scalar Control, and (2) FOC methods.

1.2.1. Scalar Control Methods

1.2.1.1. Stator Voltage Control Operation

Equation (1.9) shows that torque is directly proportional to the square of the supply voltage. Hence, a very simple method of controlling speed is to vary the supply voltage while maintaining constant supply frequency. This is accomplished through either a 3-phase autotransformer or a solid-state voltage controller.

The autotransformer method has the advantage of providing sinusoidal voltage for the IM, contrary to solid-state controllers. In large power applications an input filter is required to reduce the harmonic currents flowing in the supply line if a solid-state controller is used. Despite this inconvenience, solid-state approaches have become the most commonly used nowadays; especially with small squirrel-cage IMs [35]. This is also due to the fact that they can be used as “Soft-Starters” for constant speed squirrel-cage IMs, where the starting voltage is applied gradually to limit the stator inrush current [1].

A solid-state voltage control consists of a series-connected power switches (SRCs, GTOs, IGBTs, etc.) in the IM. The instant of voltage application can be delayed by controlling the gating signals to the power switches. If the speed command is changed, the firing angles of the switches will change accordingly in order to generate a new terminal/supply voltage to the IM and thus a new operating speed.

Neglecting the stator impedance ($r_s + jx_{ls}$) in Figure 1-1, the induced EMF approximately equals the supply voltage ($E_1 \approx V_s$). This assumption is reasonable for an integral horsepower machine, especially if the frequency is above 10% [5]. From equation (1.6), the air-gap flux can be written as

$$\Phi_{\mathrm{m}} \approx \left(\frac{1}{4.44 N_1 k_{w1}}\right)\frac{V_s}{f_s} \tag{1.11}$$

The supply voltage in (1.11) can only be reduced or maintained at its rated value. Operation above rated supply voltage is restricted by magnetic saturation. However, the reduction of supply voltage of an IM has the effect of reducing both the air-gap flux, and the induced rotor current. The developed torque will also fall roughly as the square of the supply voltage reduction, as shown in equation (1.9). Therefore, when supply voltage is reduced, torque is decreased, slip is increased, and speed is decreased.

Due to reduced torque capability and flux, the overall efficiency of the drive will also be reduced accordingly. As a result, this method is restricted to applications that require low-starting torque and narrow ranges of speed at a relatively low slip. Such applications includes small motors coupled to fans, air blowers, centrifugal pumps, etc. [4][5][8]. Moreover, as stated earlier, reduced voltage is not usually for speed control in industry, but rather for motor torque control, mainly for soft stating squirrel-cage IMs [1].

1.2.1.2. Frequency Control Operation

It is also possible to control the speed of an IM by varying the supply frequency while maintaining constant supply voltage, based on equation (1.9). If the stator impedance ($r_s + jx_{ls}$) in Figure 1-1 are neglected, in a low-slip region, the developed torque can be expressed as [5]:

$$T_e \approx 3\left(\frac{P}{2}\right)\frac{1}{r_r}\Phi_{\mathrm{m}}^2\omega_{sl} \tag{1.12}$$

The above equation indicates that T_e is proportional to slip speed at constant air-gap flux or at constant slip speed, T_e is proportional to the square of the air-gap flux. On the other hand, equation (1.11) shows that at rated supply voltage and frequency, the air-gap flux is also rated. Therefore, if supply frequency is decreased below its rated value (at constant voltage), the air-gap flux will increase and will saturate the magnetic circuit. In addition, at low frequencies, the reactances decrease and the motor current may be too high. For these reasons, this type of control is not normally used.

In order to avoid high saturation of magnetic circuit at constant voltage, the supply frequency can only be increased beyond its rated value. In this case, the air-gap flux will decrease; resulting in reduced torque capability of the motor, as it can be seen in equation (1.11). This type of frequency control operation is also referred to as *Field Weakening*.

Frequency control methods require frequency converters. There are 2 types of converters [8]: direct (cycloconverters) and indirect (rectifier-inverter). Cycloconverters are used in very large power applications, such as locomotives and cement mills, where the frequency requirement is only one-half or one-third of the line frequency [4]. For a majority of industrial applications, a wide range of frequency variation is required. So, indirect frequency converters are appropriate. They consist of a rectifier unit, a DC link, and an inverter unit. Depending on the source characteristic of the DC link, indirect converters are further divided into *Voltage-Sourced Inverters* (VSIs) and *Current-Sourced Inverters* (CSIs).

In VSIs, the converter impresses a voltage on the motor, and the impedance of the machine defines the current. In CSIs, the converter impresses a current on the motor, and the impedance of the machine

determines the voltage. Most of today's small and medium AC drives are VSIs [4]. For most small and medium industrial applications the so-called *Pulse-Width Modulation* (PWM) VSI is applied, and only this converter will be considered in this thesis.

PWM techniques translate the modulation waveforms of variable amplitude and frequency into a train of switching pulses for the inverter. In PWM VSI AC drives, the DC link voltage is uncontrolled. It is derived from a simple diode bridge (rectifier). The converter's output voltage is controlled electronically within the inverter by using one of the PWM techniques. The transistors (in the inverter) are switched on and off several times within a half-cycle to generate a variable voltage output which is normally low in harmonic content.

There are many PWM techniques, each having different performance notably in respect to the stability and audible noise of the driven motor [36]. Their common feature is that they virtually eliminate low-speed torque pulsations. Since negligible low-order harmonics are present, this is an ideal solution, where a drive system is to be used across a wide range of speed [3]. In addition, since voltage and frequency are both controlled with the PWM, quick responses of torque to changes in demand are possible. Also, with a diode rectifier as the input circuit, a high power factor (close to unity) is offered to the incoming AC supply over the entire speed and load range.

1.2.1.3. Voltage-Frequency Control Operation

To overcome the limitations of voltage and frequency control methods, a third method is incorporated to control the speed and torque independently by varying the supply voltage and frequency to maintain constant air-gap flux. The key feature of this method relies on the analysis of equation (1.11), according to which, in order to maintain

constant air-gap flux at variable frequency (or voltage), the stator voltage (or frequency) must be changed accordingly. This exceptional feature compounds the control problem of IM drives and set them apart from DC drives, which require only the voltage control.

A number of strategies have been developed to ensure constant air-gap flux operation at all time. They are classified depending on the way the voltage-to-frequency ratio is implemented [4][8]:

(1) Constant Volts per Hertz control,
(2) Constant slip-speed control, and
(3) Constant air-gap flux control.

A detailed study of these schemes is beyond the scope of this thesis. The constant Volts per Hertz method is by far the most popular in industry due to its simplicity. Hence, a brief introduction of the method is given in order to point out the limitations of scalar methods with respect to FOC schemes. The reader is referred to [4]–[7] for advanced analyses and comparison of the available scalar methods.

Figure 1-3 describes the open-loop implementation scheme of constant volts per hertz control for a VSI IM drive [5]. The power circuit consists of an uncontrolled diode rectifier, LC filter or DC link, and a PWM VSI. Ideally, no feedback signal is required for the control. The reference stator frequency ($\omega_s^* = 2\pi f_s^*$) is used as the primary control variable because it is approximately equal to the rotor frequency (ω_r), if the motor slip frequency (ω_{sl}) is neglected. The reference phase voltage (V_s^*) is generated directly from ω_s^* by the so-called volts per hertz constant ($K_{vf} = V_s^*/\omega_s^*$) as shown in Figure 1-3, so that the air-gap flux remains constant, according to equation (1.11).

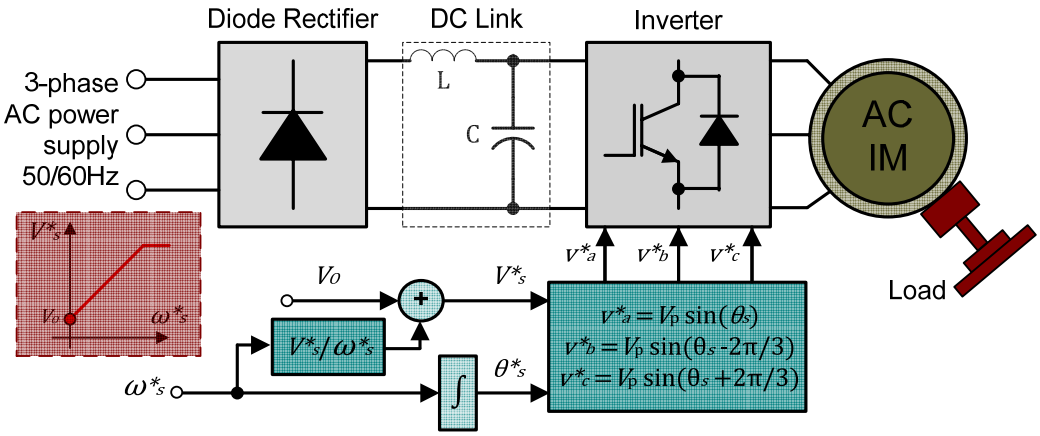

Figure 1-3: Implementation scheme of open-loop constant Volts per Hertz VSI IM drives

As the frequency becomes small at low-speed operations, the stator impedance ($r_s + jx_{ls}$) (refer to Figure 1-1) tends to absorb the major amount of stator voltage, thus weakening the air-gap flux. To overcome this effect, the boost voltage (V_o) is added so that rated flux and full torque become available down to zero speed. The boost voltage is normally defined as $V_o = I_{s1} r_s$, where I_{s1} is the stator current at fundamental frequency [8]. Note that the effect of V_o becomes negligible at higher frequencies, as shown in the V_s^*-ω_s^* function in Figure 1-3.

The ω_s^* signal is integrated to generate the angel signal (θ_s^*) and the corresponding reference sinusoidal phase voltage signals (v_a^*, v_b^*, v_c^*) are generated (with $V_P = \sqrt{2} V_s^*$). These reference voltage signals generate the gate signals that drive the inverter.

Clearly, if the load torque in Figure 1-3 is increased for the same reference frequency, the actual motor speed will drop. This speed drop is particularly small (with a low slip) and usually tolerated in low-performance applications such as pumps and fans. In such applications, accurate control of speed is not the main issue.

However, since the rotor speed is not measured and controlled, the slip speed cannot be maintained or controlled. This can lead to operation in the unstable region (pull-out torque) of the torque-speed characteristics of the IM if the reference frequency is changed abruptly by a very large amount [5][8]. This problem is, to an extent, overcome by adding an outer speed loop in the drive to regulate the slip.

In the case of close-loop control, the rotor speed is measured and compared with a reference speed, and the resulting error is processed through a (PI) controller and a limiter to generate the reference slip speed signal. The latter is added to the measured rotor speed to obtain the reference stator frequency (ω_s^*). Thereafter, ω_s^* is processed as in the open-loop scheme described in Figure 1-3. Since the slip is proportional to the developed torque at constant flux, this close-loop scheme is also referred to as open-loop torque control with a speed control loop.

When the slip is regulated, if the load is increased, the speed tends to drop accordingly. However, the speed control loop will increase the frequency until the original speed is restored. Since there is no close-loop flux control, the line voltage variation will cause some flux drifts and, as a result, the torque sensitivity with slip will vary. In addition, incorrect volts per hertz ratio, stator drop variation by line current, and machine parameter disturbances may still cause weaker flux or the flux to saturate [5].

To overcome the above limitations, a practical arrangement consists in speed control system with close-loop torque and flux controls [4][5][8]. However, additional feedback loops mean complexity of additional feedback signal synthesis, and potential stability issues [37]. Moreover, even when close-loop torque and flux controls are used, as the frequency command is increased by the torque loop, the flux temporarily deceases until it is compensated by sluggish flux control loop. This inherent

coupling effect of torque and flux in IMs slows down the torque response of the drive. It is also considered as the common drawback of scalar methods.

1.2.1.4. Some Remarks on Scalar Control Methods

So far the techniques described have been based on achieving constant air-gap flux or, if that is not possible, then the maximum (rated) flux. Constant flux is the ideal condition if the highest torque is required because the load cannot be predicted with certainty, or if fast acceleration time is desired. There is no doubt that scalar methods provide good steady-state but poor dynamic responses. They only meet the requirements of industrial applications for which details of transient behaviours are not so important.

The poor dynamic responses obtained with scalar methods are the result of deviation of air-gap flux (in both magnitude and phase) caused by the inherent coupling effect of flux and torque: in IMs, the developed torque and flux are functions of voltage, frequency and current. The deviations of air-gap flux are usually accompanied with oscillations. These oscillations generate electromagnetic torque oscillations. If left unchecked, they reflect as speed oscillations. This is undesirable in high-performance applications, where high precision, fast positioning, or accurate speed control are required at all time. Furthermore, flux oscillations result in large excursions of stator currents; requiring large peak converter ratings to meet the dynamics. As a result, the cost of the overall drive increases and the competitive edge of AC drives in the marketplace is reduced regardless of their excellent advantages over DC drives.

The coupling effect between the flux and torque in IMs makes their control system design very challenging, especially in transient regimes.

An effective dynamic control is only possible if flux deviations can be controlled by magnitude and frequency of the stator and rotor phase currents and their instantaneous phases. Scalar methods are unable to solve this problem because they use only the magnitude and frequency of the stator and rotor currents. The foregoing problems can be solved by FOC techniques with real-time processors and an accurate IM model.

1.3. Field Oriented Control of IM Drives

In separately-excited DC motors the armature and field winding fluxes are always in quadrature (i.e. orthogonal to one another). If the armature reaction is neglected, the orthogonal fluxes will have no net interaction effect on one another. It is said that field and armature fluxes are completely decoupled. The objective of FOC is to force the control of an IM (or AC machines in general) to be similar to that of a separately-excited DC motor in terms of torque and speed control.

For DC motors, the developed torque may be expressed as

$$T_e = K_a \phi(I_f) I_a \tag{1.13}$$

where K_a is a constant coefficient, $\phi(I_f)$ is the field flux (function of field current I_f), and I_a is the armature current (torque component). Due to the decoupling feature of DC motors, torque and flux can be controlled independently (since they can also readily be measured externally). The time constant of the armature circuit is generally much smaller than that of the field winding. Therefore, controlling torque through I_a (while maintaining constant field flux through constant I_f) is faster than changing I_f or both (I_f & I_a). If field flux is maintained constant at all time and the torque angle is kept 90°, the torque will always follow (directly proportional) the armature current. Such arrangement results in high-performance torque control drive.

The concept of torque control in IMs is not as straightforward as it is in DC motors due to the interaction between the air-gap and rotor fluxes. In squirrel-cage IMs (refer to Figure 1-1), the flux producing current (I_m) and the torque producing current (I_r) cannot be measured externally or controlled separately. However, as in DC motors, I_m and I_r are also roughly perpendicular to one another and their vector sum makes up the stator current (I_s), which can be readily measured. In order to operate an IM drive like a DC drive, the two current vectors (I_m & I_r) must be distinguished and controlled separately without the benefit of two separate circuits (like in DC motors) and only being able to measure and control the stator current. This is only possible by means of external controls; making the system more complex.

Many external control schemes have been introduced to ensure online independent control of torque and rotor flux in IMs. The mechanisms by which these controllers are operated are referred to as FOCs or VCs. The term "vector" control refers to the technique that controls both the amplitude and the phase of AC excitation. VC therefore controls the spatial orientation of the electromagnetic fields in the machine. The term "field oriented" control is used for controllers achieved in field coordinates to maintain a 90° spatial orientation between I_m & I_r.

The strategy of FOC for IMs is to resolve the instantaneous stator currents into 2 components: one providing the air-gap flux (I_m) and the other producing the torque (I_r). After this, I_m & I_r must be controlled separately under all speed and load conditions, while maintaining a constant field current (as in DC drives). The resolution of stator currents requires the position of rotor flux at all time. If the rotor flux position is known, then the control of the motor can be approximated to that of separately-excited DC motor by using one of the external control approaches. Therefore, the central part of FOC schemes is the *active motor model*, which continuously models the conditions inside the motor

to determine (directly or indirectly) the value of the rotor flux position at all time. For good dynamic responses of the drive, the model calculations need to be done at least more than 2000 times per second, which gives an update time of less than 0.5ms [1]. Although this is easily achieved with modern DSPs, the ability to continuously model the IM at this speed only became available within the last decade or so with the development of 16-bit microprocessors [1].

If rotor flux position is known at all time, *ideal* FOC can be obtained. The requirement of phase, frequency, and magnitude control of the currents and hence the flux is made possible by the inverter control. So, the main difference between Scalar Control methods and modern FOC drives is almost entirely in the control system and the extent to which the active model for FOC is implemented to control the switching pattern of the inverter.

1.3.1. Dynamic Model of IM

In VSDs or servo drives an IM constitutes an element within a feedback loop. Therefore, it is important that its dynamic behaviour(s) be taken into account for applications where transients are important. This is difficult to incorporate in the per-phase equivalent circuit (Figure 1-1). Besides, high-performance drive controls, such as FOCs, rely on the dynamic model of the machine to take into account the interactions between currents, fluxes, and speed for fast dynamic response.

The dynamic model of an IM is often derived from its idealized circuit model [38], shown in Figure 1-4, where the letters "*s*" and "*r*" are related to stator and rotor variables, respectively. The voltage equations of the magnetically coupled stator and rotor circuits can be expressed as:

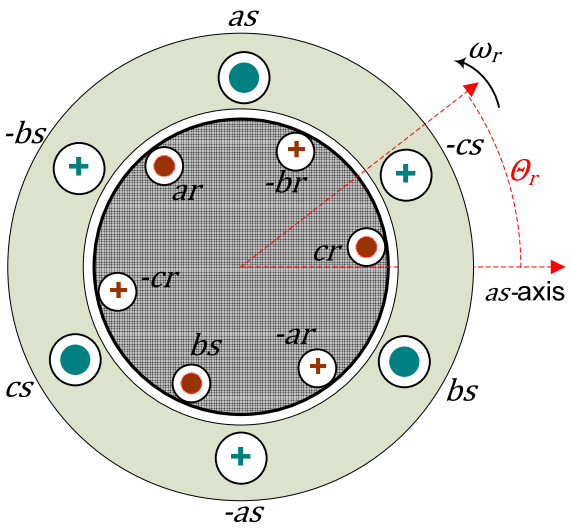

Figure 1-4: Idealized circuit model of a 3-phase IM

$$v_{as} = r_s i_{as} + \frac{d\lambda_{as}}{dt} \tag{1.14}$$

$$v_{bs} = r_s i_{bs} + \frac{d\lambda_{bs}}{dt} \tag{1.15}$$

$$v_{cs} = r_s i_{cs} + \frac{d\lambda_{cs}}{dt} \tag{1.16}$$

$$v_{ar} = r_r i_{ar} + \frac{d\lambda_{ar}}{dt} \tag{1.17}$$

$$v_{br} = r_r i_{br} + \frac{d\lambda_{br}}{dt} \tag{1.18}$$

$$v_{cr} = r_r i_{cr} + \frac{d\lambda_{cr}}{dt} \tag{1.19}$$

The flux linkages of the stator and rotor windings, in terms of winding inductances and currents are:

$$\begin{bmatrix} \lambda_s^{abc} \\ \lambda_r^{abc} \end{bmatrix} = \begin{bmatrix} L_{ss}^{abc} & L_{sr}^{abc} \\ L_{rs}^{abc} & L_{rr}^{abc} \end{bmatrix} \begin{bmatrix} i_s^{abc} \\ i_r^{abc} \end{bmatrix} \tag{1.20}$$

where:

$$\lambda_s^{abc} = \begin{bmatrix} \lambda_{as} \\ \lambda_{bs} \\ \lambda_{cs} \end{bmatrix},\ \lambda_r^{abc} = \begin{bmatrix} \lambda_{ar} \\ \lambda_{br} \\ \lambda_{cr} \end{bmatrix},\ i_s^{abc} = \begin{bmatrix} i_{as} \\ i_{bs} \\ i_{cs} \end{bmatrix},\ i_r^{abc} = \begin{bmatrix} i_{ar} \\ i_{br} \\ i_{cr} \end{bmatrix} \tag{1.21}$$

The stator-to-stator and rotor-to-rotor winding inductances are:

$$L_{ss}^{abc} = \begin{bmatrix} L_{ls} + L_{ss} & L_{sm} & L_{sm} \\ L_{sm} & L_{ls} + L_{ss} & L_{sm} \\ L_{sm} & L_{sm} & L_{ls} + L_{ss} \end{bmatrix} \tag{1.22}$$

$$L_{rr}^{abc} = \begin{bmatrix} L_{lr} + L_{rr} & L_{rm} & L_{rm} \\ L_{rm} & L_{lr} + L_{rr} & L_{rm} \\ L_{rm} & L_{rm} & L_{lr} + L_{rr} \end{bmatrix} \tag{1.23}$$

where L_{rr} is the self-inductance of the rotor winding, L_{ss} is the self-inductance of stator winding, L_{sm} is the mutual inductance between stator windings, and L_{rm} is the mutual inductance between rotor windings. The stator-to-rotor mutual inductances are dependent on the rotor angle (θ_r), and are defined as

$$\begin{gathered} L_{sr}^{abc} = [L_{rs}^{abc}]^T \\ = L_{sr} \begin{bmatrix} cos\theta_r & cos(\theta_r + 2\pi/3) & cos(\theta_r - 2\pi/3) \\ cos(\theta_r - 2\pi/3) & cos\theta_r & cos(\theta_r + 2\pi/3) \\ cos(\theta_r + 2\pi/3) & cos(\theta_r - 2\pi/3) & cos\theta_r \end{bmatrix} \end{gathered} \tag{1.24}$$

where L_{sr} is the peak value of stator-to-rotor mutual inductance. If the reluctive drops in iron are neglected, the machine inductances can be calculated in terms of the winding turns of the stator (N_s) and rotor (N_r), and the air-gap permeance (P_{ag}) as [38]:

$$\begin{gathered} L_{ss} = N_s^2 P_{ag},\ L_{rr} = N_r^2 P_{ag},\ L_{sm} = N_s^2 P_{ag} cos(2\pi/3),\ L_{rm} = \\ N_r^2 P_{ag} cos(2\pi/3),\ L_{sr} = N_s N_r P_{ag} \end{gathered} \tag{1.25}$$

Equations (1.14)-(1.19) show that the performance of an idealized IM is described by six 1st-order differential equations; one for each winding. The coefficients of these equations are coupled to one another by the mutual inductances between the rotor and stator windings. Furthermore,

the stator-to-rotor coupling terms are functions of the rotor position. So, when the motor rotates, the coupling terms change with time.

In order to reduce this complexity and the coupling effect, a change of variables is often required. It consists in transferring the IM equations to a quadrature rotating reference frame such that the mutual inductanes are no longer time dependant. There are several methods to do that. In this thesis, the well-known Clarke and Park Transformations are used, modeled and implemented digitally.

Using these Transformations, many properties of an IM can be analyzed without complexities in the voltage, current and flux equations. Furthermore, Park and Clarke Transformations make it possible and easy for control algorithms to be implemented on real-time DSPs. The following illustrates how these Transformations are performed for an IM.

The 3-phase voltages, currents and fluxes of an IM can be analyzed in terms of complex space vectors. With regard to the instantaneous stator winding currents (i_{as}, i_{bs}, i_{cs}), the space vector can be defined by

$$\bar{\imath}_s = i_{as} + \alpha i_{bs} + \alpha^2 i_{cs} \tag{1.26}$$

where $\alpha = e^{j\frac{2}{3}\pi}$ and $\alpha^2 = e^{j\frac{4}{3}\pi}$ are the spatial operators. The stator current complex space vector is shown in Figure 1-5, where (a, b, c) are the 3-phase system axes. This current space vector depicts the 3-phase sinusoidal system that needs to be transformed into a time-invariant two-axis coordinate system using the Clarke and Park Transformations.

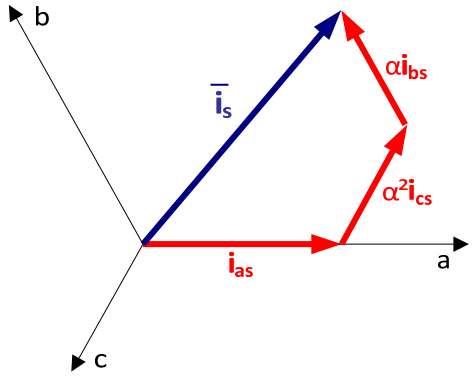

Figure 1-5: Stator current space vector and its components in 3-phase reference system axes (a-b-c)

1.3.1.1. Clarke Transformation

Developed by E. Clarke, the Clarke Transformation consists in changing a stationary circuit to a 2-phase stationary reference frame represented by α & β [39]. Using this approach, the space vector of equation (1.26) can be expressed using the 2-axis theory shown in Figure 1-6:

$$\bar{\imath}_s = i_{\alpha s} + j i_{\beta s} \tag{1.27}$$

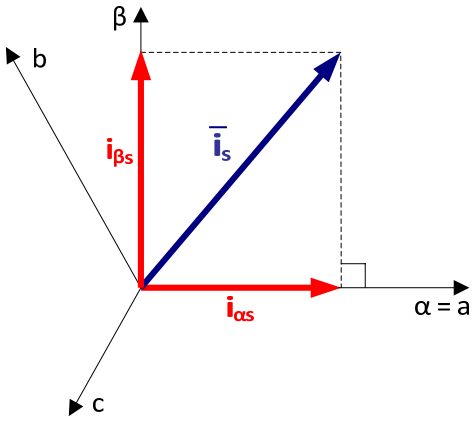

Figure 1-6: Stator current space vector and its components in (α, β) reference frame (Clarke Transformation)

The real part of the state vector is equal to the instantaneous value of the direct-axis stator current component ($i_{\alpha s}$), and the whole imaginary part is equal to the quadrature-axis stator current component ($i_{\beta s}$). Thus, the stator current space vector in the stationary reference frame attached to the stator can be written as

In symmetrical 3-phase machines, the direct and quadrature axis stator currents ($i_{\alpha s}$ & $i_{\beta s}$) are fictitious quadrature (2-phase) current components. They are related to the actual 3-phase stator currents as follows. Assuming balance system ($i_{as} + i_{bs} + i_{cs} = 0$) [38]:

$$i_{\alpha s} = \frac{2}{3} i_{as} - \frac{1}{3} i_{bs} - \frac{1}{3} i_{cs} = i_{as} \tag{1.28}$$

$$i_{\beta s} = \frac{1}{\sqrt{3}} (i_{bs} - i_{cs}) = \frac{1}{\sqrt{3}} i_{as} + \frac{2}{\sqrt{3}} i_{bs} \tag{1.29}$$

The above equations indicate that the Clarke Transformation outputs a 2-phase co-ordinate system that still depends on time and speed. The space vectors of other motor quantities (voltages, currents, magnetic fluxes, etc.) can be defined in the same way as the stator current space vector. If the 3-phase symmetrical system is assumed balanced, then only 2 stator instantaneous currents are required to perform the Clarke Transformation.

1.3.1.2. Park Transformation

Beside the stationary reference frame introduced by Clarke, the machine model can also be formulated in an arbitrary reference frame rotating at an arbitrary speed. In this case, the voltage equations can be expressed by using the transformations of the motor quantities from one reference frame to the arbitrary reference frame. Dynamic models of AC machines are often used in FOC algorithms to obtain control schemes that produce high-performance and are similar to those used to control DC machines.

In order to achieve this, as stated earlier, the reference frames must be aligned with the stator, or the rotor, or the magnetizing flux-linkage space vector. The most commonly used reference frame (and the one used in this thesis) is the reference attached to the rotor flux linkage space vector with the direct axis and quadrature axis [5][8].

Introduced in the late 1920's by R.H. Park, the Park Transformation offers a different approach to AC machine analysis [39]. It formulates a change of variables which replace variables such as voltages, currents, and flux linkages associated with fictitious windings rotating with the rotor. In other words, the stator and rotor variables are referred to a reference frame fixed on the rotor. Hence, viewed from the rotor, all variables can be seen as constant (DC) quantities. This unique feature of the Park Transformation allows the elimination of all time-varying inductances from the voltages equations of 3-phase AC machines due to the rotor spinning.

Park Transformation modifies the 2-phase orthogonal system (α, β) in the (d, q) rotating reference frame. If the d-axis is aligned with the rotor flux, as shwon in Figure 1-7, for the current vector, the relationship from the 2 reference frames will be:

$$i_{ds} = i_{\alpha s} cos\theta_e + i_{\beta s} sin\theta_e \tag{1.30}$$

$$i_{qs} = -i_{\alpha s} sin\theta_e + i_{\beta s} cos\theta_e \tag{1.31}$$

where θ_e is the rotor flux position. The components i_{ds} and i_{qs} are the flux and torque component currents of the IM, respectively. They depend on the current vector (α, β) components and on the rotor flux position. If the latter is known, then, by this projection, the (d, q) current components become constants.

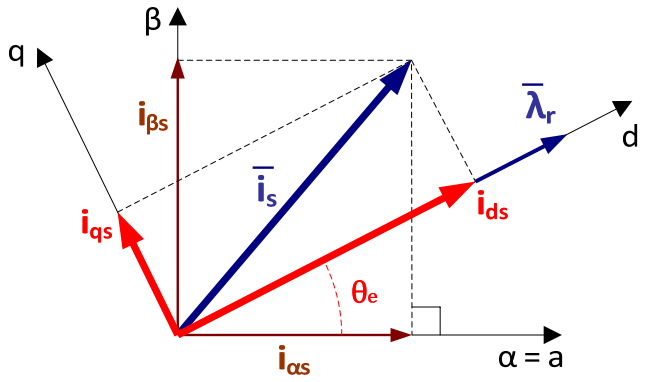

Figure 1-7: Stator current space vector and its components in (d, q) reference frame (Park Transformation)

Equations (1.30) and (1.31) indicate that the Park Transformation outputs a 2-phase coordinate system (d, q) that are time invariant. Furthermore, knowing the flux component (i_{ds}) and torque component (i_{qs}) currents, the IM drive can now be operated as separately-excited DC motor drive. To do so, the developed torque must also be described in the same reference frame as the i_{ds} and i_{qs}. The IM torque in (d, q) system can be found as follows.

Since AC machines can be modelled using an arbitrary reference frame, if an IM is rotating at speed ω (arbitrary speed) in the direction of the rotor, then its dynamic equations in stationary reference frame can be obtained by setting $\omega = 0$. Likewise, the equations in synchronous reference frame are obtained by setting $\omega = \omega_e$. Applying this transformation to the stator windings (a, b, c) voltages, the stator winding (d, q) voltages in the arbitrary reference frame can be written as [5]:

$$v_{qds} = \begin{bmatrix} 0 & 1 \\ -1 & 0 \end{bmatrix} \lambda_{qds} + p\lambda_{qds} + r_s\lambda_{qds} \tag{1.32}$$

where $p = d/dt$. Applying the transformation to the rotor voltage equation, we get

$$v_{qdr} = \begin{bmatrix} 0 & 1 \\ -1 & 0 \end{bmatrix} \lambda_{qdr} + p\lambda_{qdr} + r_r \lambda_{qdr} \tag{1.33}$$

The stator and rotor flux linkage equations are given by

$$\begin{bmatrix} \lambda_{qs} \\ \lambda_{ds} \\ \lambda_{qr} \\ \lambda_{dr} \end{bmatrix} = \begin{bmatrix} L_{ls} + L_m & 0 & L_m & 0 \\ 0 & L_{ls} + L_m & 0 & L_m \\ L_m & 0 & L_{lr} + L_m & 0 \\ 0 & L_m & 0 & L_{lr} + L_m \end{bmatrix} \begin{bmatrix} i_{qs} \\ i_{ds} \\ i_{qr} \\ i_{dr} \end{bmatrix} \tag{1.34}$$

where the rotor variables (λ_{qr}, λ_{dr}, i_{qr}, i_{dr}, L_{lr}) are referred to the stator, using the effective turns ratio given in equation (1.4). The electromagnetic torque equation is given by:

$$T_e = \frac{3}{2}\frac{P}{2\omega_r}\left[\omega\left(\lambda_{ds} i_{qs} - \lambda_{qs} i_{ds}\right) + (\omega - \omega_r)\left(\lambda'_{dr} i'_{qr} - \lambda'_{qr} i'_{dr}\right)\right] \tag{1.35}$$

After a few manipulations of equation (1.35), the torque can be written as

$$T_e = \frac{3}{2}\frac{P}{2}\left(\lambda_{ds} i_{qs} - \lambda_{qs} i_{ds}\right) \tag{1.36}$$

which is the key expression for analysis of FOC schemes.

1.3.2. Fundamentals of FOC

In order to resolve the stator currents into 2 components, the motor control system is considered in a synchronously rotating reference frame (d, q), where the sinusoidal variables appear as DC quantities in steady-state [5][8][38]. Under synchronous reference frame ($\omega = \omega_e$), the component of the current producing the rotor flux phasor (i_{ds}^e) is aligned with the rotor flux vector (λ_r) so that the q-axis component of the rotor flux in the chosen reference frame will be zero, as illustrated in Figure 1-7. The superscript "e" denotes the synchronous reference frame

Resolving the stator current phasor along λ_r reveals that i_{ds}^e is the flux-producing component current and i_{qs}^e is the torque-producing component

current. With $v_{qdr} = 0$ for squirrel-cage IMs, from equations (1.32) and (1.33), it follows that:

$$\lambda_{dr}^{e} = \hat{\lambda}_r = \bar{\lambda}_r \tag{1.37}$$

$$\lambda_{qr}^{e} = L_m i_{qs}^{e} + L_r i_{qr}^{e} = 0 \tag{1.38}$$

where $L_r = L_{lr} + L_m$. Under the condition stated in (1.38), the developed torque in synchronous reference frame can be written as [5]:

$$T_e = \frac{3}{2}\frac{P}{2}\frac{L_m}{L_r}\lambda_{dr}^{e} i_{qs}^{e} \tag{1.39}$$

If the rotor flux is kept constant (i.e. if $\lambda_{dr}^{e} = \hat{\lambda}_r = L_m i_{ds}^{e} = const$), then equation (1.39) can be written as

$$T_e = \frac{3}{2}\frac{P}{2}\frac{L_m^2}{L_r} i_{ds}^{e} i_{qs}^{e} = K_t i_{qs}^{e} \tag{1.40}$$

where K_t is the torque constant. Clearly, there is a very close analogy between the developed torque of an IM in synchronous reference frame (equation (1.40)) and that of the DC motor in equation (1.13). As in DC motors, equation (1.40) also indicates that torque can be independently controlled by regulating the torque component current (i_{qs}^{e}) as long as the flux component current (i_{ds}^{e}) is kept constant at all time.

In order for λ_{qr}^{e} to be zero at all time (to satisfy the conditions stated in equations (1.37) and (1.38)), its derivative must also remain zero at all time. This is possible only if the motor slip speed satisfies the condition stated in equation (1.41) at all time [5][7][8][38].

$$\omega_{sl} = \frac{r_r i_{qr}^{e}}{\lambda_{dr}^{e}} = \frac{L_m}{\hat{\lambda}_r}\frac{r_r}{L_r} i_{qs}^{e} = \frac{L_m}{\hat{\lambda}_r}\frac{1}{T_r} i_{qs}^{e} = K_s i_{qs}^{e} \tag{1.41}$$

where T_r is the rotor time constant and K_s is the slip gain.

In practice, the magnitude of rotor flux is adjusted by i_{ds}^{e}, and the orientation of the d-component to the rotor field is maintained by keeping

the slip speed in accordance with equation (1.41). Therefore, if the IM is operated at constant flux (which is the case considered in this thesis), the accuracy of the slip speed will rely on that of the rotor time constant or slip gain.

1.3.3. Rotor Flux Position

So far it was shown that the resolution of stator currents requires the rotor flux position. In IMs, the rotor position is not, by definition, equal to the rotor flux position. It is for this reason that rotor flux position cannot be detected directly by mechanical speed sensors (or position encoders) provided with the IM. There are 2 basic approaches to determine rotor flux position: direct method or Direct FOC (DFOC) and indirect method or Indirect FOC (IFOC).

In DFOC methods, the rotor flux position is obtained directly from measurements using field angle or Hall sensors. The sensors are embedded in the stator in close proximity of the air-gap. In IFOC schemes the rotor position (or speed) is first measured and then the slip relation described in (1.41) is used to compute for the rotor flux position relative to the rotor axis. The use of field angle or Hall sensors (which increases the drive cost) and their sensitivity to temperature and mechanical vibrations (especially at low-speeds) have favoured IFOC schemes for many industrial applications [6].

By using the slip speed value given in equation (1.41) and the measured rotor speed (ω_r), rotor flux position can be calculated as:

$$\theta_e(t) = \int_0^t \omega_{sl} dt + \int_0^t \omega_r dt = \int_0^t \omega_{sl}\, dt + \theta_r(t) \tag{1.42}$$

where θ_r is the rotor position, derived from the measured rotor speed. In literature, the process of finding rotor flux position using the calculated

slip speed and measured rotor speed is referred to as *Current Model Method*. This process uses i_{ds}^{e}, i_{qs}^{e}, and ω_r to generate rotor flux position as follows.

Since it is often convenient to express machine parameters and variables in per-unit quantities, the rotor flux position is also often written in per-unit as follows. In transient operation case, i_{ds}^{e} can be defined as [38]:

$$i_{ds}^{e} = \frac{L_r}{r_r L_m}\frac{d\lambda_{dr}^{e}}{dt} + \frac{\lambda_{dr}^{e}}{L_m} \tag{1.43}$$

By defining $i_m = \lambda_{dr}^{e}/L_m$ as the magnetizing current, equation (1.43) becomes

$$i_{ds}^{e} = T_r \frac{d}{dt} i_m + i_m \tag{1.44}$$

By using the base supply frequency ($\omega_b = \omega_s = 2\pi f_s$) and manipulating equations (1.41), (1.42), and (1.44), the rotor flux frequency (ω_e) can be written as [38]:

$$\omega_e = \omega_r + \frac{i_{qs}^{e}}{T_r i_m \omega_b} \tag{1.45}$$

Equation (1.45) indicates that the Current Model outputs the rotor flux speed, which in turn needs to be integrated to obtain the rotor flux position. It should also be noted that the rotor time constant (T_r) is the most critical parameter to correct functionality of this model. The effect of T_r on the performance of the drive is investigated in chapter 3.

1.3.4. Indirect FOC IM Drive

Figure 1-8 shows the implementation diagram of the investigated IFOC IM drive based on rotor flux linkage. Two stator currents feed the Clarke Transformation block to generate stator currents ($i_{\alpha s}$ & $i_{\beta s}$) in orthogonal reference frame. These currents provide inputs to the Park

Transformation in order to obtain i_{ds} & i_{qs}, in synchronous reference frame (the superscript "e" is omitted for simplicity). The Park Transformation outputs are compared with their respective references. The generated errors are processed through two PI controllers, the outputs of which are applied to the inverse of Park Transformation to produce voltages ($v_{\alpha s}$ & $v_{\beta s}$) in orthogonal reference frame as in equations (1.46) and (1.47). This transformation is necessary because the stator current and voltage of the IM can only be controlled by a static inverter in stationary reference frame.

$$v_{\alpha s} = v_{ds}^{*} cos\theta_e - v_{qs}^{*} sin\theta_e \tag{1.46}$$

$$v_{\beta s} = v_{ds}^{*} sin\theta_e + v_{qs}^{*} cos\theta_e \tag{1.47}$$

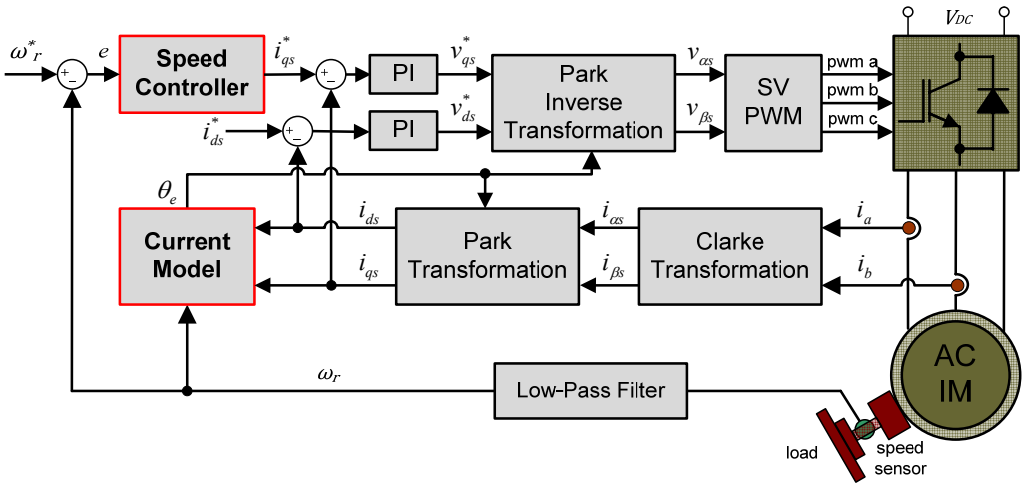

Figure 1-8: Configuration of the investigated IFOC IM drive with SVPWM

The voltage space vectors ($\bar{V}_r$) of these voltages are processed in the Space Vector PWM (SV-PWM) block to generate (six) gate signals that drive the 3-phase inverter. The choice of SV technique is justified by the fact that it generates minimum harmonic distortion of the currents in the winding

of 3-phase AC machine. It also provides an efficient use of the supply voltage in comparison with sinusoidal modulation techniques [36].

The mechanical speed of the motor in the investigated drive is measured by a speed sensor and processed through a Low-Pass Filter to reduce noises. The speed error is processed through a speed (torque) controller to generate the torque component current command (i_{qs}^{*}). The flux component current command (i_{ds}^{*}) is estimated between 40 and 60% of the nominal motor current; for operations below rated speed [38].

Note that both the Park and Clarke Transformations require an accurate value of rotor flux position, given by the current model. Therefore accurate knowledge of the motor slip gain (K_s) in real time is essential to achieve the highest possible efficiency from the control structure. As it is discussed in chapter 3, the accuracy of many available online slip gain estimation methods relies on other offline IM parameters. Besides, it is also important to have the best offline parameters for conventional control design. The process by which these parameters are estimated is referred to as Self-Commissioning.

1.3.5. Self-Commissioning for IFOC IM Drives

It is possible to identify the motor's parameters (offline) through standard no-load and locked-rotor tests with a 50Hz or 60Hz supply [34]. The lack of accuracy with this standard approach has been overcome by many other sophisticated schemes [40][41]. The study of these methods are beyond the scope of this thesis since the proposed drive topology (in Chapter 4) is designed to have less sensitivity to the accuracy of the motor's parameters. Under significant detuned conditions, the drive is designed to self-adjust its gains according to the current trend of the system. Therefore, the standard approach to self-commissioning is

sufficient if the parameters of the IM are not reported in its Nameplate or provided by the manufacturer.

The IM used in this thesis (as shown in Figure 1-8) is a 3-phase Δ-connected squirrel-cage type. Its rated parameters were measured experimentally using the standard self-commissioning approach described in [34]. The motor inertia is calculated according to the procedure described in [40]. Table 1-1 summarizes the investigated IM rated parameters, where $L_s = L_{ls} + L_m$.

Table 1-1: Nominal Parameters of the Investigated IM

Parameter	Symbol	Value	Unit
Voltage	V	230	V
Line current	I_{LL}	5.76	A
Output power	P_{out}	2.0	HP
Frequency	f	60	Hz
Rotor speed	n_r	1750	rpm
Stator resistance	r_s	3.35	Ω
Rotor resistance	r_r	3.06	Ω
Stator leakage inductance	L_s	21.6	mH
Rotor leakage inductance	L_r	21.6	mH
Magnetizing reactance	L_m	291	mH
Motor inertia	J	0.001	kgm^2
Number of poles	P	4	-

1.4. Conclusions

This chapter has clearly pointed out and summarised (in Figure 1-8) the two issues of IFOC drives investigated in this thesis: (1) the Current Model block design for the estimation of rotor flux position, and (2) the Speed Controller block design for tight control of speed/torque. As previously stated, the accuracy of the Current Model block relies on that

of the slip gain (or rotor time constant). If the system's parameters are subjected to changes during its normal operation, which is normally the case, the effects of mismatch between the instrumented and the actual slip gain in the drive can significantly affect the dynamics of the overall drive system. For high-performance applications, various methods have been proposed to reduce this sensitivity of the drive to detuned slip gain. This problem is addressed in chapter 3, along with the proposed scheme to estimate the slip gain in the entire torque-speed plane.

In many applications, the speed and/or the torque of the motor are required to change during the drive operation. The accuracy and robustness of the speed control are of high interest in high-performance drives. Chapter 4 shows that conventional approaches to close-loop speed/torque control with IFOC IM drives are insufficient for such applications. They heavily rely on the (accuracy of) motor parameters and are designed under a pre-defined operating (nominal) condition of the drive. If the drive is operated at conditions very different than the ones used during the controller design, the system responses often experience significant steady-state and dynamic changes. The parameters that affect the speed/torque control of an IFOC IM drive are discussed in chapter 4; along with the proposed method of designing a good FL controller to deal with the system disturbances and operating changes.

Chapter 2

Fuzzy Logic System and Control

Outlined by L.A. Zadeh in the 1960's, the basic framework of Fuzzy Logic (FL) systems was established by E.H. Mamdani in the 1970's to control a steam engine. The success of Mamdani's application made Fuzzy Logic Controller (FLC) one of the most fruitful areas of fuzzy systems [42][43][44]. As a result, in the 1980's Japanese engineers applied the theory of FL in many applications, where conventional control could not be used easily due to the complexity of mathematical models. Among such applications, Hitachi developed the most advanced FLC for the Sundai Subway [42].

From the early 1990's, many companies began to offer large numbers of consumer-oriented products enhanced by FLCs [42][43][45]; including in the area of high-performance AC drives [20]–[27][30]–[33][46]. Ever since, the literature on FLC has been growing rapidly; making it very difficult to present a comprehensive survey of the wide variety of applications that have been made. A more detailed discussion on some of the industrial advances of FLC may be found in [42][44][45][47][48]. The current chapter is restricted to the concepts and theories of FLCs used in this thesis.

It is evident, based on the literature, that FLCs pointed a way for effective use of FL systems in the context of complex and ill-defined systems. Such systems are common in practice. They are generally time-variant, with delays and nonlinearities, and often with poorly defined or unknown dynamics. They are difficult to describe with analytical (or quantitative) models, and unlikely to be efficiently controlled by conventional model-based techniques. To overcome this challenge, conventional techniques

tend to simplify the model of the process at the expense of the performance response. FLC offers a different approach to this problem. The current chapter is designed to describe the approach used in FLCs to overcome some of the limitations encountered with conventional techniques in the area of control system.

Many nonlinear and complex systems can be controlled successfully by skilled human operators without the full knowledge of their underlying dynamics [49]. FL, which is the logic on which FLC is based, is much closer to human reasoning and natural language than conventional logical techniques [45]. It provides an effective means of capturing the approximate or inexact nature of the real world. Viewed in this context, the fundamental of FLC is a set of linguistic control rules related by the dual concepts of fuzzy implication and the compositional rule of inference. In other words, FLC provides an algorithm capable of converting linguistic control strategies of a skilled operator (or expert knowledge) into automatic control strategies [42][45]. The control statements are captured in the form of fuzzy rules or fuzzy propositions:

IF (*process state* or p*remise*) THEN (*control action* or c*onsequent*) (2.1)

Expression (2.1) indicates that a fuzzy rule can be considered as an "IF-THEN" statement that defines the set of facts that must be true (the premise) before a set of actions (the consequent) can be executed. The premise and the consequent parts of a fuzzy rule are called *Fuzzy Propositions*.

The way an FLC performs the conversion from linguistic control strategies into control actions is the object of this chapter. In order to understand this mechanism, the concept of fuzzy system is first outlined and compared with that of conventional control system to point out some

fundamental differences between the two approaches. Next, some of the most commonly used concepts of FL are enlighten to help introduce each component of an FLC. Finally, all the components of a standard FLC are described and explained using a simple and generic close-loop speed control system problem.

2.1. Conventional and Fuzzy Sets

In conventional Boolean theory the degree to which an object or a variable is a member of a set is either 0 (False) or 1 (True). For example, a motor speed is *fast* if it is driven above 1000rpm, and it is *slow* if it is below or at 1000rpm. This is illustrated in Figure 2-1.a.

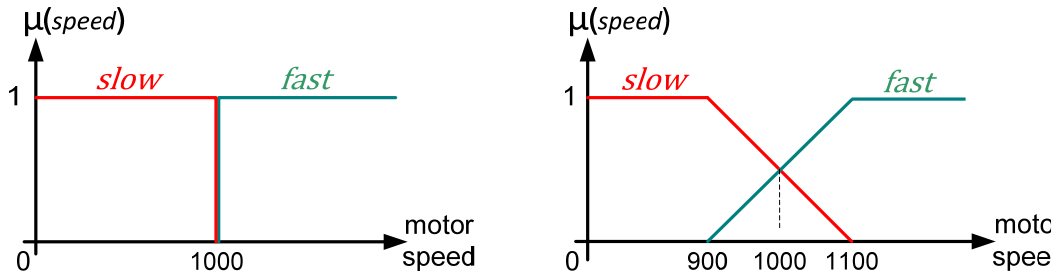

Figure 2-1: Membership Functions of: (a) conventional (crisp) sets, and (b) fuzzy sets

Human reasoning does not necessarily follow this crisp "True-False" logic (shown Figure 2-1.a). Human reasoning is often vague, qualitative (as opposed to quantitative), or fuzzy in nature. That is why in fuzzy sets, variables are assigned partial membership sets or degrees of membership. The degree to which a variable is a member of a fuzzy set can vary between 0 and 1; where 0 means "Completely False" and 1 means "Completely True". A fuzzy set allows a gradual transition from full-membership (Completely True) to zero-membership (Completely

False) and vice versa. Using this approach and Figure 2-1.b, a motor speed of 1000rpm is a member of a fuzzy set "*fast*" to degree 0.5 (i.e. 50%) and a member of "*slow*" to the same degree. A speed of 1050rpm is "*fast*" to degree 0.75 and "*slow*" to degree 0.25.

In the above example, the variable *speed* has been assigned two *Linguistic Terms* (*slow* & *fast*). The number of linguistic terms a variable can have in an FLC will be discussed later.

Following Figure 2-1, a fuzzy set can now be defined as follows. Let U be a set, called the *Universe of Discourse* and u be a generic element of U ($u \in U$). A fuzzy set A in a universe of discourse U is a function that maps U into the interval [0, 1]. The fuzzy set A is characterized by a membership function (MF) $\mu_A(x)$ that takes values in the interval [0, 1].

2.1.1. Linguistic Variables and Values

Words are constantly used to describe variables in human's daily life. Similarly, words are used in fuzzy rules to formulate control strategies. Referring to the above example, words like "motor speed is fast" can be used to describe the state of a system (in the current case, it is the state of the motor). In this example, the words "*slow*" and "*fast*" are used to describe the variable "speed". This means that the words "*slow*" and "*fast*" are the Values of the fuzzy variable "speed". Note that the variable "speed" in its turn, can also take crisp values, such as 1000rpm, 300.67rpm, 0rpm, etc.

If a variable is assigned some crisp values, then it can be formulated by a well established mathematical framework. When a variable takes words as its values instead of crisp values, there is no formal framework to formulate it in the classical mathematical theory. The concepts of Linguistic Variable and Value were introduced to provide such a formal

framework. According to these concepts, if a variable can take words in natural languages as its values, then that variable is called *Linguistic Variable*. The words that describe the value of that linguistic variable are defined by fuzzy sets in the universe of discourse in which the variable is defined [42]. These words are called *Linguistic Values*.

In general a linguistic variable is characterized by (1) a name, (2) a term, and (3) a universe of discourse. For example, in Figure 2-1.b, the variable "speed" is a linguistic variable with 2 linguistic values, namely "*slow*" and "*fast*". The variable "speed" can be characterized in the universe of discourse U = [-2000rpm, +2000rpm], corresponding to minimum and maximum speeds of the motor used, respectively. The linguistic values "*slow*" and "*fast*" can be characterized by the fussy sets described in Figure 2-1.b or by any other set (depending on the application and the designer's choice).

These definitions show that linguistic variables are the necessary tools to formulate vague (ill-defined) descriptions in natural languages in accurate mathematical terms. They constitute the first step to incorporate human knowledge into engineering systems in a systematic and efficient manner [50].

2.1.2. Membership Functions (MFs)

There are many other choices or shapes of MFs besides the ones described in Figure 2-1. A graphical illustration of typical and commonly used ones in literature is shown in Figure 2-2 [44].

The simplest and most commonly used MFs are the triangular types due to their simplicity and computation efficiency [44]. A singleton is a special type of MF that has a value of 1 at one point on the universe of

discourse and zero elsewhere. The L-function and sigmoid types are mainly used to represent saturation of variables.

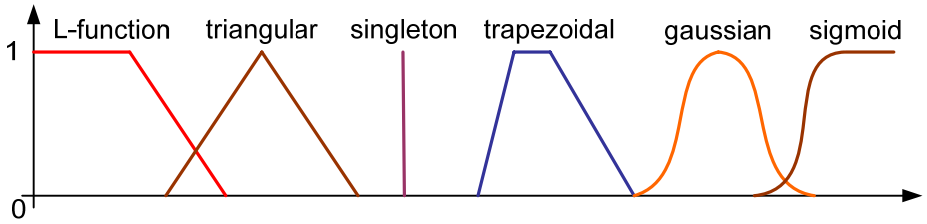

Figure 2-2: Typical shapes of MFs

2.1.3. Fuzzy Rules and Fuzzy Implication

Depending on the number of linguistic variables used, there are 2 types of fuzzy propositions (for premises and/or for consequents): atomic and compound propositions. An atomic proposition is a single statement, such as "motor speed is *fast*". A compound fuzzy proposition is a composition of atomic propositions using the connectives "AND", "OR", or "NOT". They are used as follows.

Consider a system with 2 linguistic variables x and y. If x represents the "motor speed" in the universe of discourse U and y the "motor acceleration" in the universe of discourse V, the following are some (not all) of the possible compound fuzzy propositions that can be defined in the universe of discourse (U x V):

speed is *slow* AND acceleration is *fast* (2.2)

speed is *fast* OR acceleration is *fast* (2.3)

speed is NOT *fast* AND acceleration is *slow* (2.4)

speed is *slow* OR acceleration is NOT *slow* (2.5)

Regardless of the type of rule used, the main problem is how to interpret the meaning of the "IF-THEN" statement in order to determine the influence of the premise over the consequence. The procedure for assessing this influence is called *Fuzzy Implication*. Since fuzzy propositions and relations are expressed by MFs, fuzzy implications also imply MFs as a method of interpretation.

In literature there are many ways of defining a fuzzy implication [42][47][51][52][53]:

(1) Zadeh implication,
(2) Mamdani implication,
(3) Godel, implication,
(4) Lukasiewicz implication,
(5) Dienes-Rescher implication,
(6) Larsen implication, etc.

The differences between these methods are summarized in [52][53]. Their mathematical functions indicate that the Mamdani implication is the most suitable for hardware implementation [44][52]. It is also the most commonly used in control system applications and the technique used in this thesis (unless otherwise specified). The choice for the Mamdani implication for this thesis is also strongly supported by the argument that fuzzy rules are local [42]. The rules used in this thesis, as it will be seen in chapters 3 & 4, are strictly local (as oppose to global fuzzy rules). The graphical illustration of the Mamdani implication is provided in following section.

2.2. Fuzzy Logic Controller (FLC)

They are three types of fuzzy systems [42]:

(1) Pure fuzzy systems,

(2) Takagi-Sugeno-Kang (TSK), and

(3) Mamdani or Fuzzifier-Defuzzifier system.

A Pure fuzzy system is a collection of "IF-THEN" rules that relate the input(s) and the output(s) of a system. A fuzzy *Inference Engine* combines the rules into a mapping from fuzzy sets in the input space to fuzzy sets in the output space based on FL principles. The disadvantage of pure fuzzy systems is that its input(s) and output(s) are fuzzy sets. This is a problem because in most engineering systems, the input(s) and output(s) are real or crisp values. To deal with the limitation of Pure fuzzy systems, the TSK structure was introduced in the 1980's [54][55]. The TSK system can be described as follows.

Let x be an input variable and y an output variable of a system, both defined in various universes of discourse. Rather than using fuzzy rules in the form shown of expression (2.1), TSK systems use the form:

$$\text{IF } \{x \text{ is } A\}, \text{ THEN } \{y = f(x)\} \tag{2.6}$$

where A is the input linguistic value and $f(x)$ is usually a polynomial of the input variable (but can be any function that accurately describes the output of the system within the fuzzy region specified by the premise of the rule). When $f(x)$ is a constant, the system is called *zero-order TSK*, where each fuzzy rule's consequent is specified by a singleton MF. This type of TSK FLC is utilized in the proposed slip gain online estimation scheme (in chapter 3) and in the self-tuning mechanism of the proposed STFC (in chapter 4).

The problem with TSK systems is that the consequent part of the rule is a mathematical formula. This may not provide a natural framework to represent human knowledge. In order to solve this problem, as well as the problem related to Pure fuzzy systems, the Mamdani system, also

known as standard FLC, was introduced [56]. Its basic architecture is described in Figure 2-3. It consists of:

(1) Fuzzification interface,
(2) Rule base,
(3) Inference Engine, and
(4) Defuzzification interface.

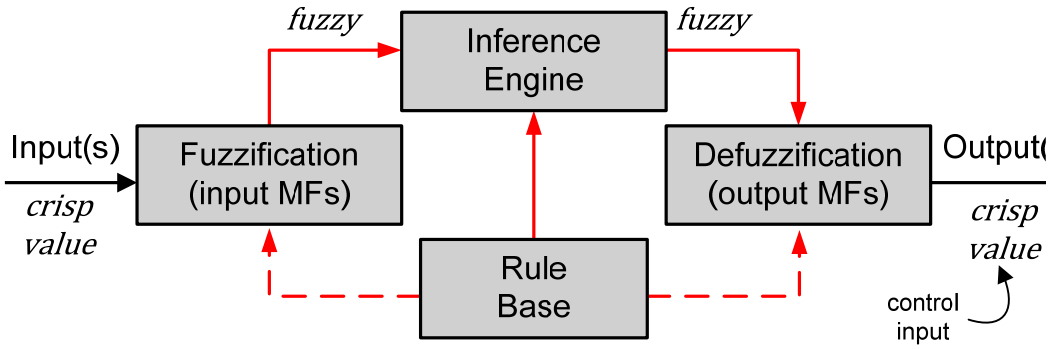

Figure 2-3: Bloc diagram of a standard (conventional or non-adaptive) FLC

The components of this FLC will be introduced by using a generic close-loop speed control problem.

Most closed-loop speed control systems react to the error ($e(t)$) between the reference speed and the output speed of the motor. When controlling processes, human operators usually compare the actual output of the system with the desired (reference) output and observe the evolution of this difference [44][46]. This is why in most FLCs, including the controllers proposed in this thesis (in chapters 3 & 4), the input variables are the system error, $e(t)$, and the change-in-error, $ce(t)$.

To complete the initial description of the investigated generic close-loop speed control, let $u(t)$ be the FLC output variable, i.e. the process input

signal. For simplicity, the input and output variables in this problem are defined by their per unit (or base) values. Hence, their universes of discourse are confined in [0, 1] interval.

2.2.1. Fuzzification Interface

Human operators often reason in terms of qualitative values (such as, small, big, high, low, tall, short, medium, etc.); rather than using quantitative values (such as 10lbs, 6feet, 23kg, etc.). The conversion from quantitative to qualitative values in FLC is referred to as *Fuzzification*. Hence, the Fuzzification interface

(1) Measures the values of the input variables ($e(t)$ & $ce(t)$ for the investigated example),
(2) Performs a scale mapping of the measured crisp values of the input variables ($e(t)$ & $ce(t)$) into the universes of discourse of these input variables, and
(3) Converts the input values into linguistic values compatible with the fuzzy set representation in the rule base.

The three operations are performed as follows. Just as ($e(t)$ and/or $ce(t)$ take on values of, for example 0.2p.u at time instant t, linguistic variables also assume linguistic values at every time instant t. The values that linguistic variables take on over time change dynamically. Let's suppose, for the investigated example, that $e(t)$, $ce(t)$, and $u(t)$ take on the following values: "Negative Big" or NB, "Negative Small" or NS, "Zero" or ZE, "Positive Small" or PS, and "Positive Big" or PB. The meanings of these linguistic values are quantified by their respective MFs. For close-loop speed control, each of the following statement quantifies different (not all) configurations of the system:

- The statement "$e(t)$ *is PB*" can represent the situation where the output speed is significantly smaller than its reference.

- The statement "$e(t)$ *is NS*" can represent the situation where the output speed is just slightly above the reference, but not too close to it to justify quantifying it as ZE and not too far to justify quantifying it as NB.
- The statement "$e(t)$ *is PB*" and "$ce(t)$ *is PS*" can represent the situation where the speed is significantly below the reference, but since "$ce(t)$ *is PS*", the motor speed is moving away from its reference value.

These statements indicate that in order to successfully quantify or "fuzzify" the dynamics of a process, one must first have a good understanding of the physics of the underlying process. Furthermore, the accuracy of the FLC relies on (1) the number, (2) the shape(s), and (3) the distribution of linguistic values or MFs used. These parameters are usually set according to the designer's choice.

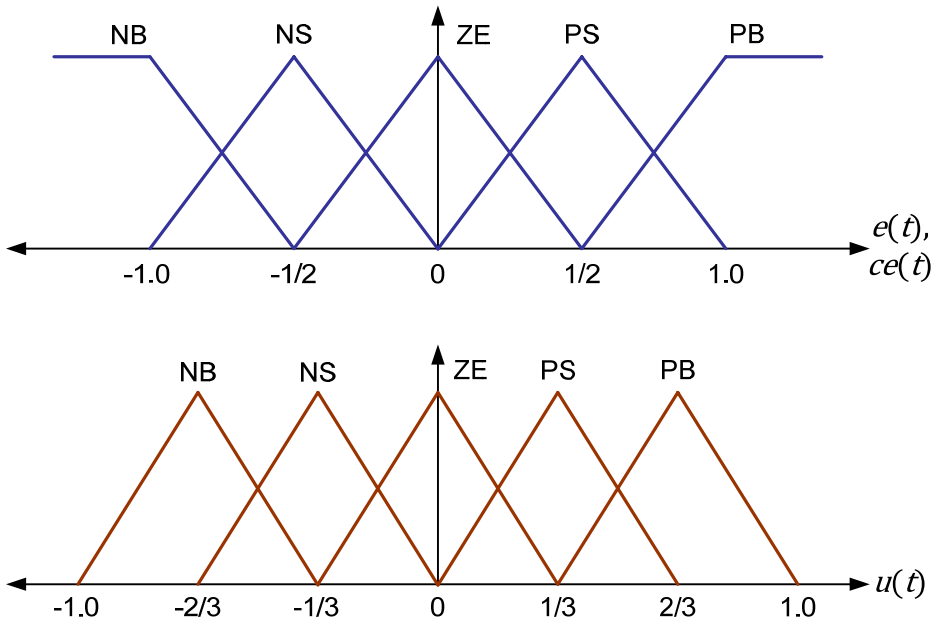

Figure 2-4: Input and output MFs of the closed-loop speed control system

The analysis of the MFs conducted in chapter 4 will show that it is possible to select these parameters according to some quantitative approaches. However for simplicity and illustration purpose, triangular MFs are considered in the current example. Their distributions, number and shapes for the input and output variables are shown in Figure 2-4 (keeping in mind that the output MFs are not part of fuzzification process).

The MFs (in Figure 2-4) are selected such that the input MFs at the outer edges saturate at values of 1 and -1, characterized by L-function MFs. Saturation makes intuitive sense as at some point the human expert would group all larger or lower values together in a common linguistic description characterizing “greater than” (for the right side) or “less than” (for the left side) [44]. For the output, the MFs at the outermost edges should not saturate for the FLC to be properly defined. This is because in decision-making processes, one seeks to take actions that specify an *exact value* (as opposite to “any value greater than” or “any value less than”) for the process input. This completes the first step of FLCs according to Figure 2-3.

2.2.2. Rule Base

While differential equations are the language of conventional control, in FLCs the dynamic behaviour of a system is characterized by a set of linguistic descriptions in terms of fuzzy rules in the form described in (2.1). Fuzzy rules serve to describe the quantitative relationship between the input and the output variables in linguistic terms such that, instead of developing a mathematical model that describes a system, a knowledge-based system is used.

In general, fuzzy rules have the following form (for a single output system):

$$Ru^{(l)}: \text{IF } \{x_1 \text{ is } A_1{}^l \text{ AND } \ldots \text{ AND } x_n \text{ is } A_n{}^l\} \text{ THEN } \{y \text{ is } B^l\} \quad (2.7)$$

where A_i^l, and B^l are the input and output fuzzy sets (with their respective linguistic values) defined in universes of discourse U_i and V, respectively, $x = [x_1, x_2, \ldots, x_n]^T$ and y are the input and output linguistic variables, respectively. If M is the number of rules in the rule base and n is the number of input variables, then $l = 1, 2, \ldots, M$ and $i = 1, 2, \ldots, n$.

It can be seen from (2.7) that several linguistic variables might be involved in the premise and consequent parts of a rule. The number of input and output variables places an upper limit on the number of elements in the premises and consequents. Since there is a finite number of linguistic variables and values, there is also a finite number of possible rules in a rule base. The FLCs designed in this thesis are limited to two input and one output linguistic variables.

There are four methods used to construct fuzzy rules [57]:

(1) Control engineering knowledge,
(2) Modelling the operator's behaviour,
(3) Fuzzy modeling of a process, and
(4) Self-learning fuzzy controller.

Methods (1) & (2) are known as *Heuristic* methods, whereas methods (3) & (4) are *Deterministic* methods [49]. Heuristic and Deterministic methods have been introduced and used by Mamdani and Takagi & Sugeno, respectively [45].

Heuristic methods are commonly used in control systems since they are based on engineering skills and experience instead of process information [49]. Among the various heuristic approaches, the so-called *Phase-Plane Trajectory* approach, introduced by [58], is the most attractive for close-loop control systems. With the Phase-Plane approach,

the rule justification is based on a generic close-loop system trajectory in phase plane. The principle of global rule modification in symmetry and monotonicity is also applied. A complete investigation of the approach is available in chapter 4.

Regardless of the method used to build the rule base, the relationship among the rules imposes interesting questions, such as: (1) Do the rules cover all the possible situations that the system may face? (2) Are there any conflicts among the rules?, etc. To answer these questions, the properties of completeness, consistence, and continuity have been introduced [42][45]:

- A set of fuzzy rules is *complete* if at any point in the input space there is at least one active rule; i.e. if the MF value of the premise part of the rule at this point is non-zero.
- A set of fuzzy rules is *consistent* if there are no rules with similar premise parts but different consequent parts.
- A set of fuzzy rules is *continuous* if it does not have neighbouring rules with consequent parts that have empty intersections. In other words, continuity means that the input-output behaviour of the fuzzy system should be smooth.

The rule bases designed in this thesis incorporated these three properties.

2.2.3. Inference Engine

The function of the inference engine is to compute for the overall value of the fuzzy control output based on individual contributions of each rule in the rule base. The inference engine is the decision-making logic of an FLC. It has the capability of simulating human decision-making based on fuzzy concepts and inferring fuzzy control actions using fuzzy implication

and the rule of inference in FL. Fuzzy inference is performed in two steps [44]:

(i) The premises of all the rules are compared with the controller inputs to determine which rules apply to the current situation. The rules that are involved in the current situation are referred to as *Active Rules*.

(ii) The conclusions (i.e. what control actions to take) are then determined using only the Active Rules. All other "inactive" rules do not take part in this step.

The conclusions reached in the second step are characterized by a fuzzy set (or a set of fuzzy sets), in the case of a Mamdani FLC. When a TSK FLC is used, these conclusions are characterized by a set of crisp values. Regardless of the FLC structure used, the conclusions must represent the certainty that the input of the process should take on various values. The inference engine mechanism is best explained in the following illustration:

Let's assume that at time instant t, the error $e(t) = 0.0\text{p.u.}$ and its change $ce(t) = 0.35\text{p.u.}$. Using the MFs described in Figure 2-4 for the investigated motor speed control example, Figure 2-5 shows the location or values of the variables $e(t)$ and $ce(t)$at the current time instant t. As it can be seen, there is only one MF involved for variable ($e(t)$) and the value of this variable at time instant t is $\mu_{ZE}[e(t)] = 1$. For variable $ce(t)$, its values at time instant t are $\mu_{ZE}[ce(t)] = 0.25$ and $\mu_{PS}[ce(t)] = 0.75$. This implies that there must be a total of two rules involved or two Active Rules at the current time instant t.

In general there is a different premise MF for each rule in the rule base, and each is a function of the input variables. So, given some specific values of input variables, a quantification of the certainty that each rule applies to the current situation is obtained. This is done as follows. The

inference engine checks the input MFs involved at time instant t. With the knowledge of the number of input MFs involved, it creates the premises and uses the corresponding fuzzy rule in the rule base to assign consequents to each premise. Only the Active Rules at time instant t are used in the output of the FLC. Thanks to the property of completeness, at any point in the input space there will be at least one Active Rule that represents the current condition of the system.

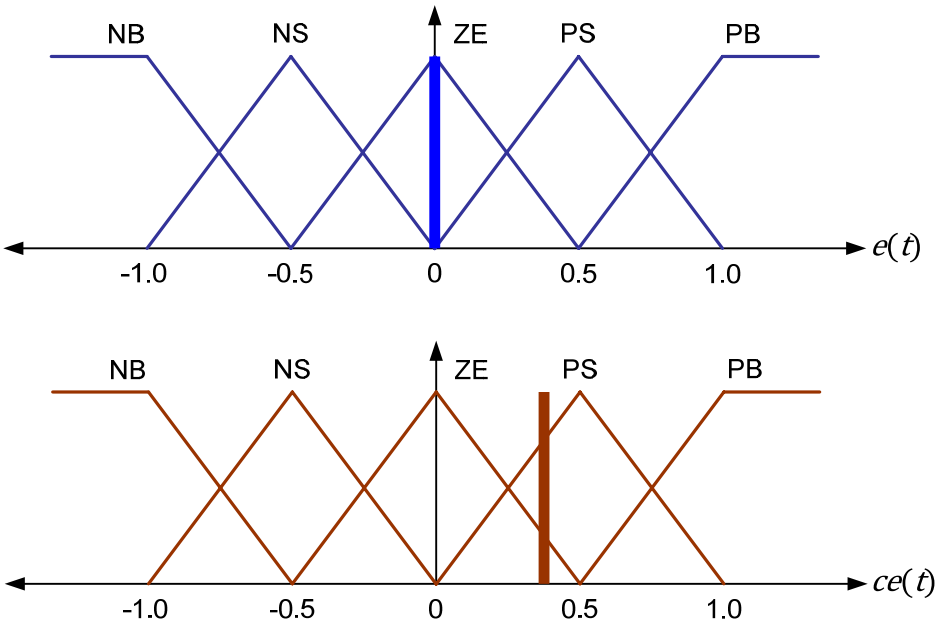

Figure 2-5: Input MFs with input values at time instant t

To complete the first step of fuzzy inference, let's assume that the Phase-Plane approach was used to formulate the rules, at time instant t the following rules may be fired from the rule base, according to Figure 2-5 (Other types of rules are possible depending on how the rule base has been formulated):

IF {$e(t)$ is ZE **and** $ce(t)$ is ZE} THEN {$u(t)$ is ZE} (2.8)

IF {$e(t)$ is ZE **and** $ce(t)$ is PS} THEN {$u(t)$ is PS} (2.9)

To perform the inference mechanism each Active Rule in the rule base must be quantified. First, the meaning of each premise is quantified by using the corresponding premise's MFs. This is illustrated in Figure 2-6.

Note that in Figure 2-6, the two terms of the premises of rules (2.8) & (2.9) are listed and quantified. At this stage, the main items of focus are how to quantify the fuzzy logical "and" operation that combines the meaning of two linguistic terms, and how to determine the conclusion that best represent the current state of the system based on the two Active Rules. The following explains how these two problems are solved.

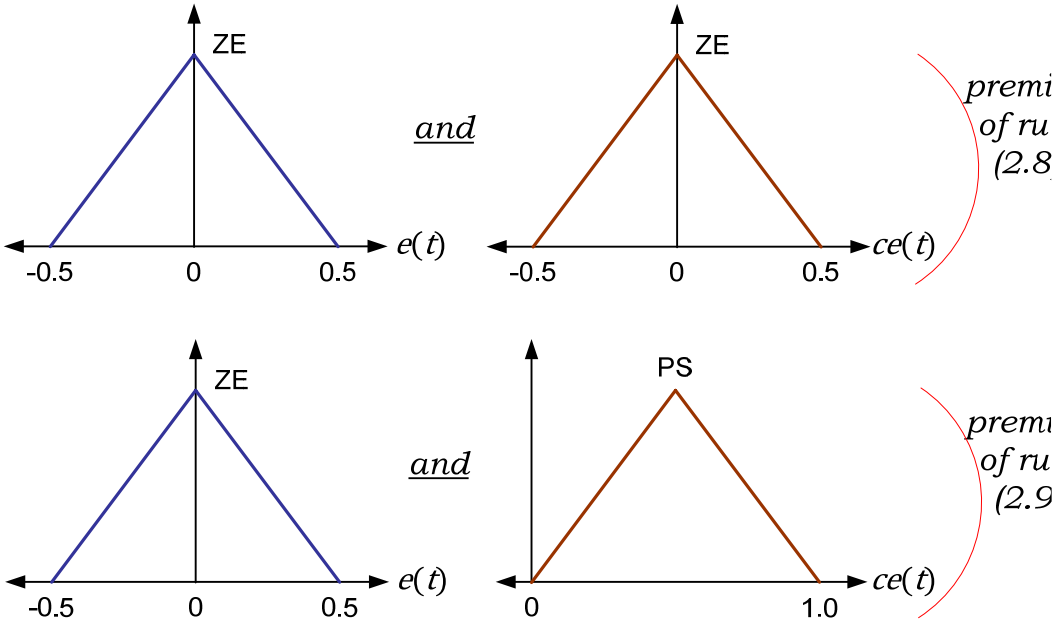

Figure 2-6: MFs of premise terms at time instant *t*

In order to quantify the fuzzy logical "and", all Active Rules must be considered independently. They will be combined later to compute for the overall value (aggregation function) of the fuzzy output at time instant *t*. This step is accomplished by using one of the implication methods

outlines previously. Using the Mamdani implication and the premises of rules (2.8) and (2.9), we get:

$$\mu_{premise_{(1)}} = min\{1.0, \quad 0.25\} = 0.25 \tag{2.10}$$

$$\mu_{premise_{(2)}} = min\{1.0, \quad 0.75\} = 0.75 \tag{2.11}$$

The MFs for the conclusions reached by rules (2.8) and (2.9) are shown in Figure 2-7, using the implication values obtained in (2.10) and (2.11).

As it can be noted, while the input to the inference mechanism is a set of Active Rules, its output is a set of implied fuzzy sets that represent conclusions reach by all the Active Rules. These conclusions are summarized in the aggregation MF shown at the bottom of Figure 2-7.

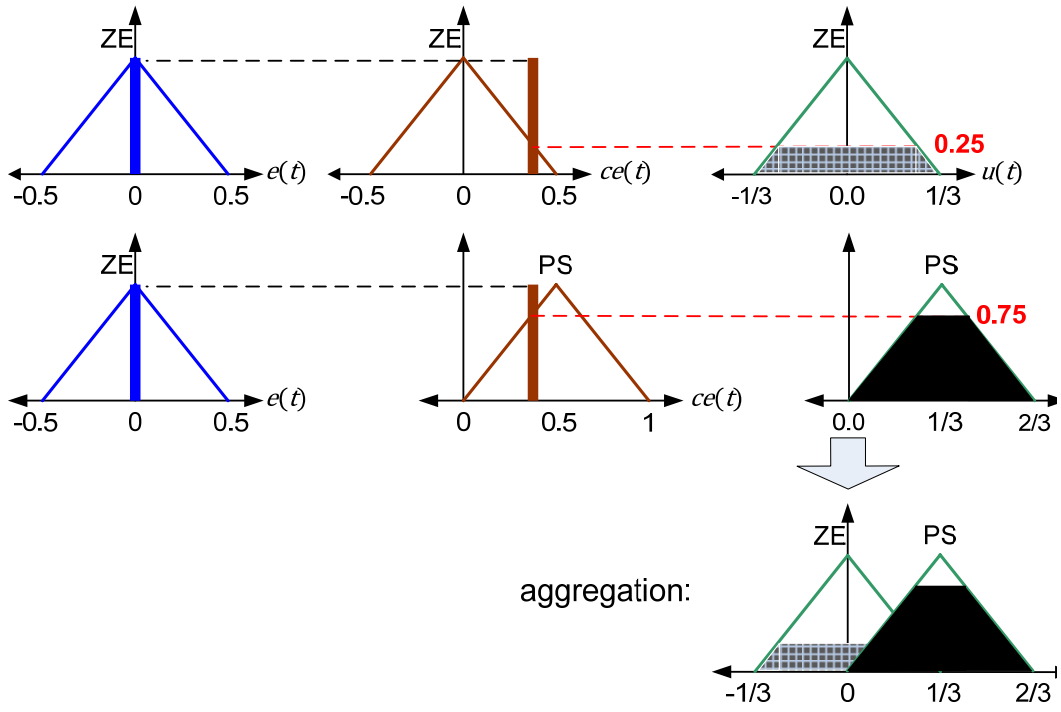

Figure 2-7: Graphical representation of FLC operation with two active rules

Figure 2-7 illustrates the case of two active fuzzy rules of a 2-inputs 1-output system. The maximum number of active rules in such systems is four if all three properties of the rule base are respected. If the number of input/output variables is increased, or if the (three) properties of the rule base are not respected, there may be cases with more than or less than four Active Rules. Clearly, if the number of Active Rules exceeds four (in the case of 2-inputs 1-output system), there will be some conflicting rules in the rule base. This is not recommended.

2.2.4. Defuzzification Inference

The result of implication and aggregation steps in the inference engine is a fuzzy output set. The latter is the union of the outputs of all Active (individual fuzzy) Rules. The conversion of this fuzzy output set to a single crisp value (or a set of crisp values) is referred to as *Defuzzification*. Hence, the Defuzzification interface performs a mapping from a fuzzy set u^{fuzzy} (the output of the inference engine or the aggregation function) to a crisp output u^{crisp}.

There are many approaches to defuzzification [42][44][59]:

(1) *Center of Gravity* (COG),
(2) *Center-Average* (CAV),
(3) *Maximum Criterion*, and
(4) *Mean of Maximum* (including *First of Maxima*, *Last of Maxima*, and *Center of Maxima* methods).

There are three criteria used in choosing a defuzzification method [42]:

(1) Plausibility,
(2) Continuity
(3) Computation efficiency, and

The plausibility criterion means that the value u^{crisp} should represent u^{fuzzy} from an intuitive point of view. Continuity means that a small change in u^{fuzzy} should not result in a large change in u^{crisp}. The computation criterion is particularly important for real time applications.

The literature shows that the COG and CAV methods are the most commonly used in control systems due to their intuitive plausibility [42][44]. The disadvantage of the COG method (with respect to the CAV) is its computation burden. The MFs of the aggregation function are usually irregular (contrary to MFs shown in Figure 2-7). This irregularity makes the computation very difficult since the COG method uses integral to compute for the crisp value. If the output variable is described by regular and symmetric MFs, the computation of the COG method can significantly be reduced [44].

Using COG and CAV methods, the output value u^{crisp} can be calculated as follows. Let b_i denote the center of the MF for the consequent of rule (i) and ω_i its height. The crisp value is computed as:

$$u_{COG}^{crisp} = \frac{\sum_i b_i \int \mu_{(i)}}{\sum_i \int \mu_{(i)}} \tag{2.12}$$

$$u_{CAV}^{crisp} = \frac{\sum_i b_i w_i}{\sum_i w_i} \tag{2.13}$$

While at first glance it may not appear so, but the integral in (2.12) is easy to compute for the case where the output variable have symmetric triangular MFs (as in the current example). Such MFs have peaks at one and base width of W. Simple geometry can be used to show that the area under a triangle "chopped off" (see Fig. 2.7) at a height of h is equal to

$$AREA = W\left(h - \frac{h^2}{2}\right) \tag{2.14}$$

Given this, the computation of (2.12) is not too significant any more. Using (2.12)-(2.14) and the aggregation function shown in Figure 2-7, we get

$$u_{COG}^{crisp} = \frac{(0)\left(\frac{2}{3}\left(0.25 - \frac{0.25^2}{2}\right)\right) + \left(\frac{1}{3}\right)\left(\frac{2}{3}\left(0.75 - \frac{0.75^2}{2}\right)\right)}{\frac{2}{3}\left(0.25 - \frac{0.25^2}{2}\right) + \frac{2}{3}\left(0.75 - \frac{0.75^2}{2}\right)} = 0.136 \tag{2.15}$$

$$u_{CAV}^{crisp} = \frac{(0)(0.25) + \left(\frac{1}{3}\right)(0.75)}{(0.25) + (0.75)} = 0.25 \tag{2.19}$$

Note that while both defuzzification methods provide reasonable command inputs to the plant (with respect to Figure 2-7), it is difficult to say which method is best without further investigations (such as simulations). This design flexibility actually extends to the general case and also arises in the specification of all the other components of the FLC. Some useful recommendations on the choices of defuzzification methods can also be found in [42][59].

2.3. Remarks

Over the past decades, the literature and experience have demonstrated the significant advantages of FLCs over conventional control approaches. Despite the success of FLCs over their counterpart conventional controllers, the design flexibility observed with FLC parameters is one of the clear indications that there are not too many guidelines or methods to calibrate the parameters of an FLC. These parameters include: input and output variables, MFs (types, shapes, number, distribution, etc.), inference method, Defuzzification methods, etc. The lack of systematic design guidelines is a result of a very strong coupling of parameters in an FLC. A change in one parameter can significantly affect the overall control system.

In order to overcome this limitation, a systematic design methodology, taking into account the coupling effect(s) of parameters, the engineering knowledge and experience, and the understanding of the system dynamics is required. Hence, a new method of designing standard FLC is introduced in this thesis and developed in chapter 4. The method is intended to reduce the design time by providing some useful guidelines on how each parameter of the controller should be calibrated. Simulation and experimental tests are provided to validate the approach. Finally, it should also be noted that the principles of FLC outlined in this chapter will also be used in the proposed slip gain online estimation method in chapter 3.

Chapter 3

Parameter Sensitivity and Adaptation

Practical temperature excursion of the rotor of a typical IM is about 130°C above ambient; corresponding to 50% increase of rotor resistance over its rated (ambient) value [8]. Magnetic saturation, on the other hand can reduce the motor self-inductance up to 80% [8]. These variations of rotor resistance and inductance correspond to approximately 33% change in rotor time constant or slip gain [8]. The slip gain (K_s) is function of rotor resistance (r_r), mutual inductance (L_m), and rotor self-inductance (L_r). Since the performance of an IFOC IM drive depends on the value of instrumented slip gain in the Current Model block (as seen in chapter 1), such variations can seriously affect its dynamics.

It is common to observe a mismatch between the instrumented (in the FOC) and actual K_s during normal operations of IFOC IM drives. This mismatch is commonly referred to as *detuned* IFOC. It is due to: (1) motor parameters changing with the operating conditions such as temperature rise and saturation or, (2) wrong instrumentation of the parameters in the vector controller [14]. The latter phenomenon is controllable through an online estimation of K_s. The former phenomenon is dependent on the operating conditions of the motor drive.

Detuned IFOC produces a coupling effect between the flux- and torque-producing channels in the IM. As a consequence [6][8]:

(1) The rotor flux linkages deviate from their reference values,
(2) The electromagnetic torque, hence deviate from its reference value, producing a nonlinear relationship between the actual torque and its reference value (making the drive unsuitable for high-

performance applications that require accurate control of torque, such as robotic), and

(3) An oscillation (from torque transients) is caused both in the rotor flux linkages and in the torque responses, with a settling time equal to that of the rotor time constant (on the order of 0.5sec or greater).

In torque controlled drives, effects (2) & (3) are very undesirable. In speed controlled drives, the nonlinear torque characteristic will not have a detrimental effect on the steady-state operation. Its effect is considered during transients. The load and the motor inertia are required to smooth these torque excursions so that they do not appear as speed ripples. This means that the type of IM drive that exhibits the highest sensitivity to incorrect parameter values is the torque drive. The existence of the speed controller in speed drives significantly reduces the negative consequence of the parameter detuning. Since the drive investigated in thesis has a close-loop speed controller, much attention is dedicated to the effects of mismatch for speed controlled IFOC IM drives.

In order to understand the requirement for online estimation of slip gain for high-performance IFOC IM drives, it is necessary to investigate the effects of detuned FOC on the steady-state and dynamic performances of the drive; using the model described in Figure 1-8. This is the primary goal of the current chapter.

The second goal of this chapter consists of describing the proposed slip gain online estimation scheme based on the principle of MRAS [17]. This scheme is designed to improve the performance of the drive under detuned conditions in the entire torque-speed plane. The estimation mechanism of the algorithm also relied on the principles of FLC, which were outlined in chapter 2. It will be shown that this approach is capable of updating the slip gain effectively with limited measured signals (stator

phase currents & voltages and rotor speed). No additional expensive sensors are required.

3.1. Parameter Sensitivity Analysis

Since variations of slip gain are very slow, their effects on the drive can be analyzed in steady-state. In this case, the IM rotor flux equations in synchronous reference frame can be written as [5][8]:

$$\lambda_{dr}^{e} = \frac{L_m r_r}{L_r}\left(i_{ds}^{e}\frac{r_r}{L_r} + \omega_{sl} i_{qs}^{e}\right)\Big/\left(\left(\frac{r_r}{L_r}\right)^2 + \omega_{sl}^2\right) \tag{3.1}$$

$$\lambda_{qr}^{e} = \frac{L_m r_r}{L_r}\left(i_{qs}^{e}\frac{r_r}{L_r} - \omega_{sl} i_{ds}^{e}\right)\Big/\left(\left(\frac{r_r}{L_r}\right)^2 + \omega_{sl}^2\right) \tag{3.2}$$

Equations (3.1) and (3.2) indicate that if the instrumented slip speed (given in (1.45)) is set using the actual motor parameters, then the rotor fluxes can be estimated according to equations (1.37) and (1.38) to obtain an *ideal* IFOC IM. However, if for example the rotor resistance is changed by a value corresponding to Δr_r, equations (3.1) and (3.2) become:

$$\lambda_{dr}^{e} = \lambda_r^{*} + \lambda_{dr}^{e} = \lambda_r^{*} + \frac{L_m (r_r/L_r) i_{qs}^{e} (\Delta r_r/r_r)\omega_{sl}}{(r_r/L_r)k_r^2 + \omega_{sl}^2} \tag{3.3}$$

$$\lambda_{qr}^{e} = \Delta\lambda_{qr}^{e} = \frac{L_m (r_r/L_r) i_{qs}^{e} k_r (\Delta r_r/r_r)}{(r_r/L_r)k_r^2 + \omega_{sl}^2} \tag{3.4}$$

where $k_r = (r_r + \Delta r_r)/r_r$ is the rotor resistance changing factor. It denotes an increase ($k_r > 1$) or decrease ($k_r < 1$) of rotor resistance.

Figure 3-1 shows the deviations of rotor flux for the investigated IM (Table 1-1) under $k_r > 1$ and $k_r < 1$. It is assumed that K_s changes are due to variations of r_r. It can be seen in Figure 3-1.a that the rated flux setting magnetic saturation occurs when $k_r > 1$ (over-excitation), i.e. when the actual r_r is larger than the instrumented one (r_r was doubled

after 2sec). On the other hand, the rotor flux will be smaller than the rated value if $k_r < 1$ (under-excitation). In this case, r_r was reduced by half after 2sec.

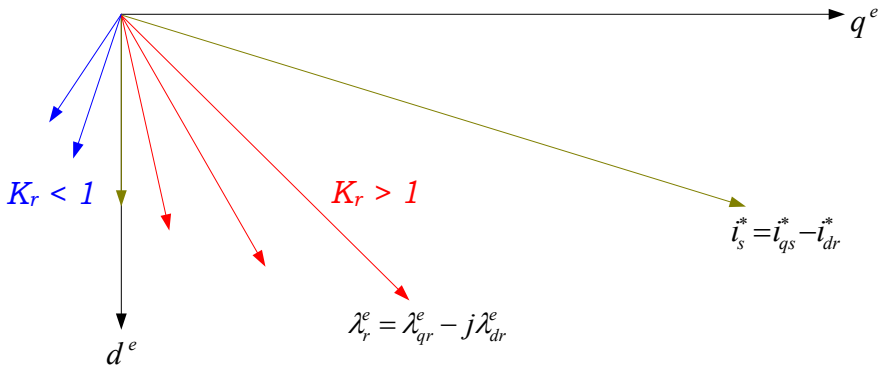

(a)

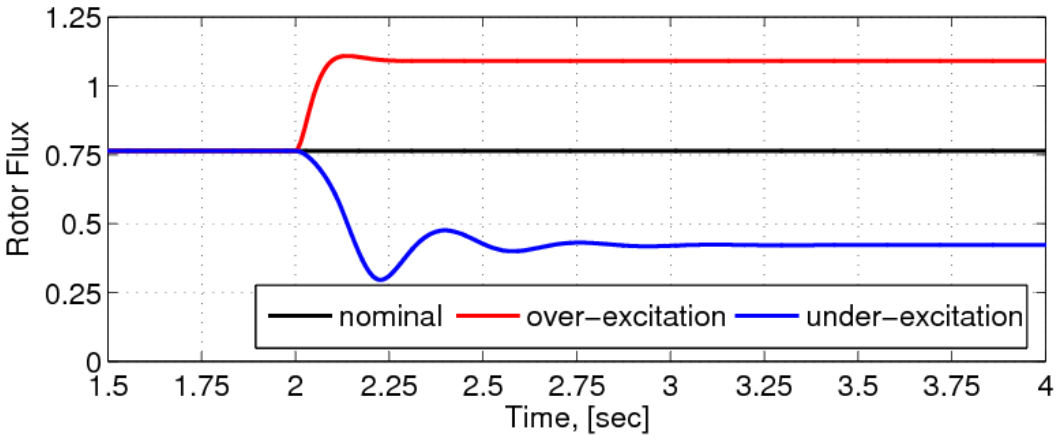

(b)

Figure 3-1: Rotor flux deviations due to slip gain changes

Over-exciting a motor can cause saturation, which increases the stator current copper losses, having a detrimental effect on the rating of the motor. On the other hand, the motor is not being effectively used if operated under rated excitation. In both cases, the steady-state and dynamic performances of the drive will be affected and its efficiency decreased (due to increase in losses). Beside the drive's efficiency, the output torque transient of the motor will exhibit an oscillatory response

and cannot follow a step change in the input torque command (reference) as quickly as expected in an *ideal* IFOC. This effect is undesirable in high-performance drives.

There are other reasons why over-excitation and under-excitation are undesirable in high-performance drives. An over-excitation condition, in particular, is a reflection of increased motor voltage, which could further cause a loss of current regulation if the inverter bus cannot support that voltage. This case is shown in Figure 3-2 for the phase voltage of the investigated IFOC IM drive under the same over-excitation condition simulated in Figure 3-1. Clearly, there is an over-voltage reaction after 2sec as a result of detuned IFOC (due to increase in rotor resistance). Figure 3-1 and Figure 3-2 explain why parameter sensitivity and adaptation are treated as one of the major issues of IFOC IM drives [14].

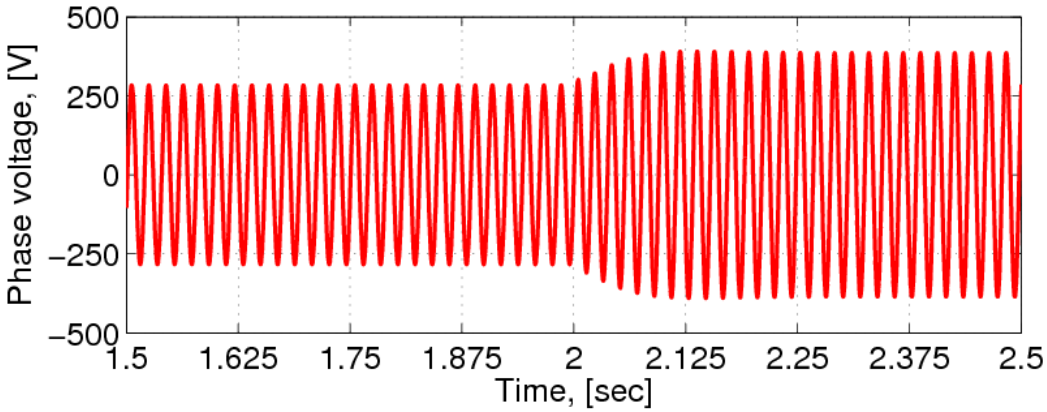

Figure 3-2: Phase voltage waveform under slip gain change

3.2. Parameter Adaptation Methods

The effects of mismatch between the motor and the controller (IFOC) can be reduced by updating the slip gain (K_s) online. Without slip gain online adaption, the torque capability of an IFOC IM drive can be reduced down to 29% or more [15]. In that case, even for applications where FOC is

used to save energy, the motor must still be oversized. With an online adaptation mechanism, it is possible to limit the torque degradation between 3% and 7% or less. This is acceptable in most high-performance applications [15]. Therefore, maintaining the instrumented K_s (in the Current Model block) as close as possible to its real value in order to maintain the drive performance and efficiency high at all time is highly recommended.

Initial calibration of K_s is straightforward if the motor parameters are available. Nominal motor parameters can be found in its nameplate or from the manufacturer. If there are not available, they can be calculated using the standard self-commissioning method mentioned in chapter 1. The online monitoring of K_s is rather very challenging while the drive is in operation. It requires advanced computation with powerful DSPs. Recently; significant efforts have been put into developing either online K_s estimation schemes or adaptive methods to deal with this problem. Depending on how the available information (of voltage, current, and speed or position signals) is processed, online K_s estimation approaches can be classified as shown in Figure 3-3 [16]. A brief description of the methods is given below; keeping in mind that some of them belong to more than one group.

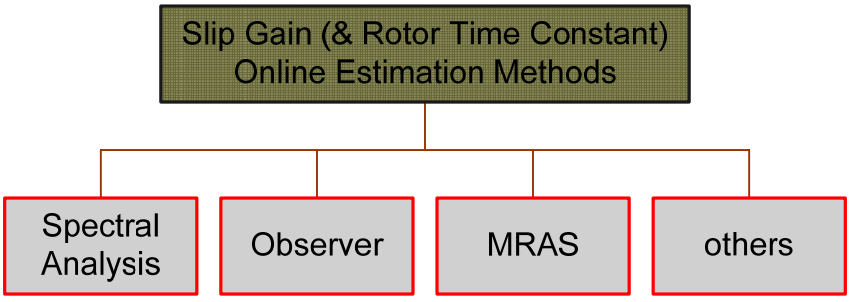

Figure 3-3: Slip gain online estimation methods

3.2.1. Spectral Analysis Methods

This group of methods is based on measurement responses to an injected test signal or an existing harmonic characteristic in voltage (or current spectrum) in order to identify the rotor resistance (r_r). For example, in [60] a method based on pseudo-random-binary sequence signal was introduced. The signal is injected into the flux axis primary current to influence the state variables of the system on the axis perpendicular to the flux axis. The influence of the signal depends on that of r_r. Hence, r_r can be identified from the response of the injected signal. Unfortunately, when the motor is not loaded in steady-state, the identification process is nearly impossible because the injected signal cannot influence the state variables on the axis perpendicular to the flux axis. In addition, the stability analysis of the algorithm has not been fully investigated.

Later on, [61][62] used some sinusoidal signals injected into the flux-producing axis of the stator current also to identify r_r even when the flux-producing current is zero. Their methods, including the method proposed by [60] require the value of stator resistance to complete the identification process: at low frequencies the performances of the algorithms are highly affected by the accuracy of the stator resistance. To obtain an accurate value of the stator resistance at all time at low-frequency operations, additional sensors (such as search coils) are required or a stator resistance online estimation method must be included.

The requirement for additional sensors is usually undesirable. It increases the drive complexity and cost; and reduces the reliability of the overall system. This is a big issue especially in hostile environments or when the physical structure of the motor must be modified to accommodate the sensors. To overcome this limitation, another approach based on injecting a test signal and sensing its corresponding output to provide compensation was introduced [63]. The problem with the

approach proposed in [63] is the difficulty of identifying r_r at zero or low-torque conditions. In addition, the injected signal(s) often generate some undesirable interference with the DPSs used for the drive, as it was observed in [14].

3.2.2. Observer-Based Methods

Observer-based methods evolve around the use of Extended Kalman Filter (EKF) [64][65][66] and/or Extended Luenberger Observer (ELO) [67]. An EKF is basically a full-order stochastic observer for the recursive optimum state estimation of a nonlinear dynamic system in real time. It uses signals that are corrupted by noises. The noise sources take into account measurement and modeling inaccuracies. The ELO, on the other hand, is a deterministic observer that uses signals without noises. It is applicable to linear-time invariant systems.

Methods that combine state and parameter estimations with EKFs were first introduced in [68][69]. It was observed that the accuracy of the estimation was highly dependent on the stator voltage and magnetizing inductance used in the filter algorithm. These variables were treated as known and constant. In practice, they are not easy to obtain, especially at low-frequency operations. To overcome this problem, in [64] the fundamental components of the stator voltage and real-time value of the magnetizing inductance are used instead. The EKF algorithm is designed such that the stator currents and the inverse of the rotor time constant (T_r) are treated as state variables. The use of stator currents as state variables offers a significant advantage since they are measured directly and are required in any FOC scheme. In addition to this arrangement of state variables, the wideband harmonic spectrum of the voltage waveform of the PWM inverter is considered as a noise input that is impressed on the motor by the inverter itself. Hence a random input for parameter

identification is inherently available, and no external signals are required for the machine parameter estimation.

A well-known disadvantage of EKFs is the computation burden of the Riccati difference equation solver, which is at the core of the algorithm. To deal with this problem, [65] introduced an approximation approach to reduce the computation burden. This approximation approach is based on the fact that in steady-state, the Kalman Gains are asymptotically constant for constant rotor speeds. This allows the Riccati equation to be replaced with a look-up table based on Kalman-Gain function. The problem with this approach arises when the motor speed is subjected to various changes during the drive operation.

Driven by the same desire to reduce the computation burden of EKFs, another method was proposed in [66]. Here, a reduced model of the IM was used and the EKF was expressed in a reference frame rotating synchronously with the stator current vector to deal with constant quantities in steady-state.

Some ELO schemes for both the state variable and parameter estimation were developed in [67][70]. The authors provided useful experimental comparisons between the ELO and the EKF methods for online estimation of slip gain. A deterministic approach is used in [70] to design the ELO with joint online estimation of IMs states and parameters. In [67], the authors implemented the scheme using three different full-order ELOs for (1) rotor time constant and rotor flux estimation, (2) rotor speed and flux estimation, and (3) rotor speed, load torque, and rotor flux estimation.

The joint state and parameter estimation method using ELO turned out to be a very advantageous solution. Since the IM is a nonlinear system, the observers from the EKF at individual time instants do not lead to an

overall optimal observation [16]. There is a great deal of flexibility in choosing the gain with the ELO than with the EKF. In addition, the rate of convergence can be tuned without adversely affecting the steady-state accuracy of the observer. Therefore, the fundamental advantage of ELOs over EKFs is that the observer performance can be greatly enhanced by simply adjusting the gain matrix for rapid convergence of the estimates, which gives an unbiased estimation in the case of the ELO.

Despite the efforts made over the years, the computation burden remains one of the main drawbacks of observer-based group of methods. However with modern DSPs, this is becoming a minor issue over the years. The other problem associated to this group of methods is the fact that the inductances are treated as constants. This is not a big issue for constant flux applications but not when field weakening operation is required. This means that for the majority of observed-based methods a simultaneous identification of magnetizing inductances (especially in field weakening operation [64]) or inclusion of the iron losses into the model [71] constitutes an additional requirement beside the identification of K_s itself.

3.2.3. MRAS Methods

This group of methods adapts for changes in the motor parameters after the initial identification. The adaptation mechanism operates by generating an error signal between two quantities. The first quantity is derived from a reference model of the motor. The second quantity is estimated from motor measured signals (voltages, currents, speed, etc.). Since the reference model quantity is independent of the slip gain changes, the generated error between the two quantities will be assigned entirely to the error in slip gain used in the control system. The generated error signal is used to modify a gain in the system by means of

adaptive mechanism (or adaptive controller) which provides correction of the slip gain.

The advantage of MRAS–based approaches over the previous two groups of methods consists in the following. In MRASs the developed IM model and outputs are based on the fundamental operation and conditions of the motor and not some unrelated signal(s). In other words, MRASs are based on fundamental component of terminal currents and/or voltages of IMs. Due to its design and implementation simplicities, this group of methods has attracted the most attention in literature and in industry; and it is the method used in the proposed K_s estimation scheme.

The number of schemes that belong to this group is vast. They differ with respect to which quantity is selected for the adaptation or estimation. The following are the most relevant adaptive quantities used in literature: reactive power [72][73], modified reactive power [8], air-gap power [74], electromagnetic torque [75], rotor back-EMF [76], stator *d*-axis and *q*-axis voltages [10][77]. Other possibilities include selection of rotor flux *d*- and *q*-axis components, stored magnetic energy, stator RMS voltage, and many more [14][16].

Despite the variety of MRAS schemes, they all share some common features regardless of the quantity used. These features also constitute their major drawbacks:

(1) Since MRAS schemes are based on the steady-state model of the motor, the online estimation mechanism is only operational in steady-state regime as well. This is not a very big issue since changes in motor slip gain are very slow and can be estimated in steady-state regions.
(2) Stator voltages are required in many of the adaptive quantities described above. They have either to be measured (with additional

sensors) or reconstructed from the inverter firing signals and measured DC link voltage.

(3) In many cases, the online estimation mechanisms are not possible at low-speed and/or low-load regions.

(4) The online estimation mechanism heavily relies on the model of the motor, in which, most frequently, all of the other parameters are treated as constants.

Due to drawback (4), it is often desirable to account for at least some of the motor parameters in the estimation process when some MRAS schemes are used. In many cases, the variations of the magnetizing inductance with saturation are the parameters that are included. Such methods were investigated in [78]–[81]. In order to deal with the difficulty of the methods at zero or low-speeds, and zero or low-load torques, some alternative approaches have also been introduced [79][82]. These methods are discussed in Section 3.3.

3.2.4. Other Slip Gain Estimation Methods

There are other possibilities for online estimation of K_s that do not belong to any of the three main groups discussed so far. For example, methods based on special switching techniques of current regulated PWM inverter to measure the induced voltage across the disconnected stator phase [83]. In this method, K_s is calculated directly from the measured stator voltage and currents. Other possibilities involve the use of AI methods, particularly, the Artificial Neural Network (ANN) [84], and FLC [21][85]. However, AI-based methods belong in vast majority to cases of one of the three main groups already reviewed.

3.3. Fuzzy MRAS Estimation of Slip Gain

The literature shows that a considerable number of solutions have been already introduced and published in the last few years for online estimation of K_s. The best possibilities for practical realisations are often awarded to procedures that are easy to implement (low in computation) and to process without additional hardware components (such as sensors or transducers) and special test signals. This includes methods that use only terminal currents and/or voltages as inputs. Such methods often belong to the group of MRASs [14][16][18][77].

The comparative studies of the various MRAS schemes conducted in [18] and [77] indicate that there is no approach that can solve the tuning problem satisfactorily in the entire torque-speed plane for the following reason. Stator voltages and currents are required in the adaptive quantities. These variables can be difficult to measure or estimate at zero (or low) speeds and torques. As a result, some online estimation mechanisms may not operate adequately in low speeds and/or low load torques while others may, and vice versa.

Among the MRAS schemes compared, those that are based on reactive power [77] and modified reactive power [8], *d*-axis voltage and *q*-axis voltage quantities [18] turn out to yield the best performances. The reactive power and modified reactive power methods are independent of stator resistance deviations. They also have acceptable sensitivity to the inductances. These special features make them very attractive when the drive is operated in zero- or low-frequency regions. They are not very effective at low-torque regions.

The *d*-axis voltage on the other hand, has a high sensitivity to detuning (even at low-load regions). It is also saturation independent. These features result in very fast and accurate convergence of the algorithm and allow IFOC in both constant torque and field weakening modes. The

q-axis voltage method offers similar performances as the *d*-axis voltage method [77].

There have been a few attempts towards expanding the torque-speed plan of MRAS schemes for slip gain online estimation. For example, in [21] the so-called FL data fusion technique was used to combine three MRAS adaptive quantities: (1) electromagnetic torque, (2) reactive power, and (3) stator voltage magnitude. Unfortunately, the data fusion mechanism used was not fully described at all. In [5], a stator resistance estimation scheme was included to an existing K_s online estimation scheme in order to extend its operation in low- and zero-frequency regions. In [19], the reactive power and *d*-axis voltage quantities were combined using a FL weight factor. In [18][77] some recommendations on adaptive quantities are given. These recommendations are based on operating conditions of the drive in terms of speed and torque. The authors also pointed out (through simulations and sensitivity analyzes) that the combination of the *d*-axis and *q*-axis voltages results in improved robustness, extended stability range to detuned motor inductances, and extended suppression of stator resistance influence at low stator frequencies. Unfortunately the mechanism combining these voltages was not fully evaluated.

Motivated by the success of the existing MRAS schemes, the analyses and recommendations of [18], the sensitivity analyzes conducted in [77], a new approach that combines the modified reactive power, *d*-axis voltage, and *q*-axis voltage is introduced in this chapter. The proposed method uses stator terminal current and voltage, and rotor speed signals to estimate K_s in the entire torque-speed plane. All three adaptive quantities are combined in a single scheme to expand the operating torque-speed plane of the algorithm through reduction of stator resistance influence at low-frequency regions and significant improvement of inductance robustness for all-load conditions. A FLC is

used to generate a weight (distribution) factor based on the drive operating conditions in terms of load torque and stator frequency. In order to describe the idea behind the approach, it is important to describe the principle of MRAS as applied to online estimation of K_s.

3.3.1. Generic Slip Gain Estimation Scheme

Figure 3-4 shows a generic MRAS scheme used for online estimation of K_s. The model makes provisions for a generalized adaptive quantity (Y^*), which is usually a function of the current/voltage commands, motor inductances, and frequency. The actual motor estimator uses some mathematical combinations of motor terminal quantities and other approximations to compute for the feedback or actual adaptive quantity (Y). The latter is compared with the reference quantity (Y^*) to generate the adaptive error signal, which is multiplied with the feed-forward current command for coherence and then compensated by an adaptive controller to generate the estimated slip gain ($\hat{K}_s$).

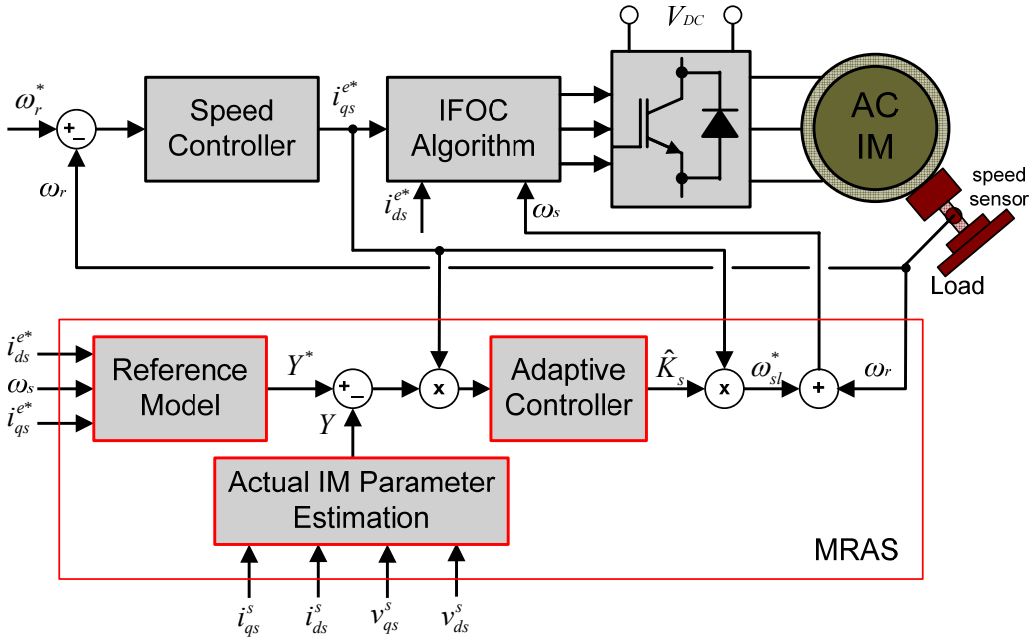

Figure 3-4: Generic MRAS scheme for slip gain online estimation

The estimated slip gain ($\widehat{K}_s$) is multiplied with the current command gain to generate the estimated slip speed command (ω_{sl}^*) that is directly used in the Current Model of the IFOC IM drive (Figure 1-8). The method proposed in this thesis follows exactly this generic topology.

3.3.2. Proposed Slip Gain Estimation Scheme

A steady-state modified reactive power can be obtained from the slip speed, flux-producing component of stator current, and rotor flux linkage as [8]:

$$Q = -\frac{L_m^2}{L_r}\omega_s(i_{ds}^e)^2 \tag{3.5}$$

Its command value is given by

$$Q^* = -\frac{L_m^{2*}}{L_r^*}\omega_s^*(i_{ds}^*)^2 \tag{3.6}$$

Where the reference stator frequency (ω_s^*) can be defined according to [5].

Equations (3.5) and (3.6) indicate clearly that any parameter change in IM will influence the actual reactive power (Q) in (3.5) and make it deviate from its command value (Q^*) in (3.6). This deviation is an indication of changes in K_s. Another important feature of the modified reactive power quantity is its independency of stator resistance under any condition of operating frequency. Although reactive power MRAS quantities offer superior performance compared to other available quantities at low-frequency regions, their sensitivity to magnetizing inductance increases significantly at low-torque regions [8][18][77].

The *d*-axis and *q*-axis voltage quantities and reference values are [18]:

$$v_{ds}^e = r_s i_{ds}^e - \omega_s L_\sigma i_{qs}^e \tag{3.7}$$

$$v_{ds}^{*} = r_s i_{ds}^{*} - \omega_s^{*} L_\sigma i_{qs}^{*} \tag{3.8}$$

$$v_{qs}^{e} = r_s i_{qs}^{e} + \omega_e L_s i_{ds}^{e} \tag{3.9}$$

$$v_{qs}^{*} = r_s i_{qs}^{*} + \omega_s^{*} L_s i_{ds}^{*} \tag{3.10}$$

where the leakage inductance $L_\sigma = L_s - (L_m^2/L_r)$ varies with saturation due to stator current (and is potentially load dependent). In (3.7)-(3.10), the stator resistance (r_s) is necessary, especially at low-frequency regions. In addition, estimations of L_σ and L_s terms are required for the *d*-axis and *q*-axis voltage quantities, respectively.

The sensitivity diagrams of the v_{ds}^{e} quantity reported in [77] showed that its most characteristic attribute is the strong detuning of K_s, combined with a reduction of stability range when L_σ is very small. This reduction requires that adaptation be switched off at high-load regions. On the other hand, the same study showed that the diagrams of the v_{qs}^{e} quantity reflected a strong influence of L_s deviations, also connected with stability deterioration at low-load regions. Similar results were also obtained in [14][18][19].

It is evident that the search for more powerful solutions is especially vindicated by the load dependency of the effects of inductance deviations connected with the stability issues, and the strong influence of stator resistance deviations at low-frequency regions. Many parameter sensitivity analyses have demonstrated that reactive power quantity is superior to other schemes at zero- and low-frequency, and high-torque regions [8][19]. At low-torque and high-frequency regions, the *d*-axis voltage followed by the *q*-axis voltage method offer the best results [18]. It was also shown in [77] that a significant improvement of the inductance effects on the adaptation under any load can be achieved by combining two adaptive error signals of the v_{ds}^{e} and v_{qs}^{e} quantities; with different

signs of their sensitivity functions with regard to r_r. (The signs of the error signals must not be changed since they represent the direction of slip gain adaptation).

A consideration of equations (3.7)-(3.10) shows that a useful combination might be given by the so-called *Voltage Vector Error* defined as

$$e_{dq} = \lambda_d e_d + \lambda_q e_q \tag{3.11}$$

where e_d and e_q are the v_{ds}^e and v_{qs}^e adaptive errors, respectively; and λ_d and λ_q are their respective weight factors [77]. Equations (3.5)-(3.11) are combined to form the proposed K_s online estimation scheme, which is described in Figure 3-5.

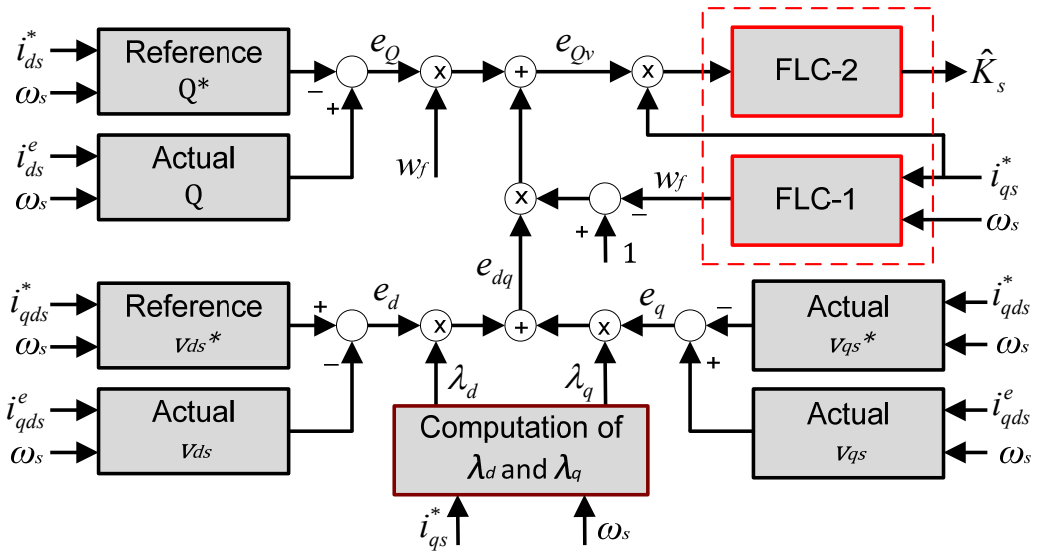

Figure 3-5: Proposed scheme for online estimation of slip gain

The first controller (FLC-1) generates the weight (or distribution) factor (w_f) which is used to determine the appropriate distribution between the reactive power error and the voltage vector error in the torque-speed plane. It uses the torque-component current (for torque estimation) and

the motor reference supply frequency to determine the values of w_f using a very simple FLC. The objective is to assign a high sensitivity to the tuning control (FLC-2) by the dominant use of reactive power control in the low-speed and high-torque regions; and the voltage vector control in the high-speed and low-torque regions.

The second controller (FLC-2) is an adaptive FLC. It generates the estimated slip gain from the combined adaptive error signal (e_{Qv}) and the reference torque component current (i_{qs}^{*}). Ideally under normal conditions e_{Qv} should be zero and $\widehat{K}_s = K_{s0}$ (where K_{s0} is the nominal slip gain). Under detuned conditions, the actual Q, v_{ds}, and v_{qs} will deviate from their reference quantities and the resulting errors will alter the value of $\widehat{K}_s$ until e_{Qv} is compensated (i.e. until $e_{Qv} = 0$).

The knowledge required for the design of FLC-1 and FLC-2 is derived by simulating the investigated IFOC IM drive (Figure 1-8). During these simulations, the slip gain online estimation algorithm was purposely disabled but the slip gain itself was varied from 0.5 to twice its nominal value (K_{s0}) at 50% rated speed. The obtained results were similar to the results obtained in [19]:

(1) The reactive power error (e_Q) tends to be very small in low-torque regions (below 30%), but increases with higher torque;
(2) The voltage vector error (e_{dq}) tends to be large except at maximum torque, indicating that w_f should be high in high-torque and low-frequency regions.

The simulations of the model also showed that the voltage vector is better in high-frequency and low-torque regions, whereas the reactive method is better in low-frequency and high-torque regions. This knowledge of the system behaviour is used to design FLC-1 and FLC-2 and to determine

the shape(s) of the MFs and the values of the scaling gains used in these controllers.

Figure 3-6 shows the MFs used for the variable "reference frequency" (ω_s^*) and the variable "torque component current" (i_{qs}^*) in FLC-1. The linguistic terms "L" is Low, "M" is Medium, and "H" is High. The value ω_b is the base (nominal) frequency of the motor, and i_{qsn} is the nominal torque component current (equivalent to twice the rated current of the motor). The number of MFs for the variables is chosen such, so that the entire torque-speed plane is represented: low, medium, and high. For example, a speed of zero is definitely a Low (L) speed, whereas as 50% of ω_b represents a speed that is 50% Low (L) and 50% Medium (M).

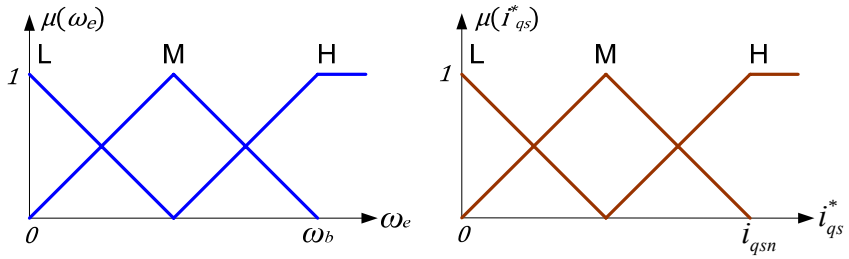

Figure 3-6: MFs for speed (ω_e) and torque component current (i_{qs}^*)

The weight factor (w_f) is generated by singleton MFs to reduce the computation burden (Table 3-1). The values of the singletons were carefully selected during simulation to coordinate how much weight should be given to a method based on the current operating condition of the drive (in terms of frequency and load torque). For example, the value of "0.80" for w_f in Table 3-1 means that when frequency and load are Low (L), the simulation results (not shown) have demonstrated that 80% ($w_f = 0.8$) of the reactive power quantity and 20% ($w_f = 1 - 0.8$) of the voltage vector quantity (see Table 3-1) are sufficient to perform an effective estimation of K_s. On the hand, as long as the frequency is Low, if

the load torque is Medium or High, only the reactive power quantities should be functional.

Table 3-1: Fuzzy rule base for w_f

w_f		speed, ω_e		
		Low	Medium	High
torque component curent, i_{qs}^*	Low	0.80	0.20	0.00
	Medium	1.00	0.55	0.20
	High	1.00	1.00	0.00

FLC-2 consists of two input variables, the combined error (e_{Qv}) and its rate of change (ce_{Qv}). There are 5 MFs for each input/output variable. The rule base matrix used to generate the estimated slip gain is monotonic and symmetrical (refer to chapter 4). While the input scaling gains of FLC-2 are fixed, its output gain is self-tuned according to the value of the weight factor (w_f).

As stated in chapter 2, in FLCs imprecision can be useful. Hence, even under detuned condition(s), FLC-1 can still be used as a measure of the motor load torque at approximately rated flux condition. Same rules apply for imprecision that can be found in rotor speed sensor or position encoder.

3.3.2. Validation of the Proposed Scheme

To validate its effectiveness, the proposed scheme was incorporated into the investigated IFOC IM drive (Figure 1-8). Initially, the tracking ability of the algorithm and its convergence time were verified at high-load and high-speed regions; where the majority of the methods perform sufficiently well. In order to do so, the drive was operated at 1500rpm at

full load torque (1.0p.u.). A PI controller was used to ensure proper speed control. The proposed online K_s estimation algorithm was activated at start-up. At first, the motor was operated with the rated K_s (which was not updated in the controller). After 1.5sec the slip gains was changed (in the IM) as a result of 50% increase in rotor resistance. Figure 3-7 shows the simulated case study.

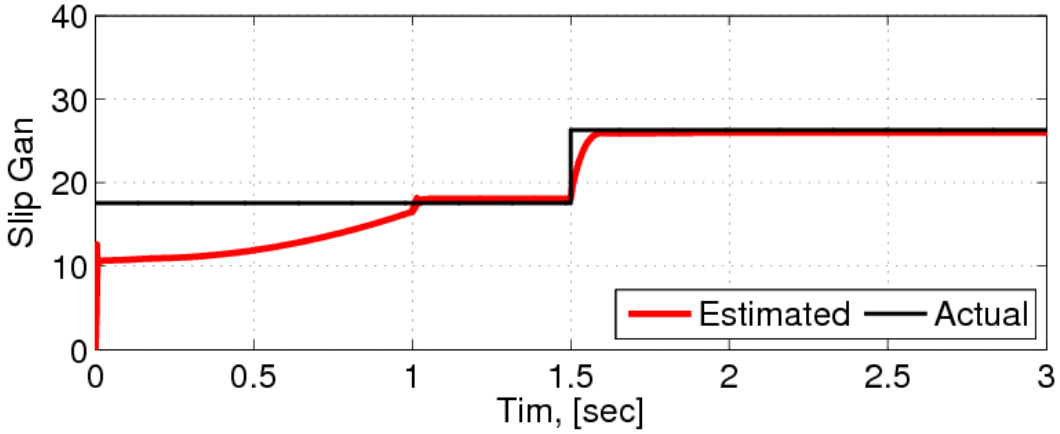

Figure 3-7: Estimated and actual slip gains at high-load and high-speed regions

It can be seen that the algorithm requires approximately 1.0sec for the estimated slip gain to converge at start-up. After the initial convergence, the settling time of the algorithm is significantly shorter. The start-up convergence time is proportional to that of the speed response. In other words, it was possible to reduce the initial convergence time by adjusting the gains of the speed (PI) controller. However, this resulted in high starting current. Therefore a compromise between the initial convergence time and starting current was made. Another alternative to reduce the initial convergence time is to start the drive with the nominal value of slip gain in the Current Model. In this case, the online slip gain mechanism can be activated a few seconds after start-up.

The ability of the algorithm to estimate K_s at high-speed and low-torque regions was also investigated through simulations. This was verified by

the ability of the drive to maintain constant flux under detuned conditions (with no over- or under-excitation). To do so, the drive was operated at 1500rpm and 0.1p.u. load torque. The online estimation was activated at start-up, as in the previous case. The slip gain of the motor was intentionally increased after 1.5sec as a result of 50% increase in rotor resistance. The FLC-1 was used to determine the sensitivity of the adaptive quantities based on the operating conditions of the drive. Since the drive is at very low-load regions, according to Table 3-1, the generated w_f was sufficiently big to reduce the effect of the modified reactive power method on the estimation process. The characteristics of the drive are shown in Figures 3.8-3.11.

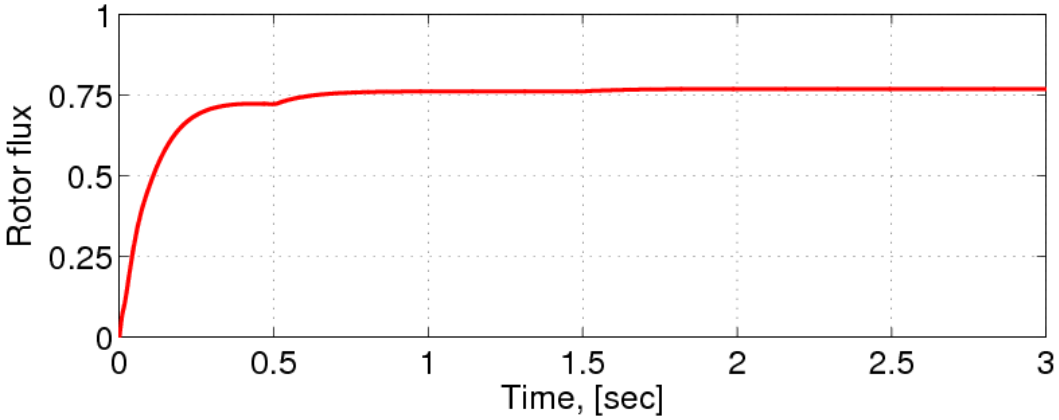

Figure 3-8: Rotor flux response under slip gain change at high-speed (1500rpm) and low-load torque (0.1p.u.)

Figure 3-8 shows that the rotor flux linkage is maintained constant despite the detuned condition (due to sudden change in K_s). This is with respect to the case shown in Figure 3-1, where an over-excitation was observed when the slip gain was increased.

The phase voltage waveform (Figure 3-9) does not show sign of over-excitation effect when compared to the waveform shown in Figure 3-2. This is a good indication that by using the proposed scheme, stator

copper losses caused by detuned IFOC can be controlled or reduced significantly at all time.

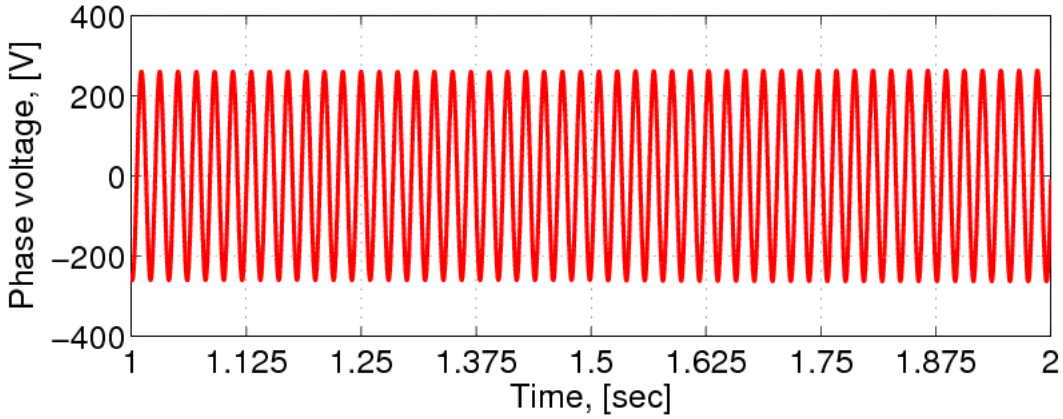

Figure 3-9: Phase voltage waveform under slip gain change at 1500rpm and low-load torque (0.1p.u.)

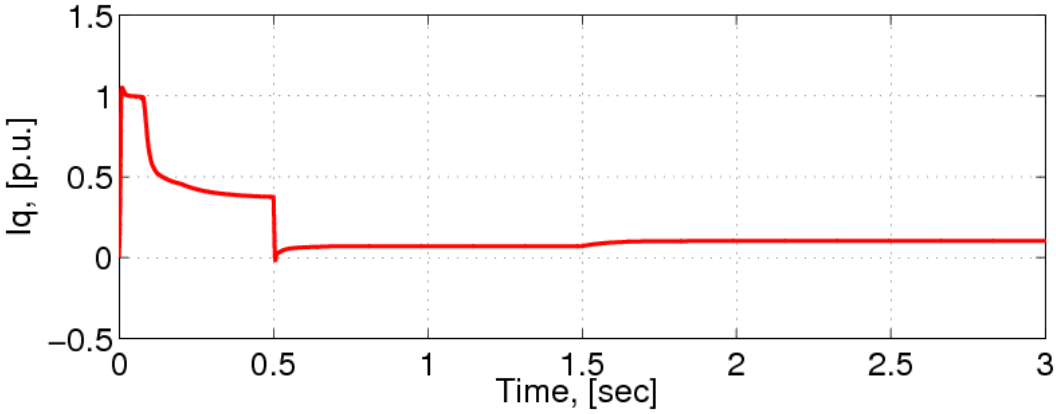

Figure 3-10: Torque component current response under slip gain change at 1500rpm and low-load torque (0.1p.u.)

Since the investigated drive utilizes an outer speed control loop, the load torque demand will necessarily be satisfied in steady-state even under detuned conditions. This is confirmed in Figure 3-10. It takes approximately 0.5sec for the torque to settle at start-up. There is a real control of torque when the slip gain is detuned at 1.5sec.

Finally, Figure 3-11 shows the response of the motor speed. The effect of detuned IFOC on the output speed is practically negligible, as expected.

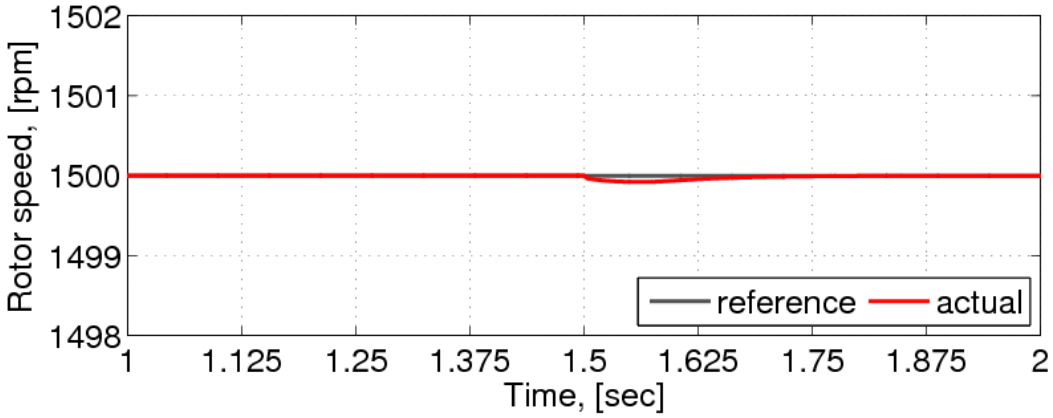

Figure 3-11: Rotor speed response under slip gain change at 1500rpm and low-load torque (0.1p.u.)

Finally, the ability of the algorithm to compensate for K_s deviations at low-speed and low-torque regions was simulated. As in the previous case, the ability of the drive to maintain constant flux in spite of detuned condition was investigated. To do so, the drive was operated at very low speed (10rpm) and very low load torque (0.1p.u.). The estimation algorithm was activated at start-up. The slip gain of the motor was intentionally increased, as a result of 50% increase of rotor resistance after 1.5sec. The system is described in Figures 3.12-3.15.

Here, as in the previous case, the rotor flux (Figure 3-12) is also maintained constant despite the sudden change in K_s. In addition, it can also be seen that the algorithm converges faster in low-speed and low-torque regions. The stator phase voltage (Figure 3-13) does not show a sign of over-excitation in spite of K_s increase. The torque response, estimated by the torque-component current in Figure 3-13 is faster than in the previous case (at start-up). It also maintains its value under detuned condition, with very short transients. Finally the motor speed

response is shown in Figure 3-15. The compensation of the motor speed under detuned conditions is slightly slower (with higher undershoots) in low-speed regions than in high-speed regions.

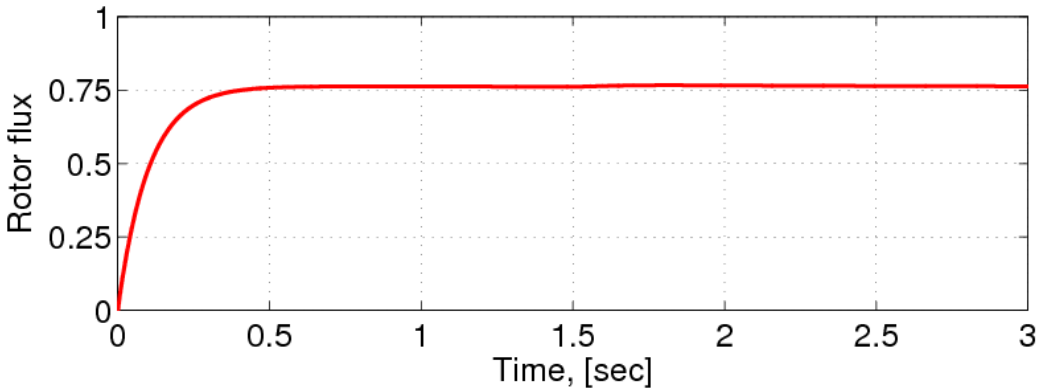

Figure 3-12: Rotor flux response under slip gain change at low-speeds (1500rpm) and low-load torque (0.1p.u.)

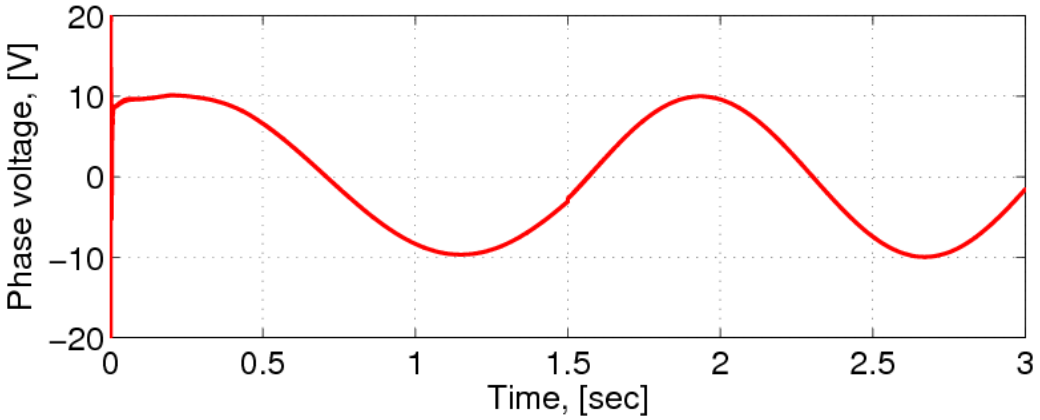

Figure 3-13: Phase voltage waveform under slip gain change at 10rpm and low-load torque (0.1p.u.)

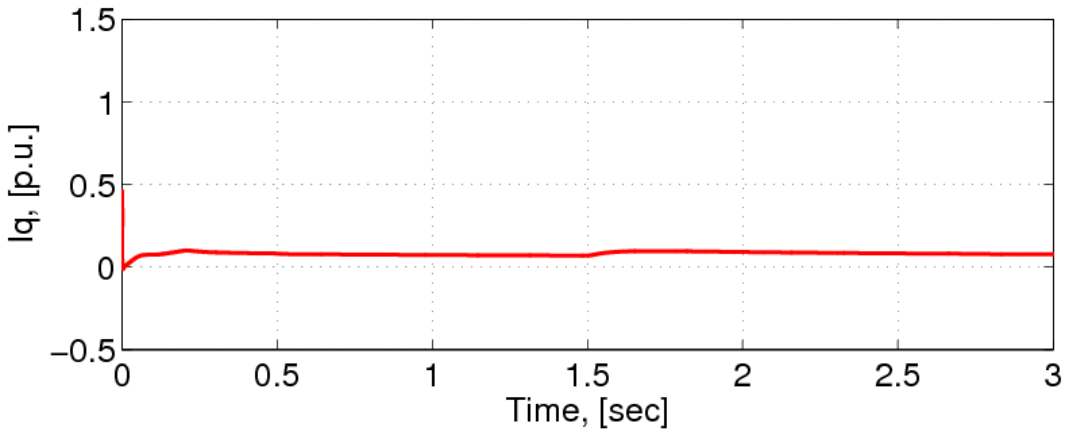

Figure 3-14: Torque component current response under slip gain change at 10rpm and low-load torque (0.1p.u.)

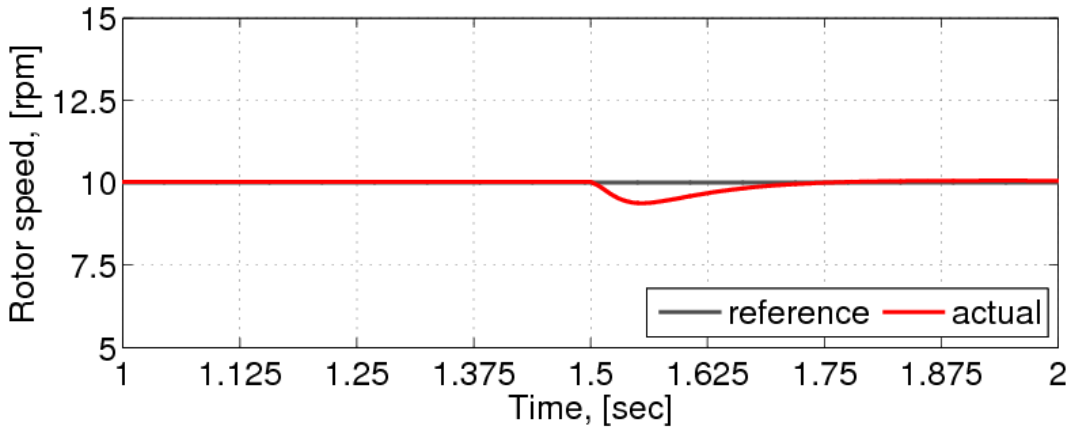

Figure 3-15: Rotor speed response under slip gain change at 10rpm and low-load torque (0.1p.u.)

3.4. Conclusion(s)

This chapter showed the importance of online estimation of slip gain for IFOC IM drives in order to reduce or to overcome undesirable effects of parameter sensitivity. These effects include the deviation of rotor flux linkage and dynamic oscillations of the electromagnetic torque. Various methods have been introduced to deal with this problem. A new method, based on the principle of FLC and MRAS is developed in this thesis. The proposed method successfully combined the features of the reactive

power, the *d*-axis voltage, and the *q*-axis voltage quantities in a single system using two FLCs. The first FLC is designed for distributing weights between the reactive power quantity and the voltage-based quantities (or the voltage vector error). It is a simple FLC, with simple linguistic rules and MFs. Its input variables are the torque component current and reference supply frequency. In practice, these variables can be obtained easily in the IFOC block. The second FLC provides an adaptive control function to the combined adaptive error for fast convergence. It is also made of simple fuzzy rules and MFs. The rule base of this FLC is designed with simplicity in mind in order to reduce the computation of the algorithm. This is done by using the so-called monotonic-symmetrical type FLC.

The plotted results validate the proposed approach. The phase waveform does not show signs of over-excitation or under-excitation effects. This is a good indication that by using this scheme, stator copper losses caused by detuned IFOC conditions can be controlled or minimized. Consequently, the overall efficiency of the drive can also be controlled or maintained.

The implementation of the proposed algorithm is straightforward and easy. It does not require modification of the physical topology of the IM to accommodate some extra sensors. It uses terminal current(s), voltage(s) and rotor speed. These quantities are required in standard IFOC schemes even when online slip gain estimation is not included. The (two) FLCs used in the scheme are designed with singleton output MFs to reduce the computation burden. These special features make the approach very attractive and suitable in many IFOC drives, where K_s estimation is a requirement in the entire torque-speed region.

Chapter 4

Self-Tuning Speed Control of IFOC IM Drives

The requirement of online estimation of slip gain for high-performance IFOC IM drives outlined in chapter 3 led to the design of a new estimation scheme based on the principles of FLC and MRAS. With the proposed scheme, it is possible to estimate the slip gain in the entire torque-speed plane. Under *ideal* slip gain estimation, the overall system can be considered as *ideal* FOC IM drive or equivalent to a linear (like a DC motor drive) system.

Under *ideal* FOC, the drive system can be operated by a linear controller with invariant parameters, designed by some simple classical methodologies. However, in modern industrial applications the electrical and mechanical parameters of the drive are rarely constant. Besides, the drive system is also subjected to load disturbances and other uncertainties (such as backlash, sensor noises, power electronics, etc.). High-performance drives require very tight control of speed/torque, usually around ±0.01% in steady state [1]. To fulfil this requirement the controller of the drive must be flexible to allow modification of its control surface to obtain significant improvements at all time.

A classical approach to servo drives or VSDs is accomplished by standard PI controllers with fixed gains. Unfortunately, fixed-gain controllers are often insufficient to deal with complex systems or systems subjected to severe parameter and operating condition changes. This is because the performance and design of PI controllers rely on the accuracy of the process model (which is usually represented by an approximate model) and on a selected (nominal) operating condition

(point). If the parameters of the system are changed or if its operating condition deviates significantly from the initial one, the system responses (torque, speed, current, etc) may also experience significant dynamic and steady-state disturbances in terms of settling time and overshoot. To overcome this problem, the gains of the controller must be updated continuously according to the actual trend of the system. Advanced conventional adaptive techniques such as, MRAS, SMC, and many more are among the first alternatives to deal with this issue [86]-[90].

Many adaptive controllers also rely on the accuracy of the mathematical model of the process. This makes the approaches sensitive to motor parameter and operating condition perturbations as well. The SMC approaches however, represent the best alternatives among the various conventional adaptive approaches in terms of alleviating the need of mathematical models. It depends on the knowledge of parameter variation ranges to ensure stability and to satisfy reaching conditions rather than relying on accurate knowledge of the control process. If the controller must operate under unknown condition of parameter variation changes, this becomes an issue.

Moreover, the majority of SMC schemes are designed to follow a 1st-order system response irrespective of the order of the controlled system [91]. In order to obtain the 1st-order system response, the control law must guarantee that the worst-case dynamics would be handled. The worst-case inputs are large and often result in chattering, which sometimes can be reduced with a boundary layer around the sliding plane [89][90]. However, chattering remains one of the main drawbacks of SMC schemes. Due to their complexity only a few conventional adaptive schemes, including SMC schemes, have been successfully implemented or verified on IFOC IM drives [20][21][22][31][32].

The difficulty related to the implementation of conventional adaptive schemes for IFOC IM drives indicates that it can be very challenging to effectively deal with all machines and drives problems through strict mathematical formulations. Alternatively, FL has emerged as one of the complements to conventional mathematical methods. Design objectives that are hard to express mathematically can be incorporated into FLC by means of simple fuzzy rules written in linguistic terms. FLCs provide effective means of capturing the approximate or inexact nature of the real world using simple linguistic statements or propositions.

The literature has shown that the performance of an FLC is similar to that of a conventional SMC for IM drives [29]. However, the design and implementation of an FLC is quite straightforward when compared to SMCs, especially if a dynamic design methodology is used for the FLC. Without a proper design methodology, the design of an FLC can be time consuming and sometimes frustrating, depending on the complexity of the system. This issue is elaborated in Section 4.2.

Recently engineers have paid significant attention to the potentials of FLCs for FOC IM drives [20]–[33][46][[92]–[96]. The available FLC schemes for FOC IM drives can be divided into:

(1) Non-adaptive FLCs, and
(2) Adaptive or Self-Tuning FLCs.

Non-adaptive FLCs (or simply FLCs) consist in finding the *optimal* calibration method for the parameters of the standard FLC in order to optimize its dynamic and steady-state responses [21][23][24][25][46][93][96]–[103]. A conventional FLC is comprised of a set of rules, MFs, and scaling gains. In a standard FLC, these parameters of the controller are fixed and selected under nominal operating conditions.

The number of methods that belong to the group of Non-adaptive is vast. For example, a special design of rules for an IFOC IM drive was introduced in [23] with rather promising results. However, if subjected to severe perturbations, the proposed FLC may require an online parameter tuning mechanism due to the way its parameters are selected. The magnetization and starting procedures of an IM are used in [24] to determine the *optimal* scaling gains for an FLC. Unfortunately, the selected scaling gains are functions of stator leakage, magnetizing reactance, and rotor inertia. This dependency on motor parameters makes the approach very sensitive to parameter changes. In addition, the authors did not validate the scheme in a wide range of operating conditions. To minimize the real-time computation burden of an FLC, a method based on reduced number of MFs was implemented in [25], also for an IFOC IM drive. Unfortunately, the controller was validated only in a very narrow range of operation and parameter changes.

The second group of approaches are designed to combine the advantages of FLCs and those of conventional adaptive or self-tuning techniques in order to increase the performance of the control system under severe parameter and operating condition disturbances [20]–[22][26][27][28][30]–[33][92][94][95][103]. The combination of MRASs and FLCs appears to be the most promising approach for drive applications and the best approach for optimal exploitation of FL methods [21]. This is because MRASs require less computation and represent a good compromise between performance and cost.

Many schemes that combine FLC and MRAS have been applied to IM drives. For example, a signal adaptation method based on model following error-driven FL adaptation mechanism is designed in [22]. Signal adaptations are known to be slower than parameter adaptation [21]. As a result, a number of schemes based on parameter adaptation with the potential ability to compensate for system perturbations were

developed [26][28]. The adaptation target in [26] is the fuzzy rules, whereas in [28] the authors aimed for the tuning of the output scaling gain to provide a faster adaptive mechanism than the output signal compensation approach used in [22] and [26]. Unfortunately, no experimental tests are provided to validate the approach used in [22].

Other approaches have also been theoretically developed [92][94][104][105], but only a few have been experimentally tested on motor drives. In many cases, the algorithms are quite complex and/or do not include practical drive constraints, such as motor current limits and computation burden of the control algorithm (and cost).

The method proposed in this chapter also exploits the advantages of MRASs and FLCs to design a new *Self-Tuning Fuzzy Speed Controller* (STFC) for IFOC IM drives. The two approaches are incorporated in a single controller, resulting in high dynamic and steady-state performances in terms of overshoot, undershoot, and settling time. The proposed STFC takes into account the constraints of motor current limitation (in order to protect the motor and the drive) and significantly reduces the computation burden of the controller. Its performance is evaluated with a conventional PI controller, designed according to the Ziegler-Nichols method. The choice of the PI controller is justified by its wide use and acceptance in industry.

Since the proposed STFC is derived from a Non-adaptive FLC, a new systematic method of designing Non-adaptive FLCs for FOC IM drives is first introduced [96]. The performance of the proposed Non-adaptive FLC is also evaluated with a PI controller through a series of simulations and experimental tests under various parameter and operating conditions. This is the first contribution of this chapter.

After the validation of the proposed Non-adaptive FLC, a self-tuning mechanism is included to it in order to maintain its dynamic performance in a wider range of parameter and operation changes. Therefore, viewed in this perspective, the proposed STFC is the combination of a Non-adaptive FLC (designed with a new methodology) and a self-tuning mechanism based on MARS approach. This is the second contribution of this chapter.

4.1. Conventional PI Speed Controller of IFOC IM Drives

An IFOC IM drive (Figure 1-8) can be divided into electrical (inner) and mechanical (outer) loops. Due to physical properties of IMs, the outer loop has a slower dynamic response compared to the inner loop. Consequently, the overall speed control performance of IM drives can be characterized by their electromechanical dynamics [106].
For an *ideal* IFOC IM the electromechanical dynamics can be written as [7][106][107]:

$$T_e = J\frac{d\omega_m}{dt} + B\omega_m + T_{load} = K_t i_{qs}^* \tag{4.1}$$

where K_t is the torque constant, J is the motor inertia, B is the viscous friction coefficient, and T_{load} is the motor load torque. By using the Laplace transformation, and assuming ideal current control in the IFOC mechanism and *ideal* IFOC, the IM drive can be reasonably represented by the block diagram of speed control system (also known as IM servo drive system) shown in Figure 4-1; where s_L is the Laplace operator.

For a PI controller, the speed control block G(s_L) is

$$G(s_L) = K_P + \frac{K_I}{s_L} \tag{4.2}$$

where K_P is the proportional gain and K_I is the integral gain. Figure 4-1 confirms that under *ideal* decoupling conditions, a closed-loop IFOC IM drive can be considered as a 2nd-order linear system.

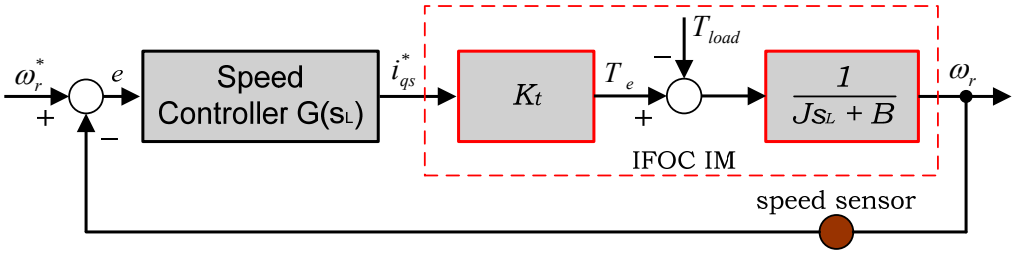

Figure 4-1: Block diagram of IM servo drive system

IFOC IM drives are globally asymptotically stable if the estimated rotor resistance is within a 200% error range [8][108]. It is also known that all signals in IM remain uniformly bounded as long as the estimated rotor resistance is within a 100% error range [108]. In chapter 3, it was shown that practical temperature excursion of IM rotor is about 130°C above ambient; corresponding to only 50% increase of rotor resistance over its rated value. So, under nominal operating conditions it is very difficult for changes in rotor time constant to drag the system into instability. Hence, the major source of instability would often be related to inadequate selection of the PI gains of the speed (and current) controller. It is therefore very important to calibrate the PI gains of the speed controller to guarantee not only stability of the closed-loop system, but also good performance at all time; especially for high-performance applications.

In literature, many approaches for PI gains calibration have been introduced: Symmetrical Optimum Criterion [8], Transfer Function-based methods [109], classical Ziegler-Nichols [13], Kharitonov Robust Stability Theory [106], Optimization-based methods [110], and many more. Among these approaches, the classical Ziegler-Nichols method is adopted in this thesis due to its wide industrial acceptance and simplicity.

Introduced in 1942, the Ziegler-Nichols method has become a classical tuning method for close-loop control systems. It is widely known as a fairly accurate heuristic method for a wide range of processes [14][111]. It is based on empirical knowledge of the so-called *Ultimate Gain* (k_u) and *Ultimate Period* (t_u) of the control process. These parameters are measured at the critical system stability condition as follows [112]:

Using the system described in Figure 4-1, the speed controller block G(s_L) is replaced by a variable gain K. A step impulse signal is applied to the speed reference (ω_r^*). Adjust K until the system's output response (ω_r) is critically stable. The value of K at which the system is critically stable corresponds to the Ultimate Gain (k_u). The period at which the system is critically stable corresponds to the Ultimate Period (t_u). In general, t_u is measured at the lowest frequency. Based on the values of k_u and t_u, the PI gains are computed as [14]:

$$K_P = 0.45k_u \quad and \quad K_I = 1/0.85t_u \tag{4.3}$$

While at first glance it may not appear so, the Ziegler-Nichols method is also parameter dependent. Its accuracy depends on that of the model described in Figure 4-1. In other words, the PI gains set according to Ziegler-Nichols method also depend on the accuracy of the off-line (nominal) parameters of the IM (K_t, J, & B). It is for this reason that in some cases or often the gains computed according to (4.3) are subsequently tuned, based on the designer experience, to achieve acceptable steady-state and dynamic responses [98]. This is an evidence that heuristic approaches are also incorporated into conventional methods.

4.2. Systematic Design of FLC for IFOC IM Drives

A well designed Non-adaptive FLC is capable of driving an IFOC IM drive to a set point with a small settling time and no overshoot. To do so, the motor current must reach its maximum value at all time. Such performances are achievable by setting good initial scaling gains, MFs and rule base. In some applications a Non-adaptive FLC may be sufficient to drive the motor satisfactorily. Unfortunately, the initial tuning of an FLC can be more difficult (and time consuming) than its conventional counterparts due to the flexibility of the knowledge base and the coupling of its parameters. This difficulty can be overcome by using a good systematic design methodology. In this section, a new but simple design methodology is introduced for IFOC IM drives.

4.2.1. Methods of Designing FLCs for Speed Control

There are two general approaches to FLC design [113]: (1) qualitative, and (2) quantitative. At the higher-level, FLCs are fuzzy are qualitative in terms of linguistic rules. This is a logic and knowledge-based design approach. At the lower-level FLCs are not fuzzy in terms of quantitative scaling gains. An ideal FLC design approach should embrace the methodology originating from logic and knowledge engineering as well as encompass the tools that are specific to control engineering [114]. A new way of incorporating these approaches in a single controller is introduced with the proposed design methodology.

The block diagram of a Non-adaptive FLC for IFOC IM drives is shown in Figure 4-2. The gains n_e, n_{ce}, and n_u are the error, change-in-error, and output scaling gains, respectively. The output variable $\Delta i_q^* = \Delta u$ is the change of current reference, defined as:

$$i_{qs}^*(k) = i_{qs}^*(k-1) + \Delta i_{qs}^*(k) \tag{4.4}$$

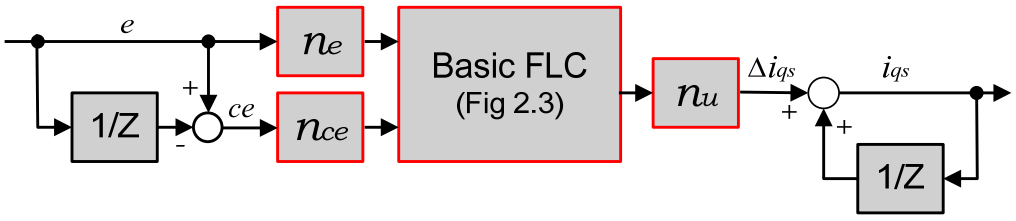

Figure 4-2: Speed control of IFOC IM Drives with PI-type FLC

The majority of available design methodologies for FLCs are developed to tune only one or two parameters of an FLC. For example, one of the earliest applications of FLC in servo drives are reported in [99][115][[116]. In [99] the scaling gain of the input variable "error" is set to the inverse of the incremental position encoder resolution while the output scaling gain is equated to the servo amplifier range. Inspired by [99], the authors in [115] proposed a new method based on formulating the rule base from a typical step response of the speed analyzed at each characteristic point. The input scaling gain of the variable "error" in [115] is also set according to the speed sensor resolution, whereas the output gain is limited to twice the rated torque of the motor. There is no recommendation(s) as to how to calibrate the MFs and/or other scaling gains.

Later on, [116] used a heuristic approach to build the rule base but failed to provide useful recommendation on the choice of scaling gains and MFs. The authors in [117] and [118] used asymmetrical MFs with dense concentration near the origin to achieve precision control near the steady-state operating point and to avoid the need of increased number of MFs. Unfortunately, as in previous researches, the scaling gain calibration method was also not provided.

In 1996, a new FLC design methodology was proposed for brushless DC motors, where only the distribution of the output MF edges was adjusted [119]. In 1997 another FLC design was experimented on IFOC IM drive for speed tracking, disturbance rejection and parameter variations [23].

In this FLC, the rules were designed such that under disturbances, the rules near the center had the ability to quickly change the motor current to keep the speed at its reference value. Similar results were achieved in other studies with output MFs concentrated around the origin [118][119]. A method designed to reduce the size of the rule base was proposed in [25] with no mention of scaling gains.

One of the most complete FLC design methodologies is reported in [24]. Although the choices of the rule base and MFs are not fully justified, the approach provides sufficient recommendations for scaling gains calibration. Another design methodology of FLCs for IM drives with particular interest on the choice of scaling gains is reported in [100]. Here, the scaling gains are selected from an analogy between an FLC and a PI controller by linearizing the FLC around a steady-state operating point, following the recommendations of [120]. However, it was assumed that the mathematical model of the system is well known. This assumption was justified by the ability of FL to handle inaccurate or ill-defined models. In other words, if the mathematical model of the machine used to calibrate the parameters of the FLC is not as accurate as the real system, FLC is capable of handling the discrepancy between the real model and mathematical or approximate model.

In 2005, the authors of [101] provided some useful guidelines on the number and distribution of MFs for AC and DC drives. It was shown that a nonlinear distribution of the output MFs around the origin offers superior responses regardless of the input MF distributions. Similar observations were also found by other engineers such as [49][119][121]. There are other heuristic-based FLC design methodologies used for IM drives [93][122][123]–[125], permanent magnet drives [98][102][126], and DC drives [49][121][127]–[133]; with no particular justification on the way the parameters are calibrated or selected.

Another group of approaches lean toward the combination of FLC with some AI-based techniques, such as the neural network (Neuro-Fuzzy) [134][135][136], and Genetic Algorithm (GA) [103][137]. In these cases, AI techniques are used to optimize the rule base, the MFs or the scaling gains. The problem with rule bases or MFs generated by quantitative AI techniques is that often they lose their original linguistic interpretation [113][138]. Besides, for Neuro-Fuzzy for example, there is also the issue of availability of training data [135]. In many cases the collected (or available) training data require further manipulations before their use [135]. GA techniques on the other hand, are usually applied to optimize the scaling gains and MFs, or the union, according to a predefined performance index.

When reviewing the existing FLC design methodologies for AC and DC drives, the following remarks can be made:

(1) Many of the existing methods emphasize on either the logic-based or the control-based nature of FLCs;
(2) The methods do not provide a complete list of recommendation and details on how all the critical parameters (MFs, rule base, and scaling gains) of an FLC must be initialized;
(3) Although some of the methods (like the AI-based ones) prove to be successful under certain conditions, such control tuning methods are not simple enough in cases when the tuning must be done by less experienced field engineers; and
(4) The calibrations of FLCs are not always and totally subjective. Most of the calibration methodologies are dictated by common sense relating design requirements, control resolution and specification, and range of process variables.

Remarks (1) and (4) are the foundations on which the proposed design methodology relies on.

4.2.2. Calibration of a Non-adaptive FLC for IFOC IM Drives

There are three critical parameters of interest when designing Non-adaptive FLCs for motor drives:

(1) Input and output MFs (shape, number, and distribution),
(2) Rule base, and
(3) Input and output scaling gains.

The difficulty of design comes from the coupling of these parameters in the knowledge base. To overcome this difficulty, in this thesis, the design and calibration of the controller is carried out in two stages: (1) *Nominal Design* and (2) *Optimal Tuning*; following the hierarchical path described in Figure 4-3 [113]:

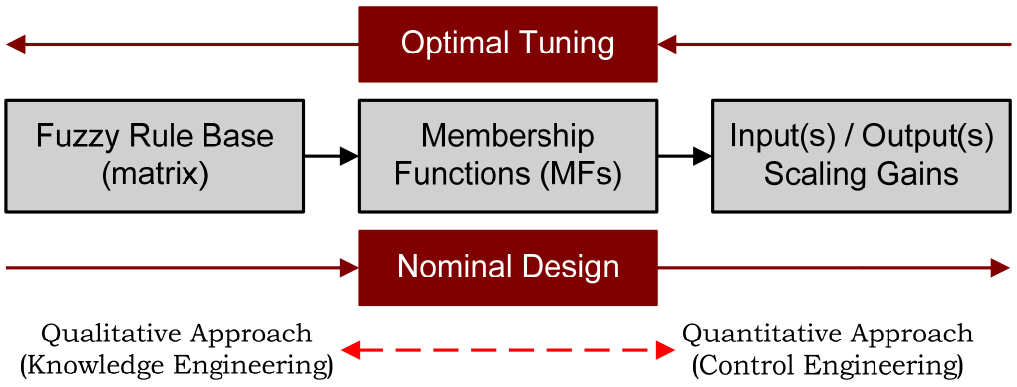

Figure 4-3: Hierarchical standard FLC design methodology

The Nominal Design approach is the left-to-right path, starting from qualitative (higher) level to quantitative (lower) level. It is the beginning stage of the design. It consists of finding the initial rule base (or the rule base matrix) and MFs; after which, the design effort is shifted to scaling gains. The scaling gain initialisation can be handled by some existing

quantitative approaches, using the available information about the system.

The Optimal Tuning is only useful if the Nominal Design is not satisfactory. It is accomplished by following the reverse order of the Nominal Design or by some other adaptive or optimal control systems. The proposed Non-adaptive FLC follows the Nominal Design path. Its Optimal Tuning is accomplished by the second controller, i.e. the proposed STFC. Using the Nominal Design path described in Figure 4-3, the Non-adaptive FLC for an IFOC IM drive can be designed using the following steps:

4.2.2.1. Fuzzy Rule Base

Due to its ability to bridge the gap between process dynamic and rule base, and its computation simplicity [45][139], the Heuristic method based on Phase-Plane analysis has found a wide acceptance in motor drive applications for rule base design [5][29][46][97][99][101][102][115][116][119][133]. The choice of Heuristic approach is also justified by the hierarchical methodology shown in Figure 4-3, according to which: at higher level, FLC are qualitative in terms of rule base. With the Phase-Plane approach, a rule base is built according to the general performance of control systems. By using such a generic approach the generated rule base is universal and less subjective.

Usually a time step response of a typical 2nd-order closed-loop system (see Figure 4-4.a) is used to derive the rule base [139]. Following Figure 4-4.a, the system response can be divided into:

(1) Four Areas: A1, A2, A3, A4
(2) Two Cross-over: b_1, b_2

(3) Two Peak-valleys: c_1, c_2.

The mapping of the response in terms of error (e) vs. its change (ce) constitutes the Phase-Plane of the system. It is shown in Figure 4-4.b for the case of a typical 2nd-order closed-loop system. Clearly the equilibrium point is the origin of the Phase-Plane trajectory. This particular feature of the equilibrium point will be exploited in later sections for the stability analysis of the Non-adaptive FLC and the STFC.

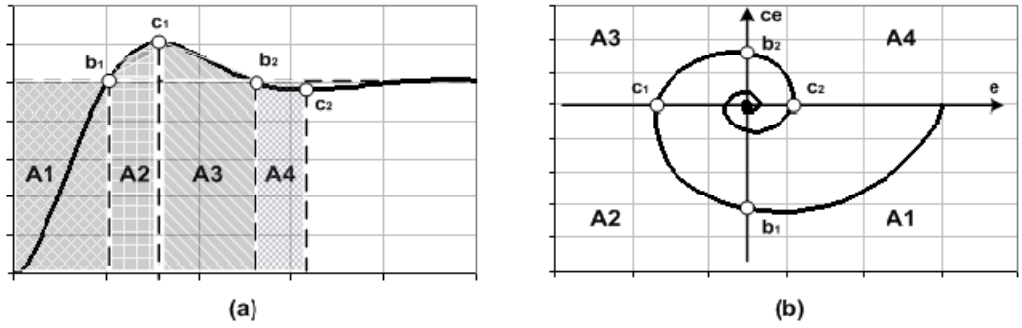

Figure 4-4: Step response of a typical 2nd–order system (a) and its Phase-Plane trajectory (b)

The 4 points described in Figure 4-4 (b_1, c_1, b_2, c_2) define all the possible step responses of a control system (including the system described in Figure 4-2). They can be used to define the frame of the rule base as follows [139][140]:

- If e and ce are zero, then maintain present control setting ($\Delta i_q^* = 0$).
- If conditions are such that e will go to zero at a satisfactory rate, then $\Delta i_q^* = 0$.
- If e is not self-correcting, then Δi_q^* should not be zero and should depend on the sign and magnitude of e and ce for e to be zero.

More details on statement (3) can be extracted by analyzing Figure 4-4.b; keeping in mind that the equilibrium point of the system is at the origin of the Phase-Plane trajectory. The reader is also referred to [138]–[142] for additional information on Phase-Plane method.

Nominal rule bases designed by the qualitative Phase-Plane approach are known to be symmetric and monotonic. They are also referred to as the *Generic MacVicar-Whelan Rule Base* [97][8][140].

To validate the approach, a Phase-Plane rule base was compared with an optimized (by Evolutionary Programming) one in a control system problem [138]. It was found that both approaches showed identical performances. In addition, the authors discovered that with symmetric-monotonic rule bases (i.e. with rule bases designed from Phase-Plane approach) the performance and robustness of FLCs stem from the property of driving the system into SMC in which the controlled system is invariant to parameter changes. This observation was also found in other studies [29][91][97][143]. This is because the structure of a system (whose rule base is designed by Phase-Plane) is changed each time the system's trajectory crosses either of the coordinate axis, as shown in Figure 4-4. In view of this, symmetric-monotonic rule base types (based on Phase-Plane trajectory approach) are highly recommended for Non-adaptive FLCs in the design methodology proposed in this thesis.

Without loss of generality, Table 4-1 shows the symmetric-monotonic rule base used for the investigated IM drive. The linguistic terms are defined as:

NVB: Negative Very Big	NS: Negative Small	PM: Positive Medium
NB: Negative Big	ZE: Zero	PB: Positive Big
NM: Negative Medium	PS: Positive Small	PVB: Positive Very Big

Table 4-1: Rule base of the proposed Non-adaptive FLC

Δi_q^*		error, $e(t)$						
		NB	NM	NS	ZE	PS	PM	PB
change-in-error $ce(t)$	NB	NVB	NVB	NVB	NB	NM	NS	ZE
	NM	NVB	NVB	NB	NM	NS	ZE	PS
	NS	NVB	NB	NM	NS	ZE	PS	PM
	ZE	NB	NM	NS	ZE	PS	PM	PB
	PS	NM	NS	ZE	PS	PM	PB	PVB
	PM	NS	ZE	PS	PM	PB	PVB	PVB
	PB	ZE	PS	PM	PB	PVB	PVB	PVB

Clearly, there is symmetry of linguistic terms with respect to the origin of the Phase-Plane and a monotonic increase in linguistic terms from left to right (or top to down). Note that the rule base) is a 7 x 7 matrix; meaning that the input variables "error" (e) its change (ce) are each characterized by 7 fuzzy subsets with 7 MFs. The output variable Δi_q^* is defined by 9 fuzzy subsets with 9 MFs. The number of input and output MFs can be different than the ones without affecting the property of Phase-Plane trajectory approach. The number, distribution and shapes of the MFs are discussed in the next step of the Nominal Design path.

4.2.2.2. Membership Functions

By using the input and output scaling gains, linguistic variables are confined within ±1p.u. (or base value). In this case, the universes of discourse of the variables can be determined by the scaling gain values and the design of the MFs can be reduced to their (1) shapes or types, (2) number, and (3) distribution.

There are many types of MFs. There are also provisions to custom-design MFs in some FLC software tools. For example, in many Neuro-Fuzzy

applications, the sigmoid MFs have been found to be very useful in training FLCs. Sometimes, the input MFs can be different from the output ones, as a result of Neuro-Fuzzy processing techniques. With the advent of global optimization techniques, such as GA and other evolutionary techniques, MFs have also been optimized and automated. Although there are no doubts that these AI techniques can generate *optimal* MFs, often their designs are difficult to interpret meaningfully and linguistically [138].

In the theoretical analysis of FLCs, MFs have not received as much attention as other parameters (i.e. scaling gains and rule base). One of the rare sensitivity analyzes of MF shapes for IM drives are reported in [141][144]. In these studies, an FLC is implemented with different types of input and output MFs of symmetrical and equal distribution, using a symmetric-monotonic rule base. It was found that the triangular MFs offer the best drive performances in addition to their computation efficiency. Such conclusions were also reached in other studies conducted for speed control of AC and DC drives [5][23][24][33][44][46][49][101][104][110][141][145]. It is for this reason that triangular MFs are also recommended and used in the proposed design methodology.

The number of MFs influences the control performance of the drive. More MFs usually leads to improved performances. The number of output MFs does not affect the rule base size but influences its richness content. The size of the rule base is determined by the number of MFs of the input variables. Research and experiments have demonstrated that the speed responses of motor drives are not improved further if the number of input MFs is increased beyond seven and that of the output beyond eleven [46][101][131]. In addition, the greater the number of input MFs, the bigger the rule base size, and the greater the DSP memory requirement. For this reason, it is recommended to use a 7 x 7 matrix for

the rule base [5][46][101][131]. This justifies the size of the rule base proposed in Table 4-1.

Figure 4-5 shows the input and output MFs for the proposed Non-adaptive FLC before the distribution factor effect is investigated.

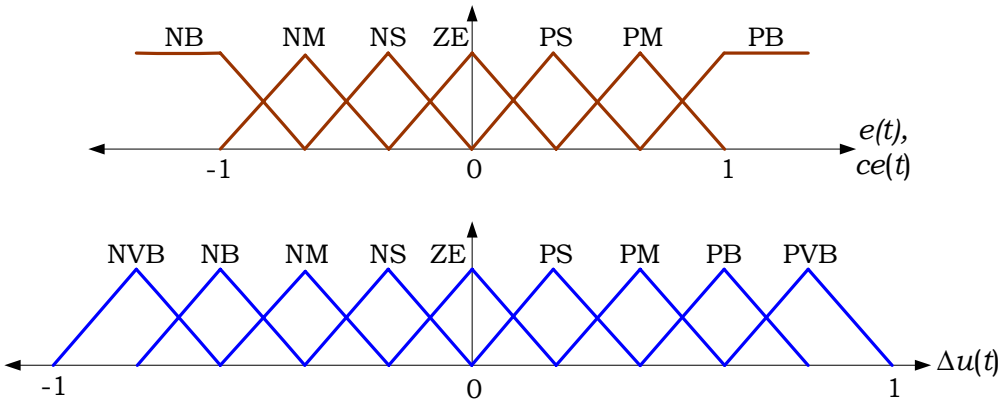

Figure 4-5: MFs of the Non-adaptive FLC for IFOC IM drives

MF distribution effect is often evaluated by the so-called *Distribution Factor* (σ). To include this factor in triangular MFs, they are often described by the set [*Left-foot*; *Peak*; *Right-foot*]. Without loss of generality, the nonlinear distribution of the output MFs described in Figure 4-5 can be represented as:

NVB: [-1; -1; (-3/4 + σ)]
NB: [-1; (-3/4 + σ); (-1/2 + σ)]
NM: [(-3/4 + σ); (-1/2 + σ); (-1/4 + σ)]
NS: [(-1/2 + σ); (-1/4 + σ); 0]
ZE: [(-1/4 + σ); 0; (1/4 - σ)]
PS: [0; (1/4 - σ); (1/2 - σ)]
PM: [(1/4 - σ); (1/2 - σ); (3/4 - σ)]
PB: [(1/2 - σ); (3/4 - σ); 1]
PVB: [(3/4 - σ); 1; 1]

If $\sigma = 0$, the fuzzy set is said to be *linearly* or symmetrically distributed. This is the case shown in Figure 4-5. If $\sigma < 0$, the fuzzy set is said to be *divergent* with nonlinear or asymmetric distribution. Finally if $\sigma > 0$ the fuzzy set is said to be *convergent*, also with nonlinear or asymmetric distribution.

It is well known that linear control surfaces are often inadequate for nonlinear processes. They result in poor performances compared to nonlinear control surfaces [130][145]. For this reason, when dealing with highly nonlinear systems in FLC, most engineers adopt for nonlinear triangular MFs to cope with real nonlinear control problems [49][101][127][131][145]. Intuitively the closer the control response to the set point, the narrower the MFs range should be. This means that for *optimal* design of an FLC, σ should be selected based on the "degree" of nonlinearity of the control system.

The effects of distribution factor (σ) on drive performances have already been experimentally investigated for a pendulum-car [145], DC motor drives [119][121][130], and AC motor drives [101][144]. A number of useful recommendations have been made [101][119][121][129][141][145]. Unfortunately, many modern FLC designs are failing to incorporate such recommendations. For example, the simulation and experimental tests performed in [101] clearly showed that a Non-adaptive FLC with linear (inputs and output) distribution can also provide an excellent speed control performance with sufficient number of output MFs (up to 11). However, the performance of the drive with linear distribution will be achieved at the expense of excessive current harmonics (due to poor regulation of i_{qs}^{*}), as a result of linear MF distribution. If the system inertia is small, the current ripple can generate significant torque ripples. In contrast, when the authors used nonlinear distributed output MFs, a significant decrease of current harmonics was observed; making the controller less sensitive to parameter changes by compromising the speed

performance slightly. It was also seen that the distribution range of the output fuzzy sets should be wide during transient operations so that i_{qs}^{*} can vary quickly and the motor can track the reference speed. It should be small during steady-states so that Δi_{qs}^{*} is small, and i_{qs}^{*} can be controlled with little ripples. This was accomplished by a self-tuning mechanism for the output scaling gain.

In order to incorporate the recommendations of [101] in the proposed design, the distribution factor (σ) was set to 0.1 (validated by simulations). This value represents a compromise between the speed response and current harmonics. Figure 4-6 shows the proposed nonlinear output MFs after the distribution factor is included.

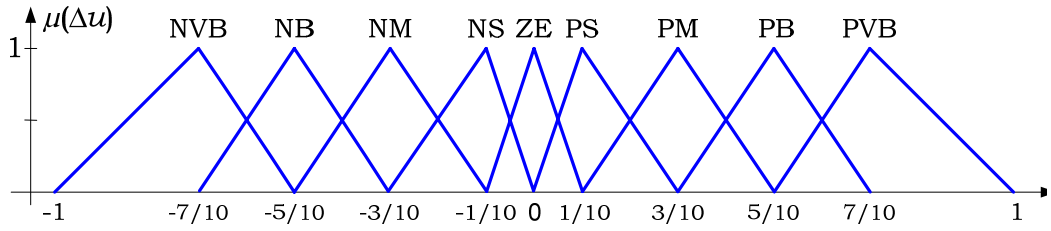

Figure 4-6: Output MFs of the Non-adaptive FLC for FOC IM drives

4.2.2.3. Scaling Gains

So far it has been shown that 7 input MFs for each input variable and 9-11 output MFs with a distribution factor of 0.1 may be sufficient, that the *Mac Vicar Whelan* rule base is suitable for motor drive applications, that the minimum inference gives nonlinear features for the controller, and that the CAV method for defuzzification gives a reliable decision table due to its computational efficient, continuous, and plausible features [42]. Now the remaining (Nominal) Design effort can be shifted to the initialisation the scaling gains.

Following the hierarchical methodology (Figure 4-3), the scaling gains are at the lowest level of FLC design; corresponding to quantitative approach. Therefore, an "optimal" design of scaling gains must incorporate a quantitative control engineering approach.

There are 3 approaches used for setting the scaling gains for AC and/or DC motor drives:

(1) The expert knowledge [23][25][27][93][98][101],
(2) The position encoder (or speed sensor) resolution [99][115][116],
(3) The available information of the system [24][46][97][119].

Since at the level of scaling gains FLCs are quantitative, methods (2) and (3) are preferred. Method (3) is selected for the proposed methodology since it is based on the information of the motor drive itself. In this thesis, the scaling gains are computed according to the starting procedure of IMs following a sudden step speed command at rated and constant flux. Under this condition, the scaling gain of the variable "error" can simply be defined by the rated rotor speed of the motor as

$$n_e = 1/\omega_{r\_nom} \tag{4.5}$$

where ω_{r_nom} is the nominal or rated rotor speed in [rpm]. The scaling gain of variable "error" (e) in (4.5) is chosen such because the input scaling gains results in scaling the horizontal axis of their respective MFs by inverse of their value (i.e. $1/n_e$) [44]. Same rule will be applied to the scaling gain of variable change-in-error (ce).

The scaling gain of the variable "change-in-error" (ce) can be deduced from the mechanical description of the drive, referring to equation (4.1). Neglecting load and friction, and replacing the torque constant (K_t) by the expression given in equation (1.40), the discrete form of (4.1) can be written as [21]:

$$\frac{2}{P}J\frac{\omega_r(n+1)-\omega_r(n)}{\Delta T}=\frac{3}{2}\frac{P}{2}\frac{L_m^2}{L_r}i_{ds}^{e}i_{qs}^{*} \tag{4.6}$$

The maximum speed variation during a sampling time ΔT is

$$\Delta\omega_r^{max}=\frac{\Delta T}{J}\frac{3}{2}\frac{P^2}{4}\frac{L_m^2}{L_r}i_{ds}^{max}i_{qs}^{max} \tag{4.7}$$

where $i_{ds}^{max}=i_{ds}^{*}$ is the reference flux-component current, estimated at 40% of nominal current [38], and i_{qs}^{max} is the maximum allowable value of the q-axis or torque-component current, estimated at twice the rated current [24][119]. Assuming constant reference speed operation or steady-state conditions, the change-in-error can be expressed as

$$ce(n)=e(n)-e(n-1)=-\omega_r(n)-\omega_r(n-1)=-\Delta\omega_r(n) \tag{4.8}$$

Using equations (4.7) and (4.8), n_{ce} can be determined as

$$n_{ce}=\pm 1/\Delta\omega_r^{max} \tag{4.9}$$

The output scaling gain is computed from equation (1.17), which can be written for i_{qs}^{e} as

$$i_{qs}^{e}=\frac{\lambda_r L_r}{L_m r_r}(\omega_s-\omega_r)=\frac{L_m i_{ds}^{e}L_r}{L_m r_r}(\omega_s-\omega_r) \tag{4.10}$$

From equation (4.10), it is possible to obtain the discrete q-axis torque component current expression able to maintain constant slip speed:

$$\frac{\Delta i_{qs}^{e}}{\Delta T}=-\frac{L_r}{r_r}i_{ds}^{e}\frac{\Delta\omega_r}{\Delta T} \tag{4.11}$$

To guarantee a maximum acceleration during the motor start-up, the speed FLC output can be computed from (4.11). In that case, equation (4.11) becomes

$$\left(\frac{\Delta i_{qs}^{e}}{\Delta T}\right)^{max} = \left(\frac{\Delta i_{qs}^{*}}{\Delta T}\right)^{max} = n_u = \frac{3}{2}\frac{P^2}{4}\frac{L_m^2}{r_r}\frac{1}{J}(i_{ds}^{max})^2 i_{qs}^{max} \quad (4.12)$$

Equation (4.12) represents the output scaling gains of the proposed Non-adaptive FLC. It is defined such (as opposed to the input scaling gains) because there is a proportional effect between the output scaling gain and the output MFs [44].

Equations (4.5), (4.9), and (4.12) complete the Nominal Design path, and hence the selection and initialization of the three major components of an FLC. The Optimal Tuning of the controller, as stated earlier, will be necessary only if the Nominal Design fails to meet the performance requirements of the drive system. This will be verified after a series of simulations and experimental tests.

4.3. Performances of the Proposed Non-adaptive FLC

The effectiveness of the proposed design methodology was verified through simulations and experimental tests. Its performances were evaluated with that of a PI controller, designed according to Ziegler-Nichols method. Both controllers were incorporated alternatively in the IFOC IM drive scheme described in Figure 1-8. The PI gains initially calculated according to equation (4.3) and subsequently tuned during simulations in order to obtain satisfactory steady-state and dynamic responses. Their final values were set at 21.60 and 0.6786 for the proportional and the integral gains, respectively.

The FLC scaling gains were computed according to (4.5), (4.9), and (4.12). The sampling rate was set at $\Delta T = 0.001$sec for both controllers (PI & FLC). The CAV method was used to compute for the output variable with the rule base matrix provided in Table 4-2. The MFs of the FLC are the same as the ones reported in Figs 4.5 and 4.6 for the input and the

output variables, respectively. The nominal parameters of the investigated IM are summarized in Table 1-1.

Figure 4-7 shows the speed responses of the FLC and PI controller following a sudden step change in reference speed from 1200rpm to 1650rpm (at 1.5sec) at full load (1.0p.u.). The results show that the PI has a very small (negligible) overshoot and as a result, the FLC response is slightly faster than the PI controller in terms of settling time. It was possible to reduce the settling time of the PI controller as well, but at the expense of its transient response (by increasing its overshoot percentage slightly).

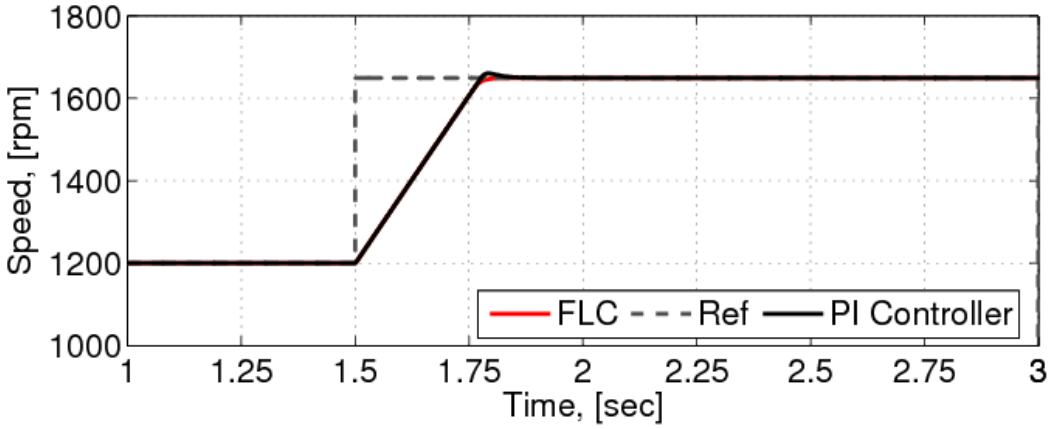

Figure 4-7: Simulated FLC and PI speed responses due to sudden change of speed reference from 1200rpm to 1650rpm at full load

The torque-component current responses are shown in Figure 4-8. They show that the FLC needs less current to track the speed reference. In other words, the FLC torque response is slightly faster than the PI controller. Finally, the flux-component currents are shown in Figure 4-9; indicating that both controllers are able to maintain decoupled field control and constant flux operations under sudden reference speed change at full load.

The results of Figs 4.7-4.9 show that two controllers perform in a similar way, as far as their settling time and overshoot percentages are concerned.

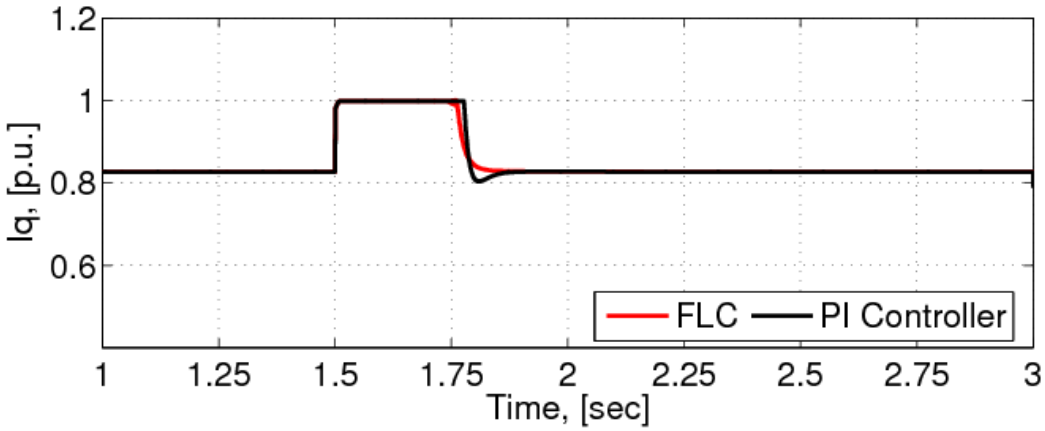

Figure 4-8: Simulated FLC and PI responses of torque component currents due to sudden change of speed reference from 1200rpm to 1650rpm at full load

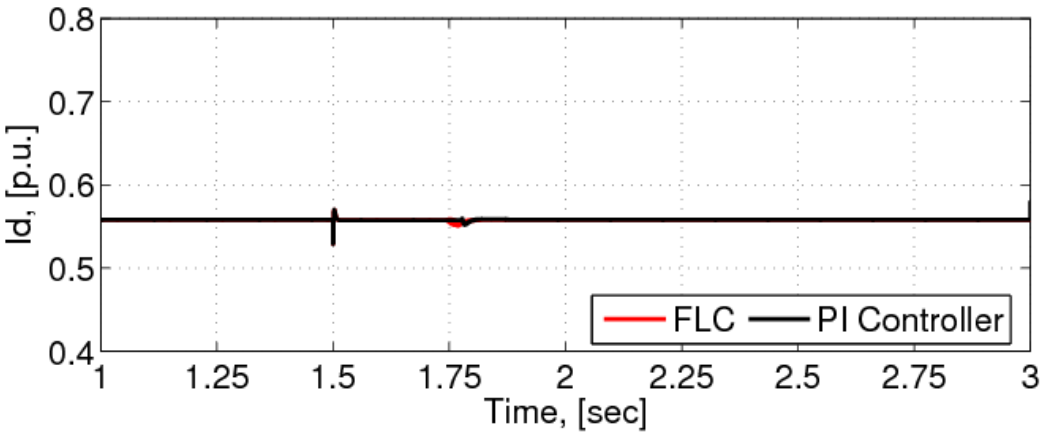

Figure 4-9: Simulated FLC and PI responses of flux component currents due to sudden change of speed reference from 1200rpm to 1650rpm at full load

Next, a sudden change of speed reference from 1650rpm to 1200rpm is applied at 1.42sec at full load. This is shown in Figs 4.10-4.12. This time, the responses of the proposed FLC are definitely faster than the PI controller which exhibits a speed overshoot of approximately 30rpm. The

torque- and flux-component current responses are shown in Figs 4.11 & 4.12, respectively. As it can be seen, the torque capability of the proposed FLC is higher than that of the PI controller. Their flux-component current responses show that it is possible to maintain constant flux operation with both controllers under sudden reduction of speed reference at constant and full load torque.

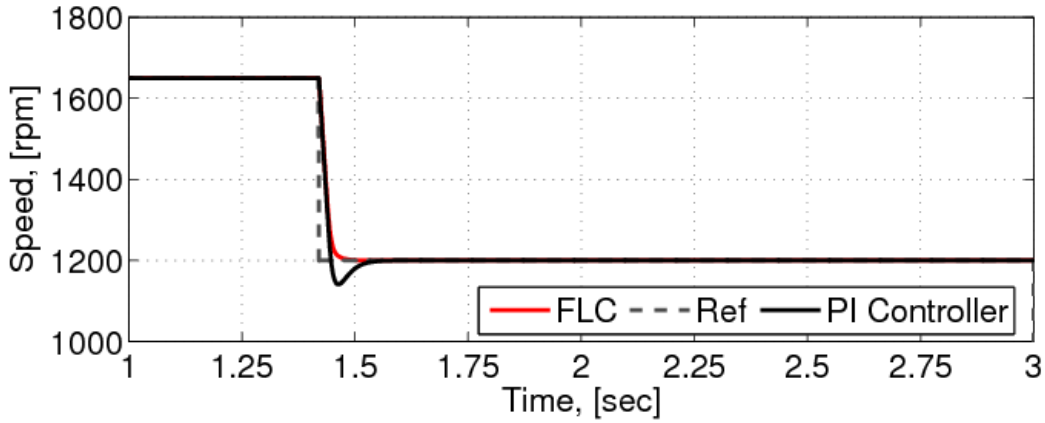

Figure 4-10: Simulated FLC and PI speed responses due to sudden change of speed reference from 1650rpm to 1200rpm at full load

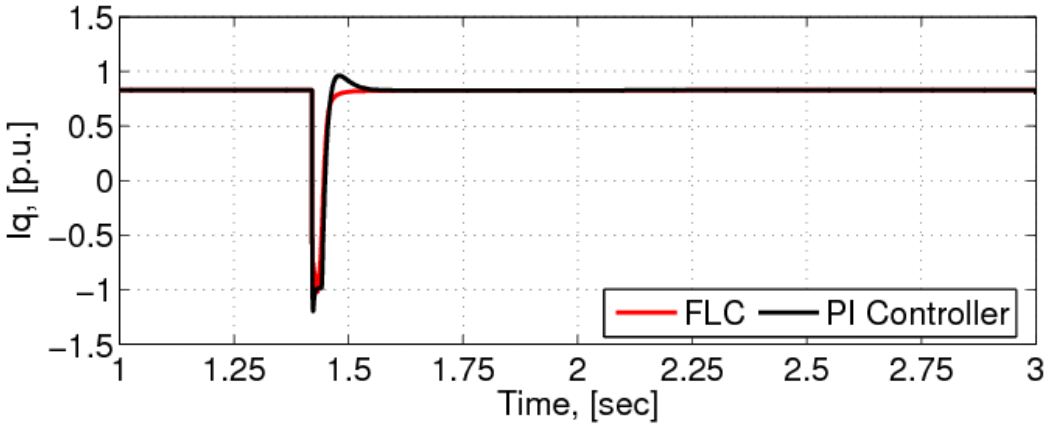

Figure 4-11: Simulated FLC and PI responses of torque component currents due to sudden change speed reference from 1650rpm to 1200rpm at full load

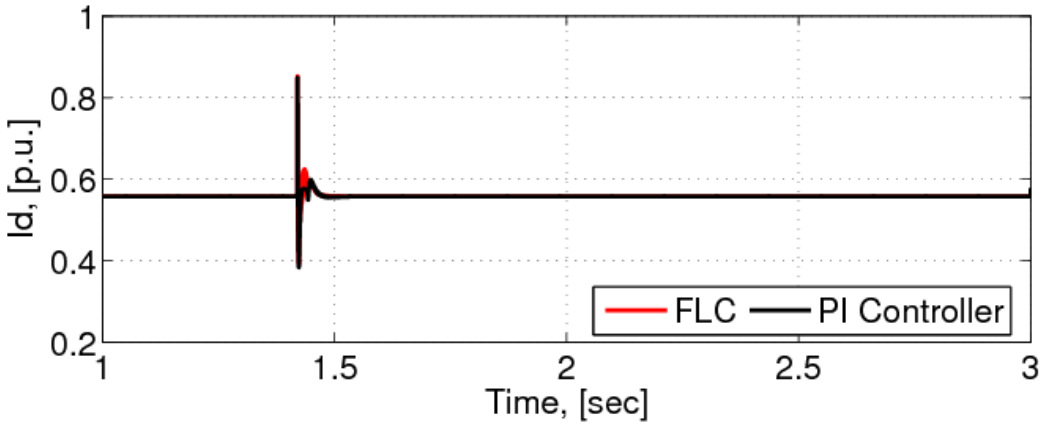

Figure 4-12: Simulated FLC and PI response of flux component currents due to sudden change speed reference from 1650rpm to 1200rpm at full load

The abilities of the controllers to reject load disturbances at constant speed operation are investigated in Figs 4.13-4.15. The drive was initially operated at 1500rpm with no-load. A sudden increase in load from zero to 85% is applied after 2.10sec. The results show that the dynamic performances of the proposed FLC are significantly better than those of the PI controller for the speed and torque. Once again, both controllers are able to maintain constant flux operation, as expected.

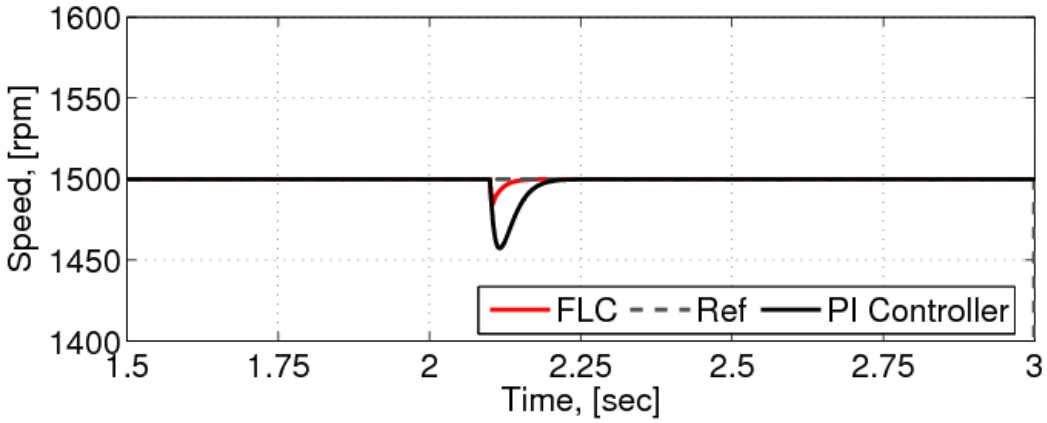

Figure 4-13: Simulated FLC and PI speed responses to sudden application of 85% load at constant speed of 1500rpm

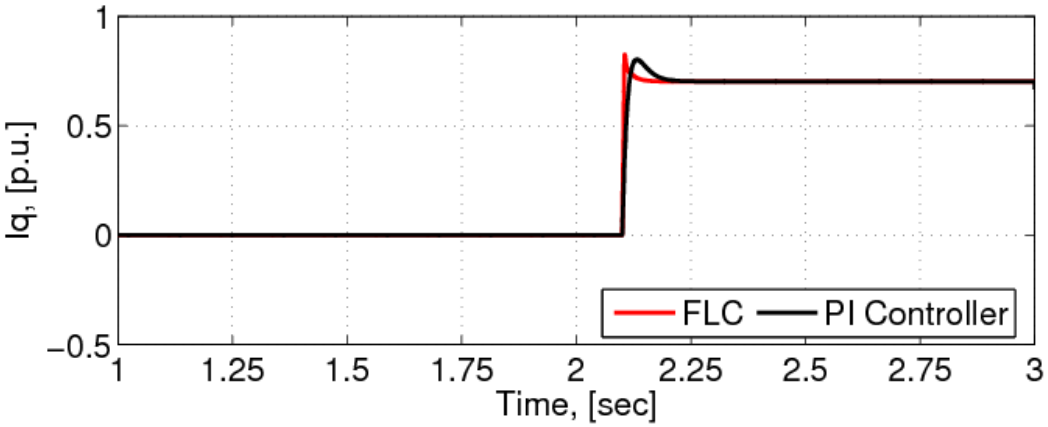

Figure 4-14: Simulated FLC and PI speed responses to sudden application of 85% load at constant speed of 1500rpm

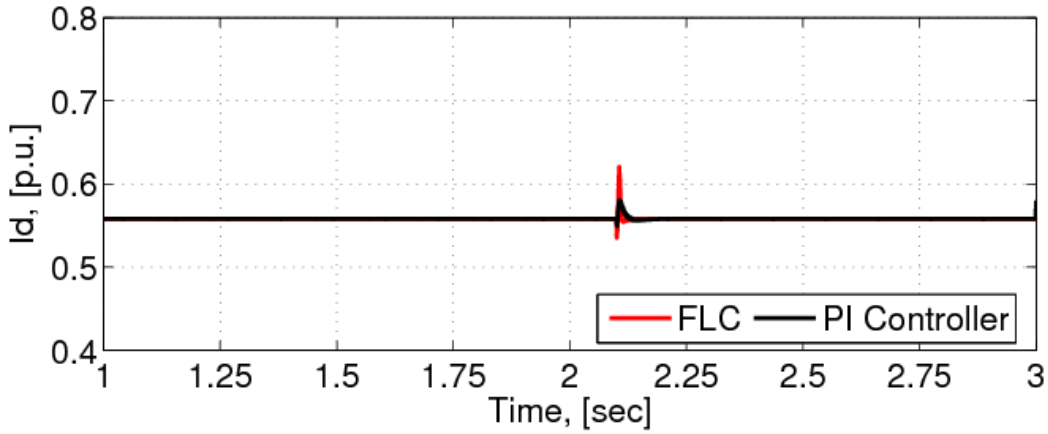

Figure 4-15: Simulated FLC and PI flux component current responses to a sudden application of 85% load at 1500rpm

So far the simulation results can be used to validate the Nominal Design of the proposed FLC for IFOC IM drives. By using the methodology described in this chapter, the design of the FLC is less subjective and dictated by fundamental concepts of control and motor operation. If necessary, it is possible to improve the design by employing the Optimal Tuning. This objective is rather assigned to the second proposed controller, i.e. the STFC.

A laboratory prototype was set to verify the validity of the proposed FLC design methodology experimentally. It consists of a DSP driving board, a control PC, a DC generator mechanically coupled to an IM, and a switching load resistor box. The IM is indirectly loaded through the DC generator by changing the values of the resistors electrically connected to it. A 600V, 20A, 3-phase IGBT inverter is used as power stage with 330V_{DC} rectifier output. The control board includes Analog Devices with 16-bit EZ-KIT fixed-point DSP.

The motor currents are measured by 2 LEM sensors and processed by a 12-bit A/D Converter. The rotor speed of is sensed by a 60-bit/revolution sensor (designed at the Power Lab/University of Alberta). It is well known that the use of speed sensors in place of position encoders in IFOC results in extra offsets, which may contribute to non-ideal IFOC [6]. The control algorithms are implemented with an ADMC21992 160-MHz DSP, using Assembly code.

The PWM switching pattern is generated with 10kHz switching frequency using a SV-PWM modulation technique. The internal data of the DSP are displayed through an 8-channel 12-bit D/A Converter. The sample data are transferred into a Tektronix scope and captured as .csv files for plotting purposes. During the experimental tests, the responses of the FLC and that of the PI controller were not synchronized. They are plotted together in some figures for comparison purposes only.

Figs 4.16-4.18 show the experimental responses of the controllers similar to the situation simulated in Figs 4.7–4.9. Clearly, the proposed FLC outperforms the PI controller in terms of speed and torque responses. The settling times of the controllers for speed (Figure 4-16) are evaluated at approximately 0.50sec and 0.625sec for the FLC and the PI controller, respectively. Both controllers exhibit no overshoot although the PI controller showed a small percentage of overshoot in the simulated cases.

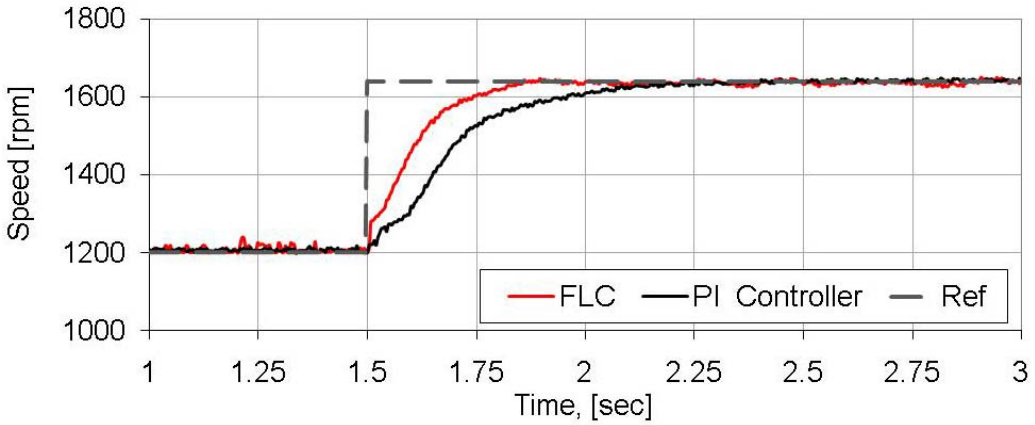

Figure 4-16: Experimental FLC and PI speed responses to sudden change of speed reference from 1200rpm to 1650rpm at full load torque

Figure 4-17 shows that in spite of sudden change of speed reference, both controllers are able to maintain constant rotor flux operation, with an overshoot of approximately 0.25sec. Figure 4-18 also shows torque can be properly controlled with the two controllers under sudden speed reference changes.

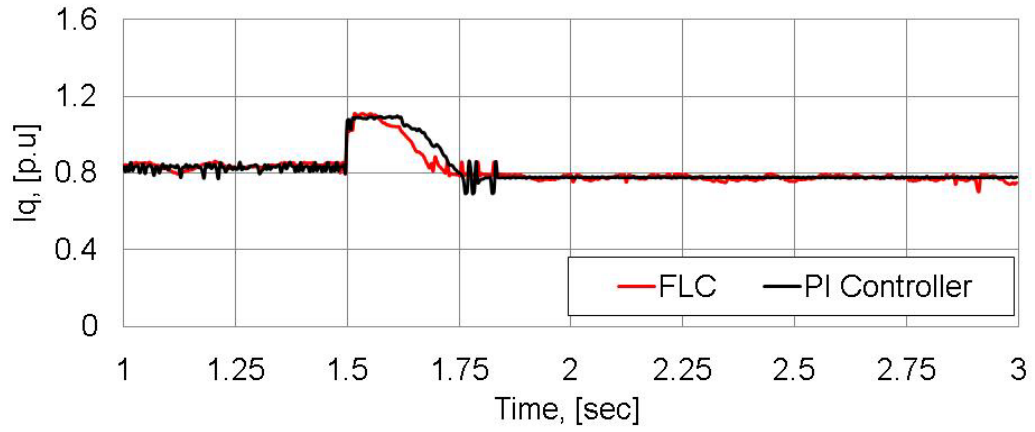

Figure 4-17: Experimental FLC and PI responses of torque component currents to sudden change of speed reference from 1200rpm to 1650rpm at full load torque

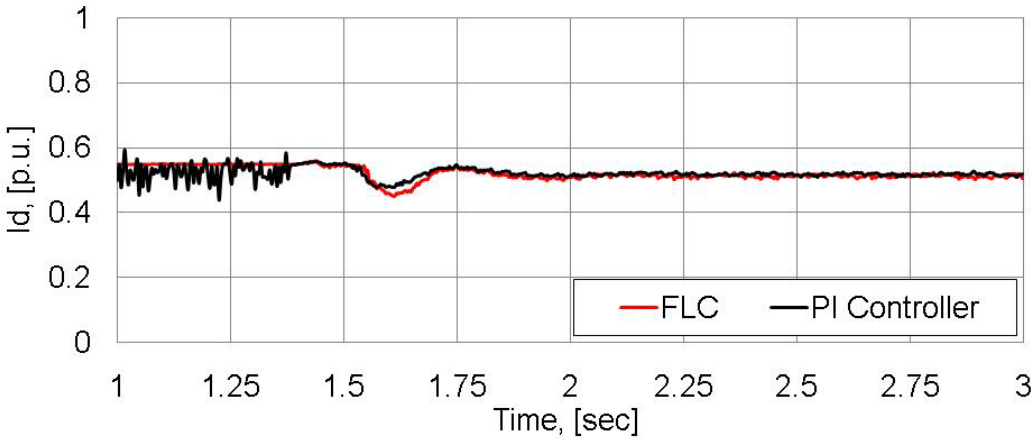

Figure 4-18: Experimental FLC and PI responses of flux component currents to sudden change of speed reference from 1200rpm to 1650rpm at full load torque

The ability of the controllers to track the speed reference was also investigated for the case of sudden reduction of speed from 1650rpm to 1200rpm at full load torque. The results are shown in Figs 4.19-4.21. The speed response of the proposed FLC (Figure 4-19) has no undershoot compared to that of the PI controller. Their settling times are slightly longer compared to the case of sudden increase of speed (Figure 4-16). As a result, their torque disturbances (Figure 4-20) are smaller than in the previous case; with the FLC showing a smaller undershoots percentage than the PI controller. Here, as in the previous case, constant rotor flux is also possible with the two controllers (Figure 4-21).

Finally, the ability of the drive to reject a load disturbance was also investigated experimentally. This is shown in Figs 4.22-4.24. The drive was started and operated at 1500rpm with no load (except for the DC generator coupled to the investigated IM). After approximately 2.05sec a sudden application of 85% rated load was applied. The speed responses of the controllers are shown in Figure 4-22. It can be seen that the proposed FLC is indeed faster than the PI controller, with no overshoot percentage.

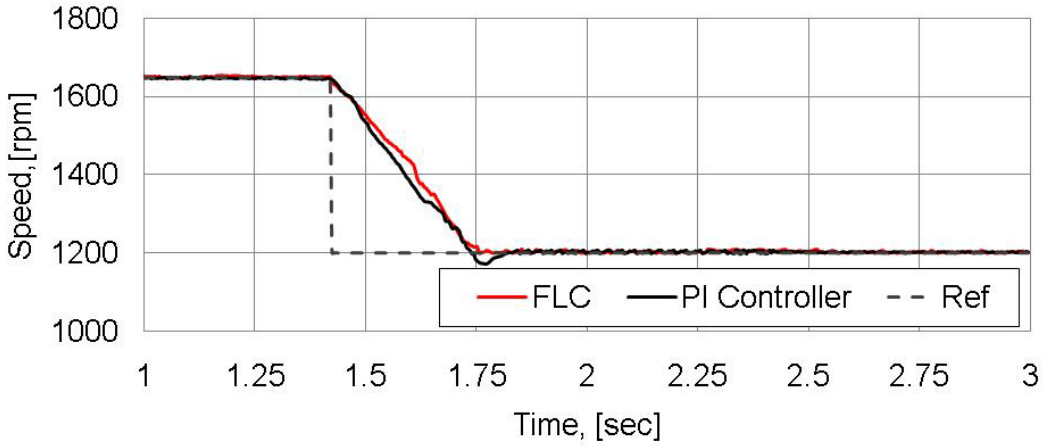

Figure 4-19: Experimental FLC and PI speed responses to sudden change of speed reference from 1650rpm to 1200rpm at full load torque

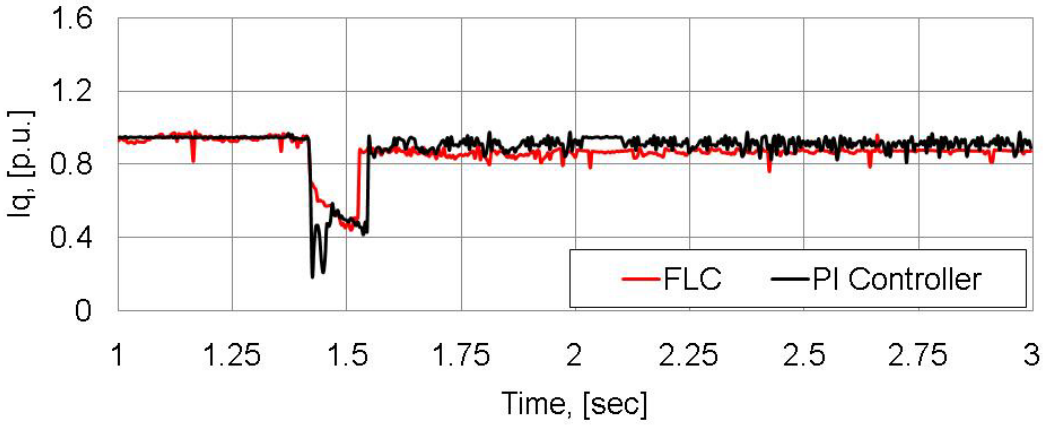

Figure 4-20: Experimental FLC and PI responses of torque component currents to sudden change of speed reference from 1650rpm to 1200rpm at full load torque

The torque responses of the drives are shown in Figure 4-23, where the values are shifted up by 1.0p.u. The FLC exhibits better steady-state performance compared to the PI controller. The flux characteristics plotted in Figure 4-24 show that both controllers can maintain constant rotor flux operation under severe load perturbations at constant speeds.

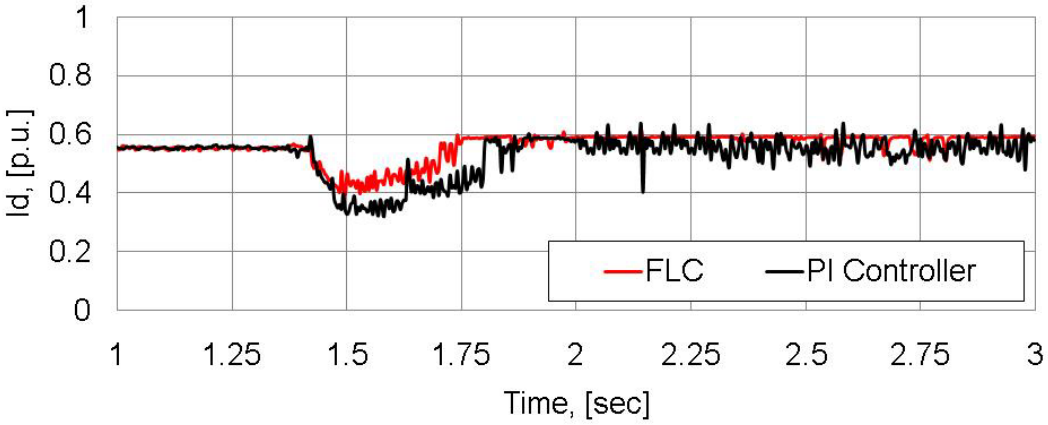

Figure 4-21: Experimental FLC and PI responses of flux component currents to sudden change of speed reference from 1650rpm to 1200rpm at full load torque

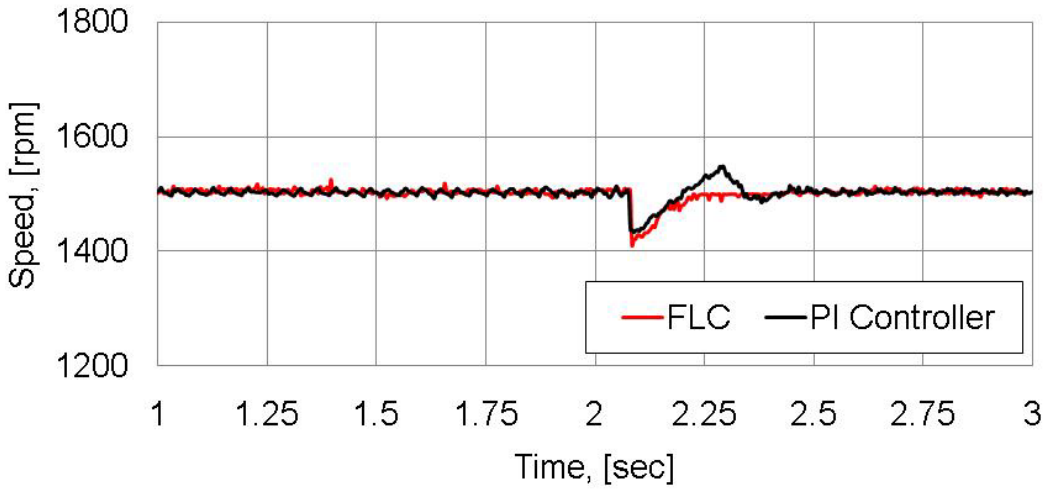

Figure 4-22: Experimental FLC and PI speed responses to sudden application of 85% load torque at constant speed of 1500rpm

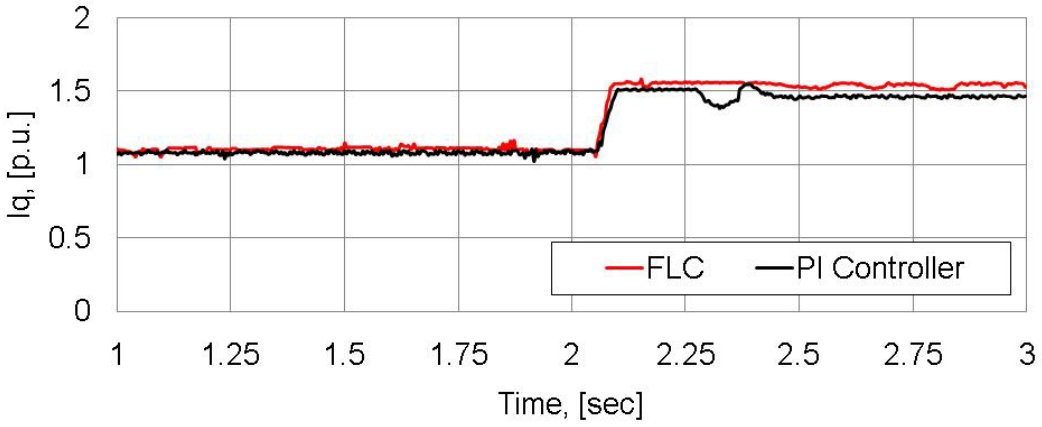

Figure 4-23: Experimental FLC and PI responses of torque component currents to sudden application of 85% load torque at constant speed of 1500rpm

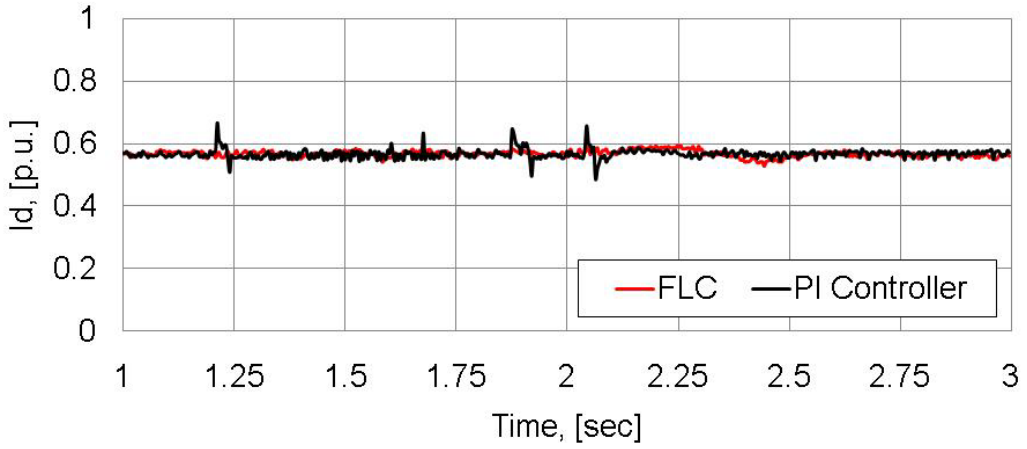

Figure 4-24: Experimental FLC and PI responses of flux component currents to sudden application of 85% load torque at constant speed of 1500rpm

Based on the simulation and experimental results obtained, the following conclusions can be made about the proposed FLC design methodology:

(1) Although the performances of FLCs are similar to that of conventional SMCs for FOC IM drives [29], the proposed FLC design approach is more straightforward than that of SMCs. The responses of the torque-component currents for all investigated cases show that it is possible to improve the performance of the

proposed FLC with additional scaling gain tunings, by allowing more current consumption for short periods of time during transients. This could have been done by using the Optimal Tuning path. However, even without the Optimal Tuning, the proposed methodology showed excellent performances in terms of speed tracking and load rejection capabilities.

(2) A significant reduction in the design time and tuning effort can be obtained with the proposed methodology compared to trial-and-error methods that are often used to tune FLCs.

(3) The method proposed is adaptable to any size of IMs operating with FOC scheme. This is possible by simply updating or calculating the scaling gains using the Nameplate information of the motor. The rule base and MFs can be designed exactly recommended in this thesis. If an Optimal Tuning is require, the designer may do so by following the hierarchical path described in Figure 4-3

The scaling gains of the proposed FLC depend on the parameters of the motor used. Although FLCs have the ability to handle ill-defined system, it is important to point out that if the motor parameters deviate significantly from their rated or instrumented values, the drive performance may also be affected to some degrees. For example, consider the motor inertia (J) which is one of the parameters in computing the change-in-error and output scaling gains, according to equations (4.7) & (4.12). The motor inertia is rarely constant in many industrial applications. For a fixed-gain controller, an increase of the J will reduce the loop gain; deteriorating the dynamic and steady-state performances of the system. Similarly, a sudden increase of load torque or motor inertia will temporarily reduce the speed until it is compensated by sluggish speed loop [5].

These effects of motor inertia are shown in Figure 4-25 and Figure 4-26 for the speed and torque-component current responses of the proposed FLC and PI controller. FLC-1 & PI-1 represent situations where the instrumented J (in the FLC) is equal to its rated and real value (in the IM). FLC-2 and PI-2 are situations where the instrumented J is twice its rated value.

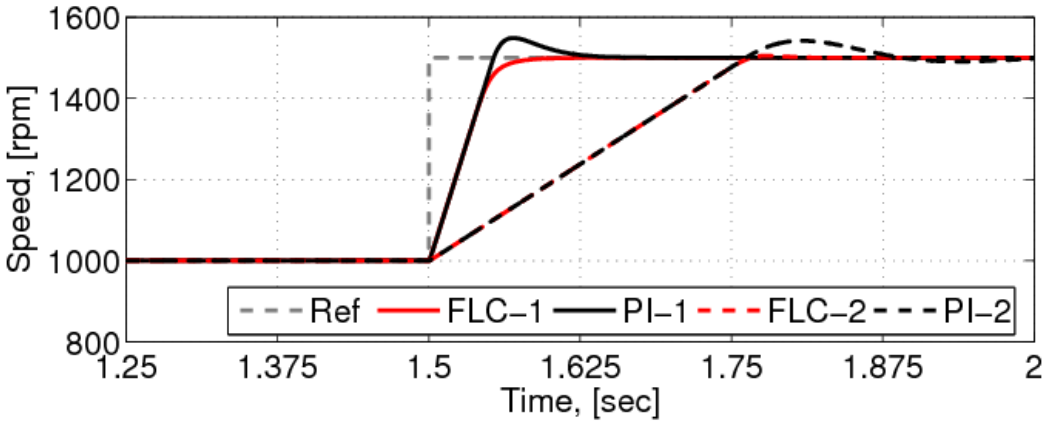

Figure 4-25: Speed responses of FLC and PI controller to a sudden change of speed under various motor inertia at constant speed and load

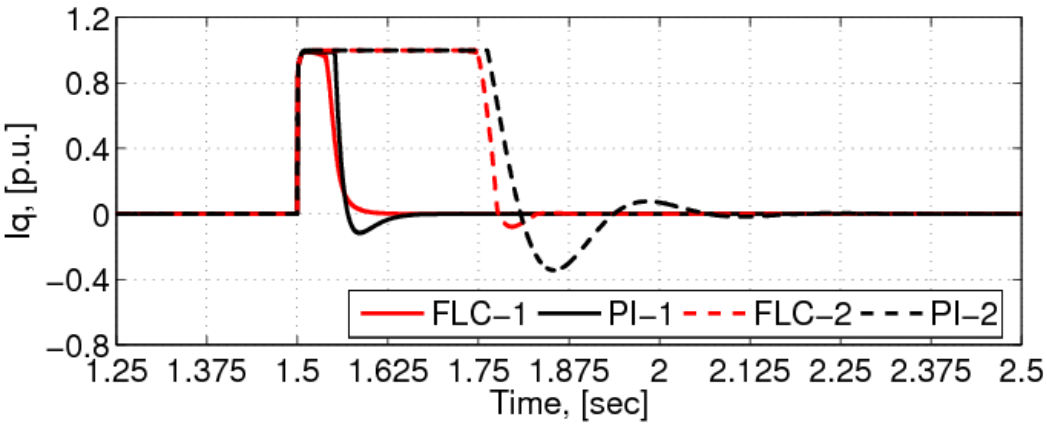

Figure 4-26: FLC and PI Controller torque component current responses to a sudden change of speed under various motor inertia at constant speed and load

It can be seen that when *J* is increased (or doubled in this case), the speed responses (Figure 4-25) of both controllers are affected severely. Their settling times are increased, with the PI controller showing the worse case. The FLC showed no overshoot or undershoot. Figure 4-26 shows that when *J* is increased, the torque capability of the drive is also affected; with the proposed FLC still offering better responses than the PI controller.

The effect of parameter change can be reduced by a high-gain negative feedback loop, especially for PI controllers. However, excessive gain may lead the system to an under-damping or instability condition. For the FLC, an Optimal Tuning approach can be used to further calibrate the scaling gains or the rule base, or the union to compensate for any parameter or operating condition change.

Beside the issue of parameter changes affecting the initial setting of the scaling gains of an FLC, there is also the issue of availability of motor parameters. It is very difficult to compute for the scaling gains adequately if the motor parameters are not available a priori. In this case, the designer often relies on experience and trial-and-error methods to calibrate the controller. Such approaches result in excessive design time and luck systematic design methodologies.

The problem of parameter variations and available information about the drive are solved by the STFC proposed in this thesis. Here, a very simple self-tuning mechanism is incorporated in the proposed Non-adaptive FLC. This mechanism is designed to tune the scaling gains of the controller according to the current trend of the system. By doing so, the STFC increases the use of the drive for applications where the system must operate under many uncertain conditions and where the available a priori information about the system is limited. The performance of the STFC does not heavily depend on complete information about IM

parameters at start-up (since the drive can be started with unity scaling gains). However, in some cases, if transient time needs to be shortened, the available motor parameters can be utilized in the controller determine the initial scaling gains according to proposed design methodology for scaling gains calibration.

4.4. Self-Tuning Fuzzy Control (STFC) of IFOC IM Drives

A self-tuning FLC can be developed by applying a tuning algorithm to directly adjust: (1) the MFs, (2) the rule base, and/or (3) the scaling gains. The tuning of scaling gains in real time has received the highest priority in literature due to their influence on performance and stability of systems [28][142]. It is for this reason that they constitute the first step of the Optimal Tuning path.

Equations (4.9) and (4.12) are also good indicators of the necessity of tuning the scaling gains of an FLC online. This is of particular interest when the system must operate under wide ranges of parameter and operating condition changes. The self-tuning controller introduced in this thesis utilizes the MRAS approach combined with FLC principles. The tuning mechanism is based on a desired control objective provided at each time step. The following paragraphs outline the idea behind the approach.

The structure of the proposed STFC is described in Figure 4-27. It consists of an IFOC IM drive (Figure 1-8) with a Non-adaptive FLC (Figure 4-2) for speed control, and a Self-Tuning Mechanism. The latter consists of a 2nd–order Reference Model, an Evaluation Mechanism block, and a Takagi-Sugeno-type of FLC (TS-FLC or TKS-FLC), designed to tune the Non-adaptive FLC in real-time.

The rotor speed (ω_r) is compared with the Reference Model output (ω_r^r) to generate the speed tracking error (e'_ω). This error is first assessed in the Evaluation block. If $e'_\omega = \pm 2$rpm, the Self-Tuning Mechanism is not operational; otherwise the Evaluation block will generate the tuning error (e_ω) to be injected into the TS-FLC block. The TS-FLC generates the online updating factors (w_e, w_{ce}, & w_u) that tune the scaling gains (n_e, n_{ce}, & n_u) of the Non-adaptive FLC in real time. The tuning is performed such that the closed-loop system behaves like the Reference Model ($H_m(s_L)$. The TS inference (with singleton output MFs) is selected in order to reduce the computation burden of the controller.

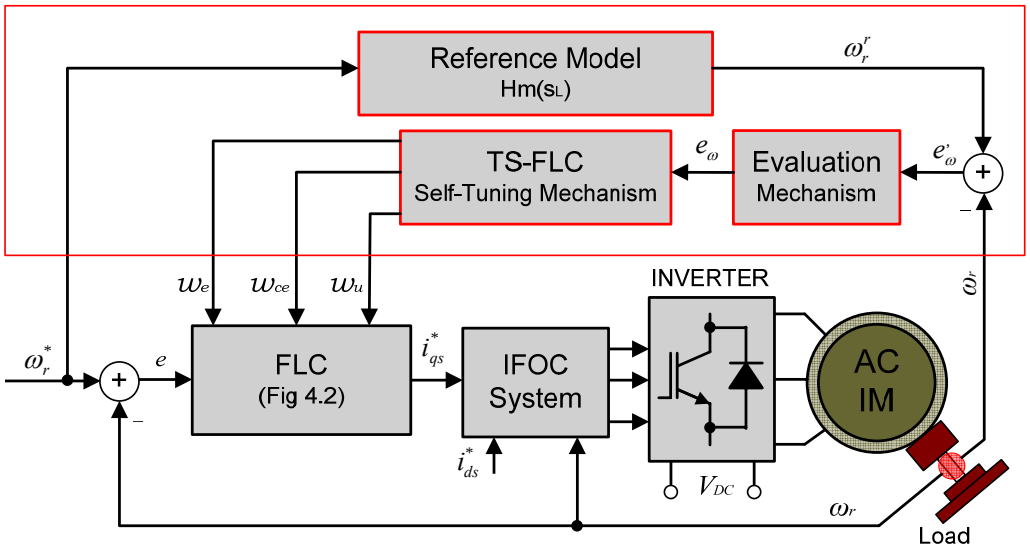

Figure 4-27: Structure of proposed STFC

The effective scaling gains are derived at each time step as functions of the updating factors:

$$n_e(k) = n_e(k-1)[\alpha \cdot w_e(k)] \tag{4.13}$$

$$n_{ce}(k) = n_{ce}(k-1)[\beta \cdot w_{ce}(k)] \tag{4.14}$$

$$n_u(k) = n_u(k-1)[\gamma \cdot w_u(k)] \tag{4.15}$$

where w_e, w_{ce}, and w_u are nonlinear fuzzy functions of the tuning error (e_ω); and α, β, and γ are the weight factors (constants). These fuzzy functions are selected such that the fuzzy gains remain within 1.0p.u. of the values required to maintain safe drive operation (currents are still allowed to exceed 1.0p.u. for very short durations).

For simplicity all the updating factors are generated using a single look-up table. The normalized tuning error signal (e_ω) and its rate of change (ce_ω) are fuzzified by 5 symmetrical MFs (NB, NM, ZE, PM, PB) with a distribution factor of zero. The performance of the STFC is not degraded by using only 5 input MFs (instead of 7 as in the Non-adaptive FLC) thanks to the Self-Tuning Mechanism function. With 5 input MFs for the input variables, each updating gain is derived from a 5 x 5 TS-FLC look-up table with 25 fuzzy rules.

The look-up table is generated offline using Matab/Simulink as follows. The FLC algorithm was built using the Matlab M-file with C-codes. Initially the drive was operated with the proposed Non-adaptive FLC only, with unity scaling gains. The drive was then simultaneously subjected to various load and parameter changes between 10 and 200% of their rated values. For every simulated condition, the scaling gains of the Non-adaptive FLC were adjusted according to a predefined performance indicator. In this case, the integral of the time multiplied by the absolute value of the error (ITAE) criterion was used:

$$(S)_{ITAE} = \int_0^{t_{stop}} t \cdot |e_\omega(t)| \cdot dt \tag{4.16}$$

The ITAE criterion was used to *locally* optimize the scaling gains and evaluate the degree in which the current set parameters satisfy the formulated objective.

Every simulated condition generated a crisp value (or singleton output MF) that was used in the look-up table. For example, when $e_\omega \neq \pm 2$rpm, the TS-FLC block operates the following type of rule to update the updating factors (based on the value of the tuning error):

$$\begin{aligned} &\textbf{IF } \{e_\omega \text{ is PM and } ce_\omega \text{ is ZE}\}, \\ &\textbf{THEN } \{w_e \text{ is } \mathbf{u};\ w_{ce} \text{ is } \mathbf{v};\ \text{and } w_u \text{ is } \mathbf{w}\} \end{aligned} \tag{4.17}$$

where **u**, **v**, and **w** are singleton MFs. Table 4-3 shows the generated (offline) look-up table used in the STFC. The weight factors α, β, and γ were set at 30, 16, and 6, respectively. They were determined during simulation tests.

Table 4-2: Self-Tuning TKS-FLC Rule Base

(w_e, w_{ce}, w_u)		tuning error $(e_\omega(t))$				
		NB	NM	ZE	PM	PB
change-in-tuning error $(ce_\omega(t))$	NB	0.875	0.750	0.375	0.375	0.125
	NM	0.750	0.750	0.625	0.375	0.250
	ZE	0.720	0.875	0.025	0.375	0.250
	PM	0.625	0.125	0.625	0.500	0.375
	PB	0.250	0.805	0.750	0.625	0.875

The Reference Model block defines the desired dynamic response of the system. It is selected based on the idea of the performance *achievable* by the drive and to prevent excessive control action. A full-order reference model can provide the best effectiveness of the adaptation mechanism, but a reduced-order one is generally preferred because of simple design and computation burden (for digital implementation) [146].

For FOC IM drives, the reference model is generally approximated by a 2nd-order system, $H_m(s_L)$, where the delay between the command and the actual currents is neglected [4][116][146]:

$$H_m(s_L) = \frac{a}{s_L^2 + bs_L + a} \tag{4.18}$$

where a and b are the Reference Model coefficients. In the proposed STFC, the values of these coefficients are determined from the so-called Symmetrical Optimum Criterion. According to this criterion, a 2nd–order reference model that is used to determine the desired dynamic characteristics of a high-order system can be written as [7][146]:

$$H_M(s_L) = \frac{1}{\frac{T_{P1}}{K_{P1}} s_L^2 + \frac{1}{K_{P1}} s_L + 1} \tag{4.19}$$

where K_{P1} and $T_{P1} = T_\omega$ are the parameters of the reference model and T_ω is the time constant of the filter in the angular speed feedback path. The value of K_{P1} depends on [8][146]: the motor nominal parameters (reported in Table 1-1), the angular speed feedback gain coefficient, the gains of the PI speed controller (designed according to Symmetrical Optimum Criterion), the inverter maximum control voltage, and the PWM switching frequency.

The parameters K_{P1} & T_{P1} were calculated using the procedure and recommendations given in [8] for IFOC IM drives. It should be noted that these parameters were set according to the laboratory prototype used for the investigated drive. After a few manipulations, the values of the coefficients in equations (4.18) were found as $a = 48000$ and $b = 190$ uniquely for the investigated IM IFOC drives.

Even though reference models designed according to Symmetrical Optimum Criterion are derived from a series of approximations (such as approximation of current loop as a 1st-order system), their responses are very close to the actual high-order systems [7][8][47][146]. Other methods can also be used to derive a reference model for FOC IM drives [147].

4.4.1. Simulation Results

As in the case of the proposed Non-adaptive FLC, the effectiveness of the STFC is also validated by several simulations under various operating conditions and parameter disturbances. Prior to testing the control approach, its Reference Model performance is confirmed by considering the response of the model to a step change in reference speed (Figure 4-28).

It can be seen that the performance of the 2nd-order model is satisfactory, i.e., the Reference Model output follows closely the motor output. A faster response may result in an unachievable control objective. The overshoot in the speed response was left purposely to compensate for a shorter settling time.

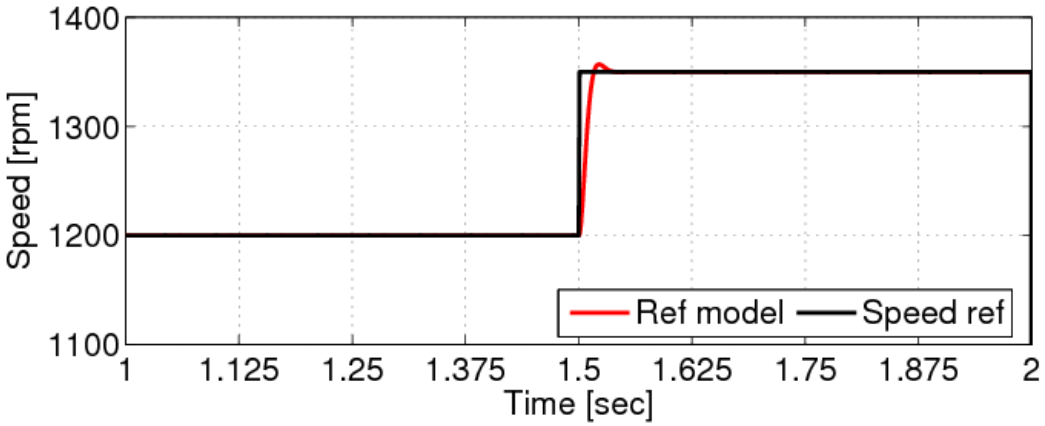

Figure 4-28: Simulated response of the second-order reference model to a step change in speed

The effect of applying a step load torque (from 10 to 85% rated load torque) at 1.0sec and then removing the load at 1.5sec is shown in Figure 4-29 and Figure 4-30, respectively.

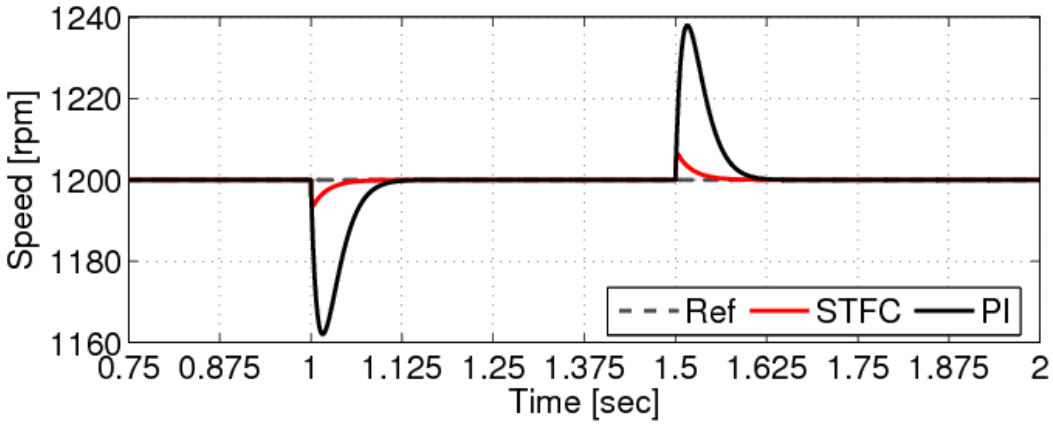

Figure 4-29: Simulated speed responses of STFC and PI controller to application and removal of 65% of rated load at 1200rpm

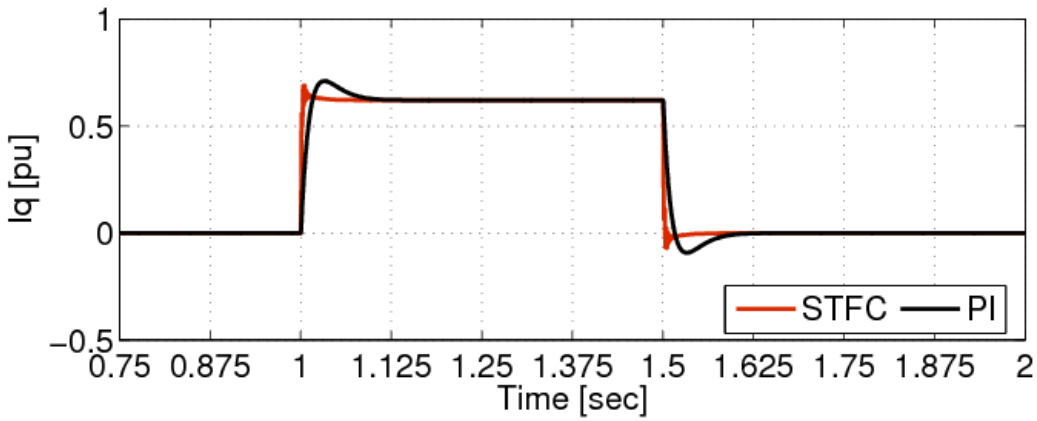

Figure 4-30: Simulated torque component current responses of STFC and PI controller to application and removal of 65% of rated load at 1200rpm

Comparing the responses, it is clear that the STFC offers better dynamic and steady-state performances compared to the PI controller. The responses of the STFC are faster, with smaller overshoot and undershoot of ±7rpm (±38rpm for PI controller). The predicted *q*-axis currents (or torque-component currents) of both systems show acceptable overshoot percentages, with shorter transient for the STFC.

The response of the system to a step change in reference speed (at 50% rated load) is shown in Figure 4-31 for a step change of 100rpm at

2.1sec. A relatively small difference in speeds is chosen purposely in order to minimize the effect of current limits on the motor and drive. Analyzing the responses of the systems, both of them exhibit equal settling times, but the STFC does not overshoot the command signal (the PI controller does).

The final simulation tests are for the case of sudden change in rotor time constant simulated by a 50% increase in rotor resistance (at 1.5sec) and removal of rotor resistance change (at 2.5sec). This is not a practical occurrence but it is included to allow comparison with the results published by other authors. The simulation assumes that the rotor time constant estimation is inaccurate in the Current Model block (Figure 1-8) at low-speed and low-torque regions (where the majority of online estimation of onlip gain methods fail to operate adequately).

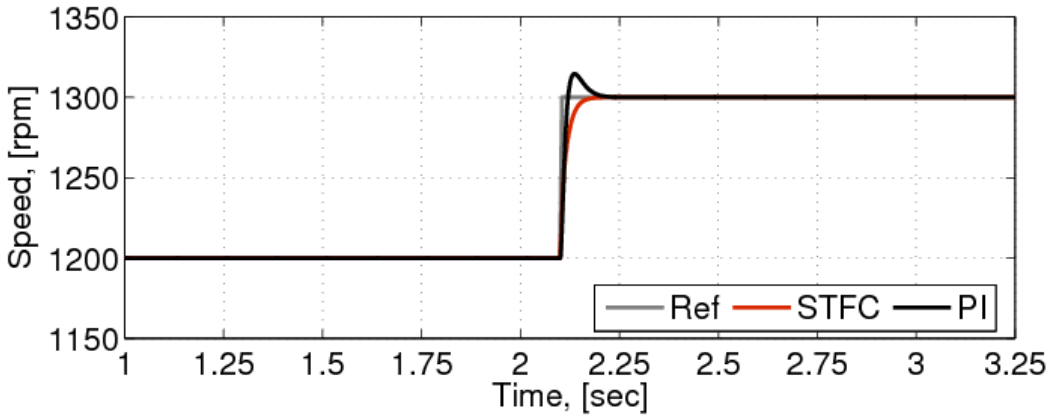

Figure 4-31: Simulated speed responses of STFC and PI controller to a step change in speed reference from 1200rpm to 1350rpm at 50% rated load

The responses of the systems at 100rpm with 30% rated load torque are shown in Figure 4-32. The simulation results show that transients are significantly smaller with the STFC than with the PI controller (even though the overshoot and undershoot percentages observed with the PI controller are not very significant).

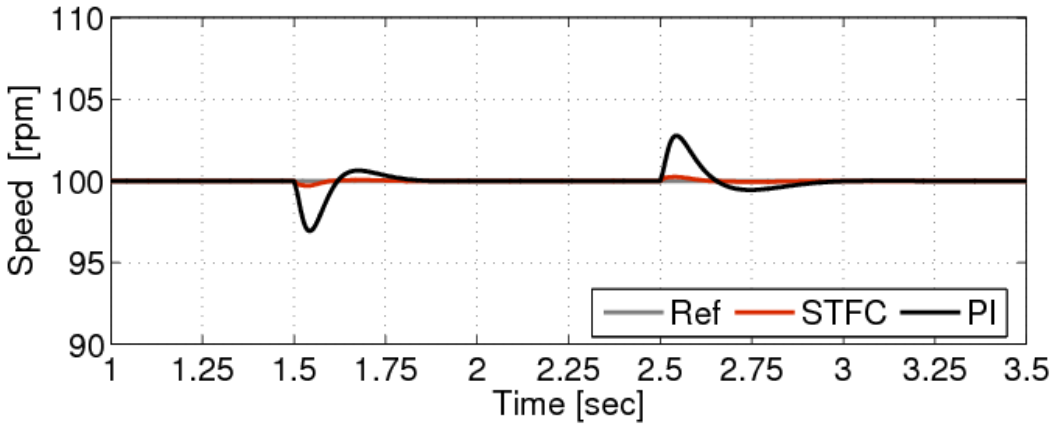

Figure 4-32: Simulated speed response of STFC and PI controller to a sudden +50% change in rotor time constant at low speed and torque

4.4.2. Experimental Results

The laboratory prototype used to validate the STFC is identical to that used for the Non-adaptive FLC. The speed controller was replaced by the STFC algorithm. The computation time of the approaches are given in Table 4-3 for comparison. These were calculated during experimental tests.

Table 4-3: Control Computation Time

	Maximum control time	Total time
PI Controller	0.5 μsec	21 μsec
STFC	0.7 μsec	28 μsec

As in the simulation tests, the implementation of the 2nd-order Reference Model following a step change in speed reference is investigated prior to testing the rest of the control algorithm. The response of the drive is shown in Figure 4-33. Clearly, the output response of the Reference Model is identical to the simulated model reported in Figure 4-28.

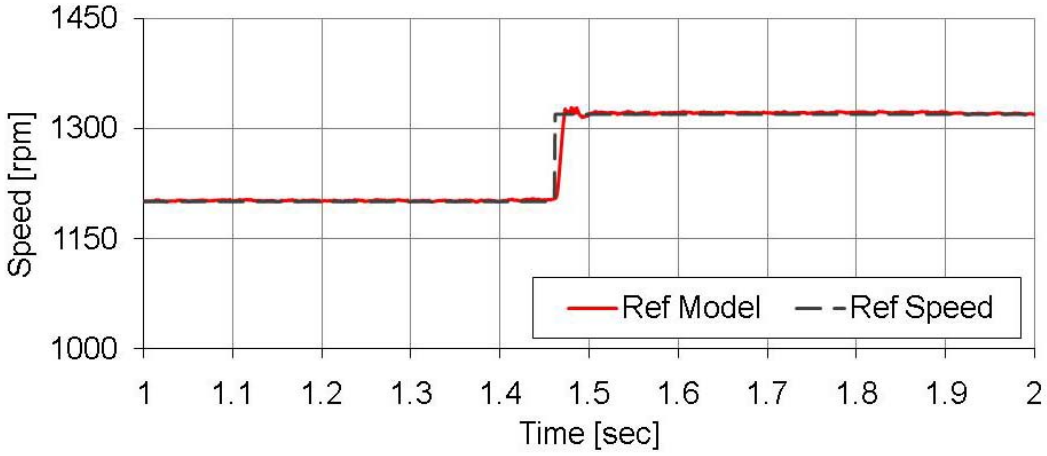

Figure 4-33: Experimental speed response of the second-order Reference Model

Investigating the ability of the drive to reject load disturbances, the drive was initially operated at 1200rpm with 10% rated load torque. A step increase of 65% rated load torque is applied at 1.3sec (for PI) and 1.4sec (for STFC), and then removed at 2.25sec (for PI controller) and 2.20sec (for STFC). The responses of the drives are shown in Figs 4.34-4.36 (for PI) and Figs 4.37-4.39 (for STFC).

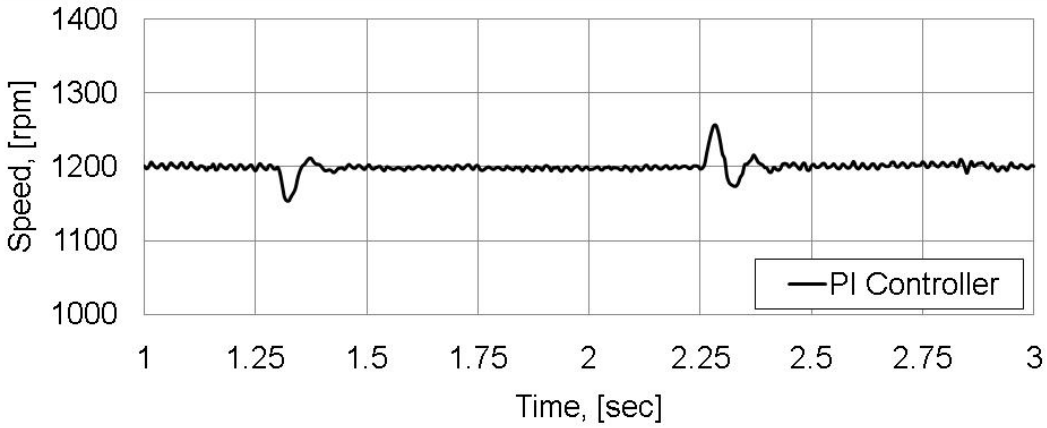

Figure 4-34: Experimental speed response of PI controller to sudden application of 65% load torque at constant speed of 1200rpm

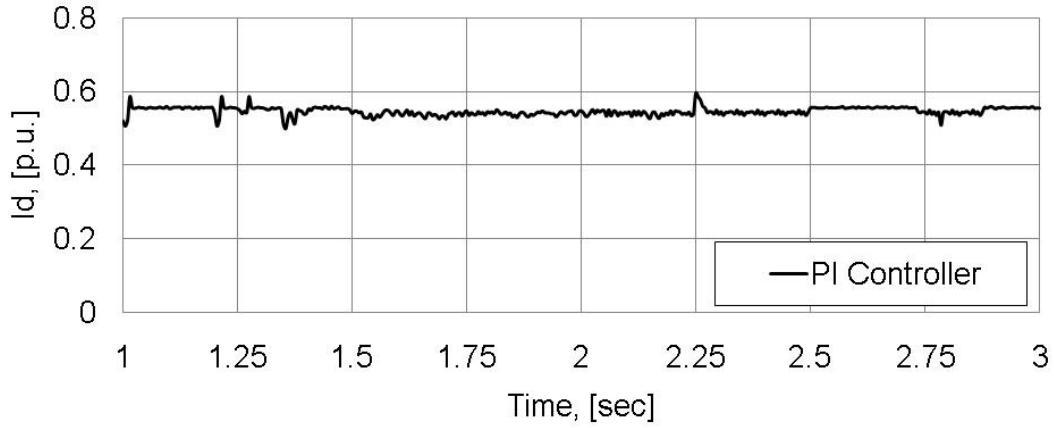

Figure 4-35: Experimental flux component current response of PI controller to sudden application of 65% load torque at constant speed of 1200rpm

Figs 4.34-4.39 validate the simulation results shown in Figs 4.29 & 4.30. It can be seen that the STFC exhibits very small undershoot and overshoot percentages (<8rpm) compared to the PI controller (50rpm). The responses of the actual torque-component currents show that the STFC is faster than the PI controller within current limits (±1.0p.u.).

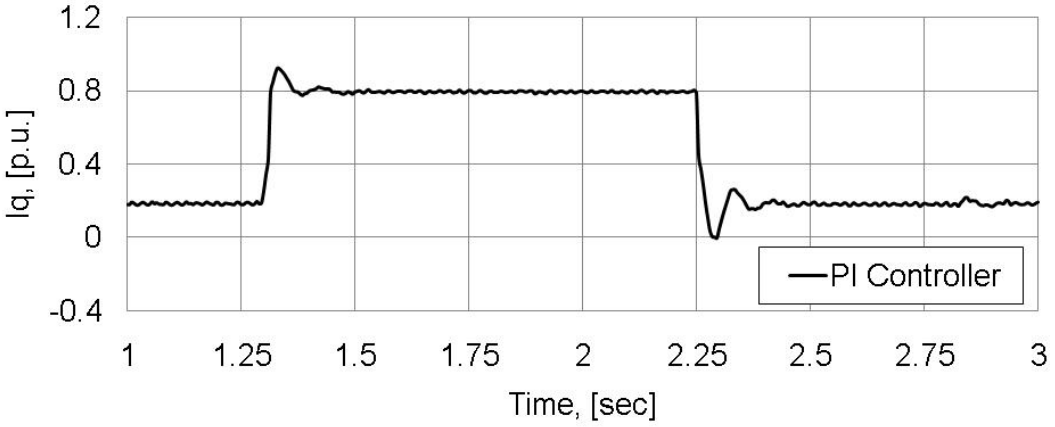

Figure 4-36: Experimental torque component current response of PI controller to sudden application of 65% load torque at constant speed of 1200rpm

The actual flux-component currents of both controllers regain their reference values after the loading and unloading of the motor (even though a speed sensor is used instead of position encoder). Note also that during implementation the loading of IM was accomplished indirectly through the DC generator using a resistor load box switches. This was not the case for the simulated situations. Consequently, the simulated loading behaviour of the motor is slightly different than the implemented one.

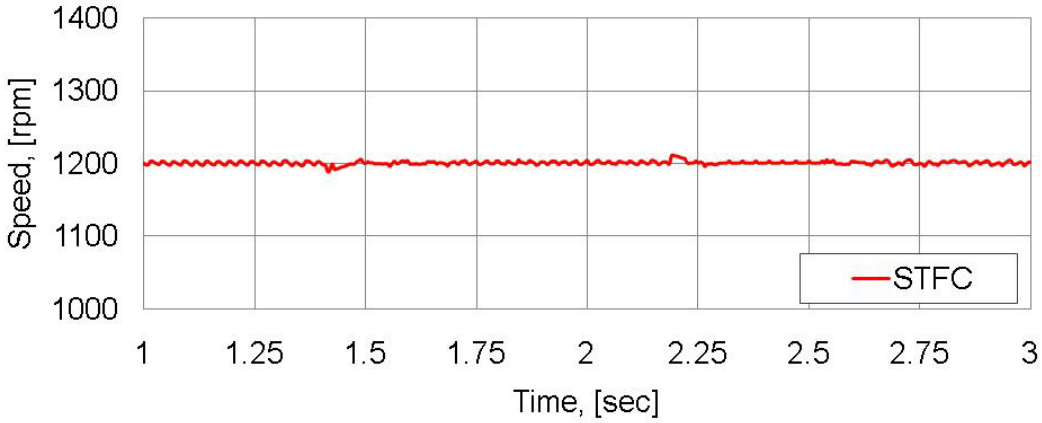

Figure 4-37: Experimental flux component current response of STFC to sudden application of 65% load torque at constant speed of 1200rpm

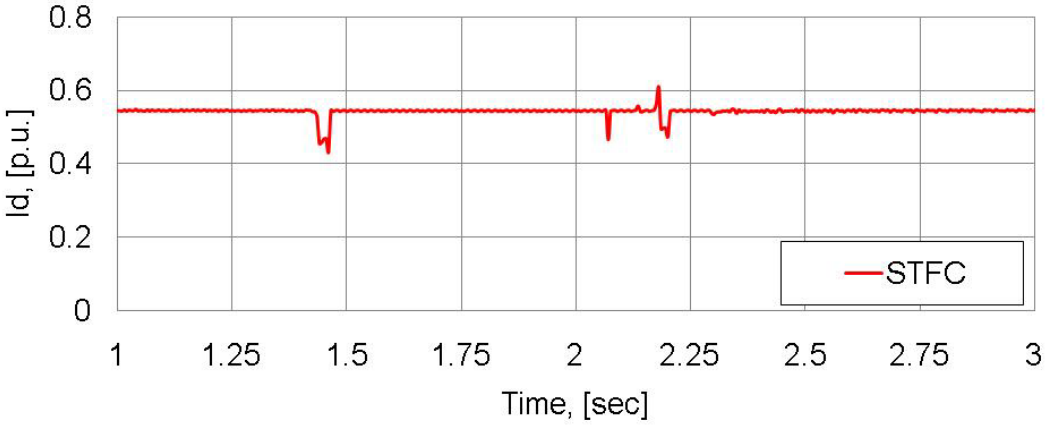

Figure 4-38: Experimental flux component current response of STFC to sudden application of 65% load torque at constant speed of 1200rpm

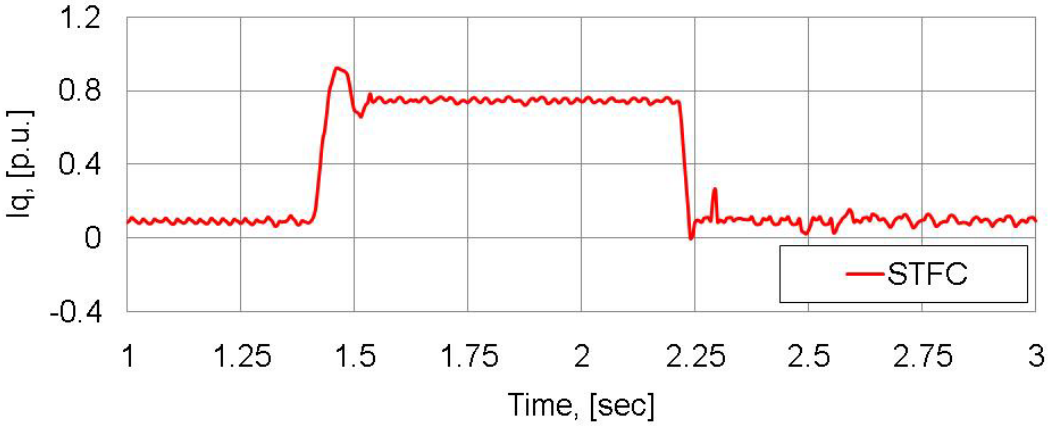

Figure 4-39: Experimental torque component current response of STFC to sudden application of 65% load torque at constant speed of 1200rpm

The speed tracking capabilities of the PI controller and STFC are investigated in Figs 4.40-4.42 and 4.43-4.45, respectively. As the motor is initially operating in steady-state at 1200rpm with 50% load, a sudden change of 100rpm in reference speed is applied at 2.1sec. The results indicate that the STFC exhibits no overshoot with a fast response, confirming the simulation results obtained in Figure 4-31.

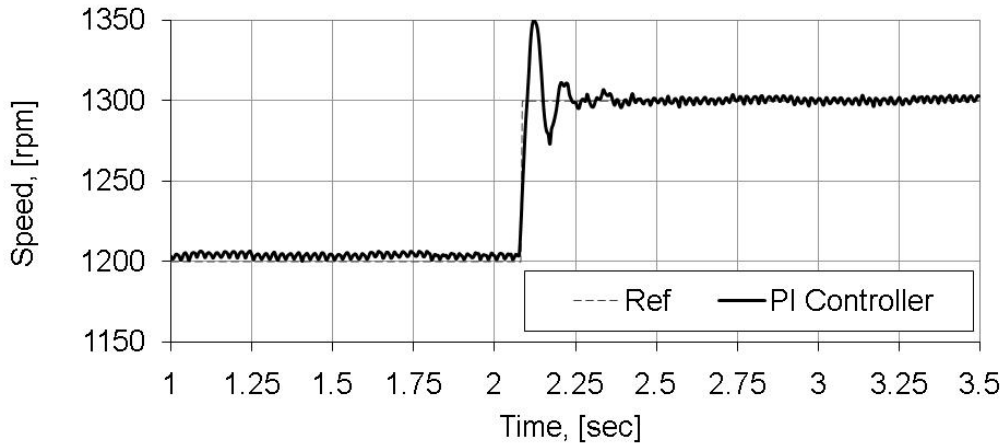

Figure 4-40: Experimental speed response of PI controller to sudden change of speed from 1200rpm to 1300rpm at constant torque

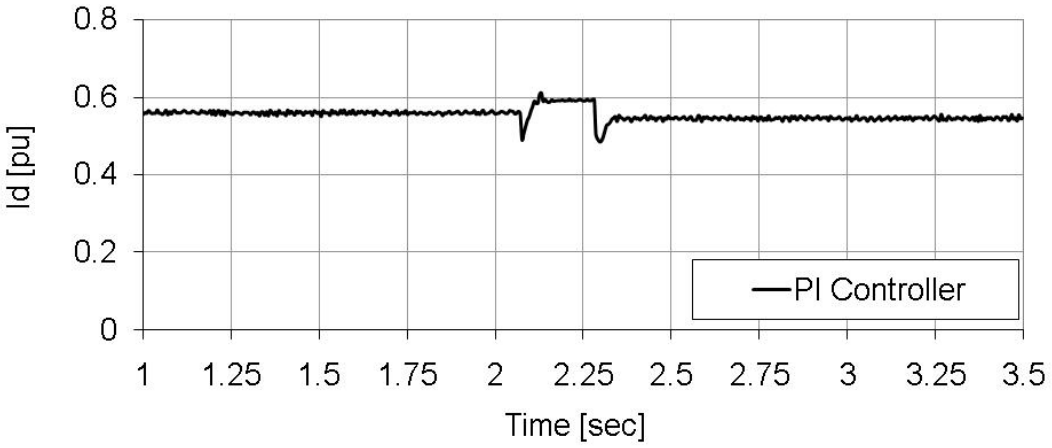

Figure 4-41: Experimental flux component current response of PI controller to sudden change of speed from 1200rpm to 1300rpm at constant torque

The actual flux-component currents of both controllers are able to settle down shortly with small undershoots. The actual torque-component current response of the STFC is faster than that of the PI controller and has no undershoot.

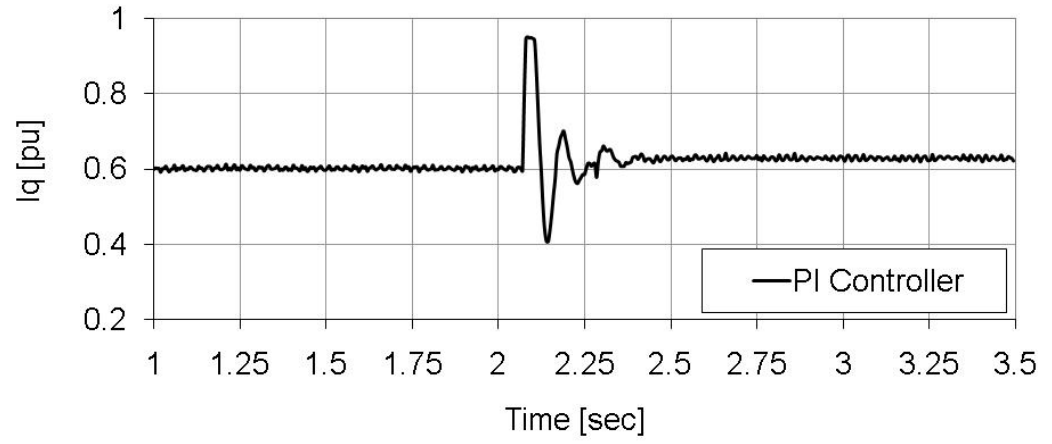

Figure 4-42: Experimental torque component current response of PI controller to sudden change of speed from 1200rpm to 1300rpm at constant torque

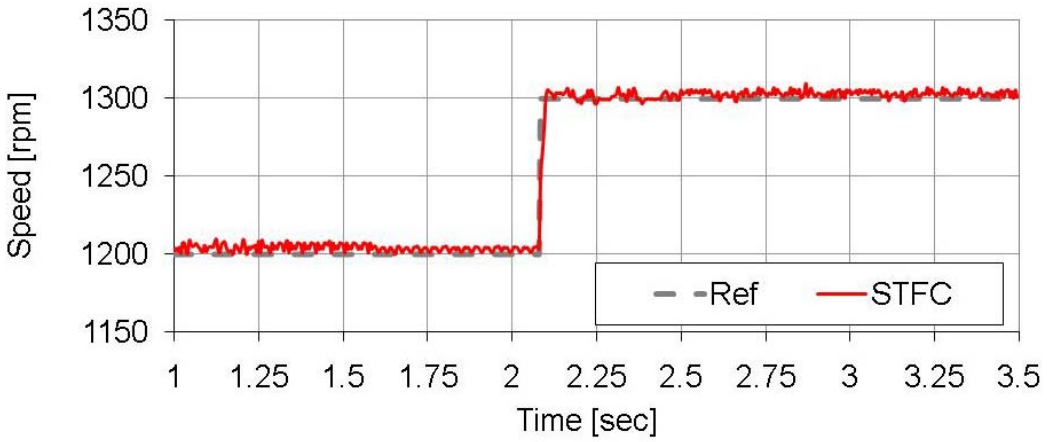

Figure 4-43: Experimental speed response of STFC to sudden change of speed from 1200rpm to 1300rpm at constant torque

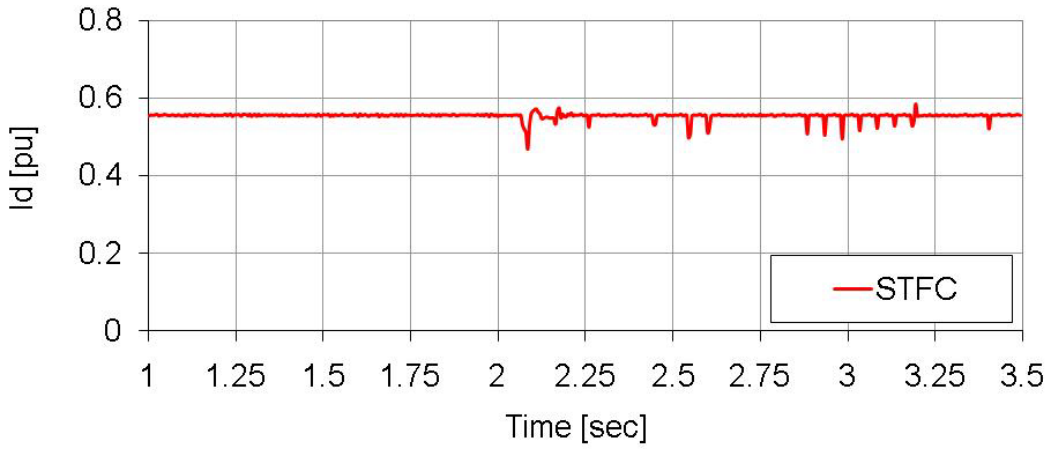

Figure 4-44: Experimental flux component current response of STFC to sudden change of speed from 1200rpm to 1300rpm at constant torque

Other experimental tests were also conducted to validate the proposed STFC under special conditions. For example, the speed tracking capability of the STFC was investigated at low-speed regions. The motor was operated at a starting speed of 100rpm with 30% rated load. A step change of 200rpm in speed reference was applied after 2.90sec. The speed reference was brought back to 100rpm at 3.75sec. The experimental results, described in Figs 4.46-4.48, validate the excellent low-speed tracking capabilities of the STFC.

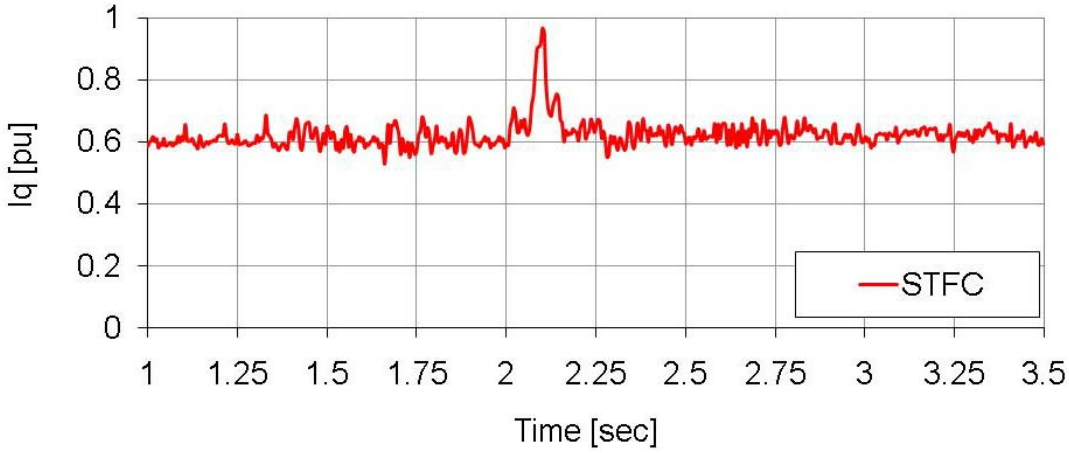

Figure 4-45: Experimental torque component current response of STFC to sudden change of speed from 1200rpm to 1300rpm at constant torque

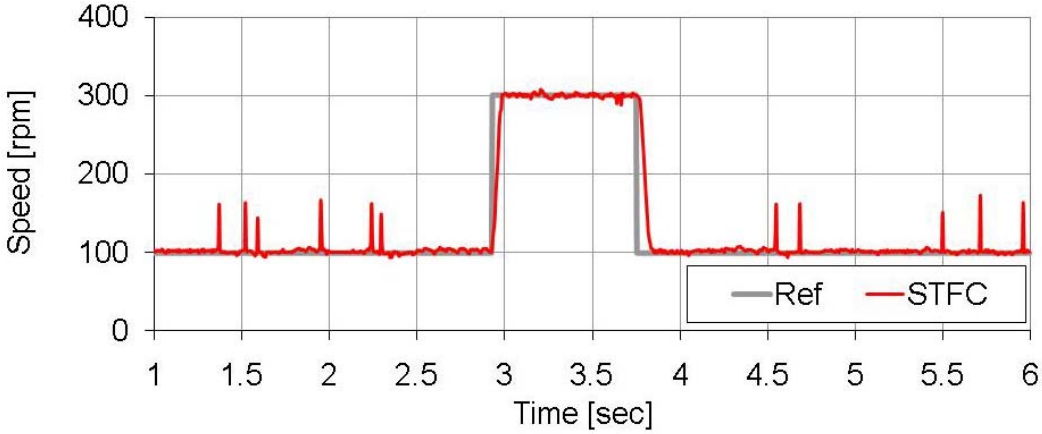

Figure 4-46: Experimental speed response of STFC to sudden change of speed between 100rpm and 300rpm at 30% rated load

The noise in the responses (Figs 4.46 & 4.48) is due to the experimental set-up topology: the speed sensor has a (low) resolution of 60 bit/revolution and is attached to the load DC generator. The backlash in the coupling and the slow updating of the speed signal (relative to the control loop) introduced noise and noise sensitivity. These effects are reduced at higher speeds and loads. It was possible to reduce the noise

at low-speed regions with proper and further tuning of the Low-Pass Filter on the speed signal at the expense of transient responses. Therefore, at low-speed operations, a compromise between noise and transient response had to be made.

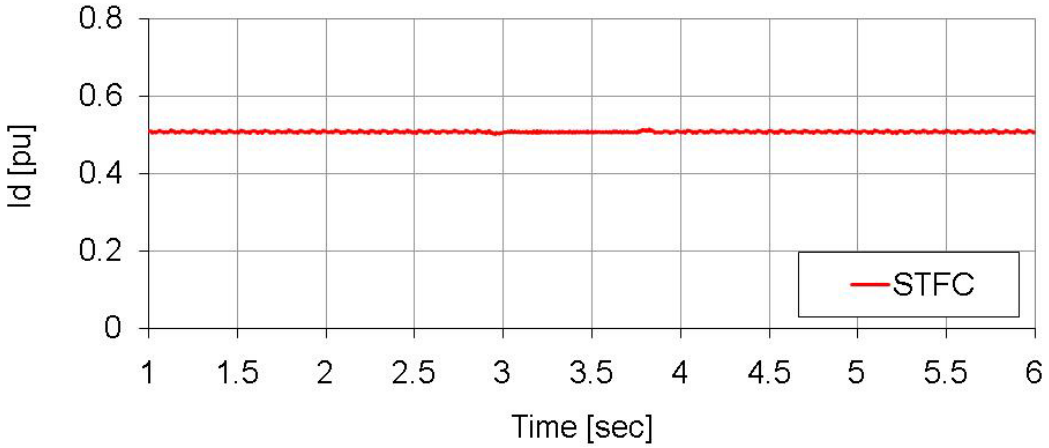

Figure 4-47: Experimental flux component current response of STFC to sudden change of speed between 100rpm and 300rpm at 30% rated load

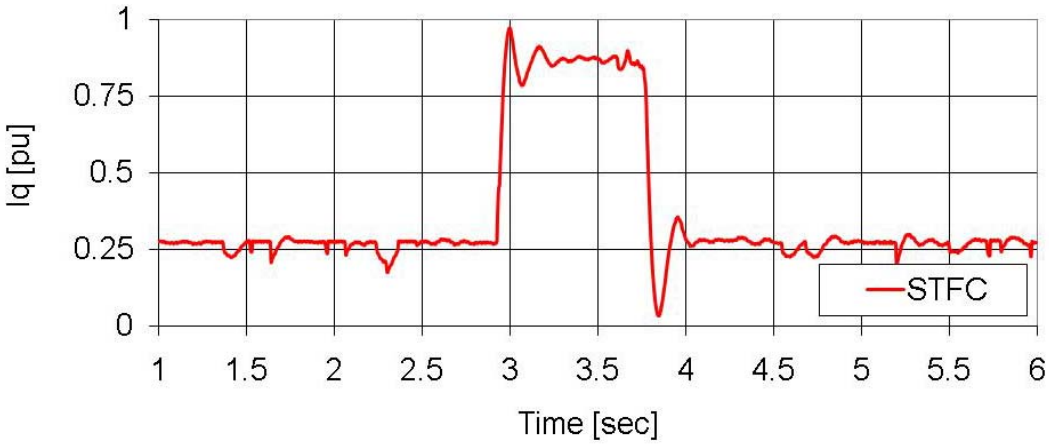

Figure 4-48: Experimental torque component current response of STFC to sudden change of speed between 100rpm and 300rpm at 30% rated load

Figs 4.49-4.51 show the experimental responses of the STFC following a very large step change in speed reference (from 100 to 1200rpm) at

constant (low) load torque. During this test, the drive was initially operated at 100rpm at low load. At approximately 1.815sec, the speed reference was increased to 1200pm at constant torque. After a short time (at 2.80sec), the speed was brought back to 100rpm. The results obtained confirm the tracking capabilities of the STFC at low- and high-speed region and its ability to handle very large step changes in speed reference. The oscillations observed in the low-speed regions are also due to the experimental set-up topology as in the previous case. It can also be seen that the speed oscillations are transferred to the torque-component current. The actual flux-component current remains constant after the step changes in speed reference, as expected.

The ability of the STFC to reject a sudden application of load torque at low-speed regions is investigated and shown in Figs 4.52-4.54. The drive was operated at 300rpm with approximately 60% load torque (as apposed to the case described by Figs 4.37-4.39). At 6.375sec a 20% load increase was applied. Figs 4.52-4.54 show that the responses of the drive are relatively identical to the case previously reported in Figs 4.37-4.39.

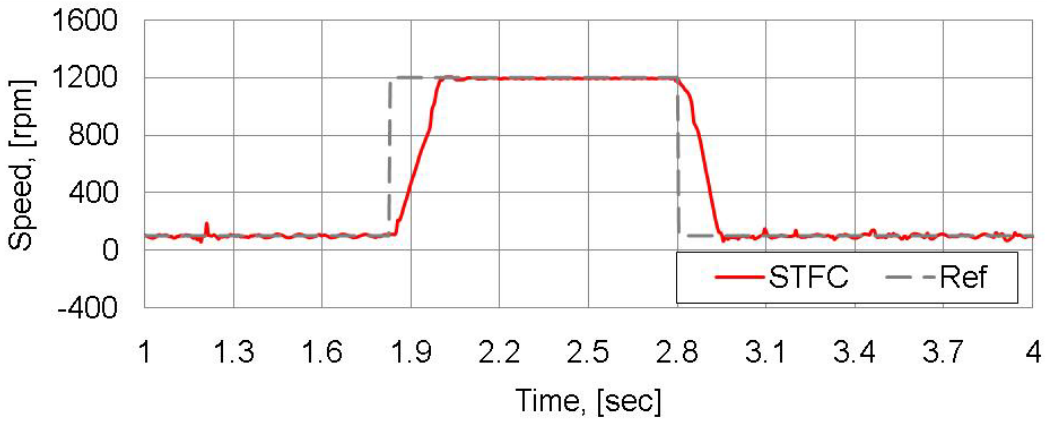

Figure 4-49: Experimental speed response of STFC due to sudden changes of speed reference between 100rpm and 1200rpm at constant load

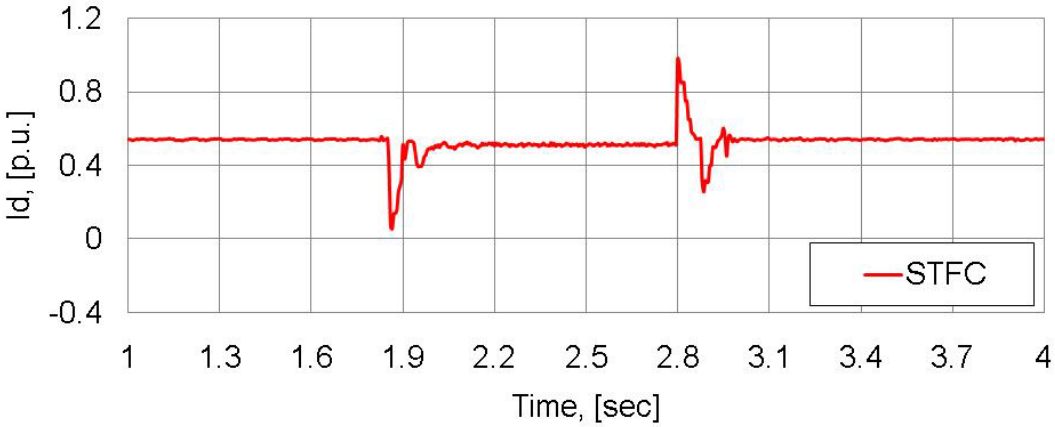

Figure 4-50: Experimental flux component current response of STFC to sudden changes of speed reference between 100rpm and 1200rpm at constant load

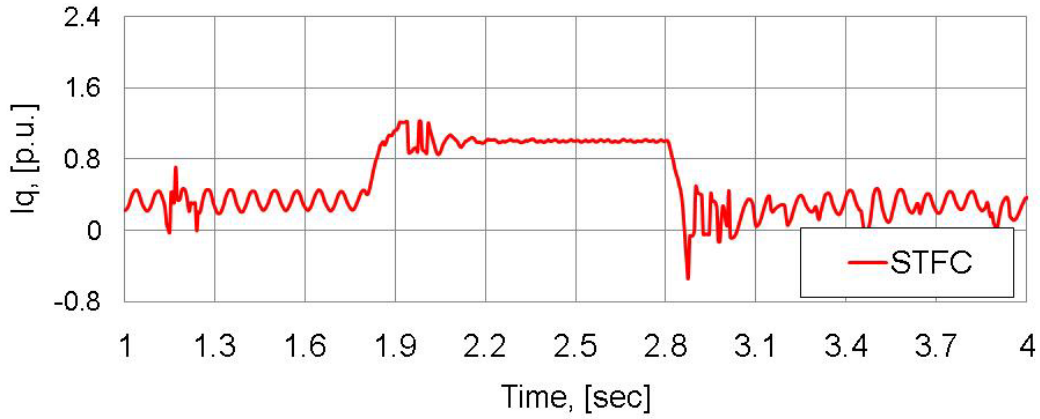

Figure 4-51: Experimental torque component current response of STFC to sudden changes of speed reference between 100rpm and 1200rpm at constant load

The final experimental results are for the case of step change in slip gain to validate the simulation result shown in Figure 4-32. As the IM was operating at 100rpm with 30% rated load, the value of the rotor resistance was suddenly doubled in the Current Model block (Figure 1-8) after 3.60sec and returned to its nominal value at 4.55sec. Since the investigated IM was of squirrel-cage type, it was impossible to change the value of the rotor resistance or rotor inductance in the actual motor

directly. Figs 4.55-4.56 show the responses of the STFC speed and torque component current. It can be seen that the speed response is stable and fast (similarly to the result obtained in Figure 4-32).

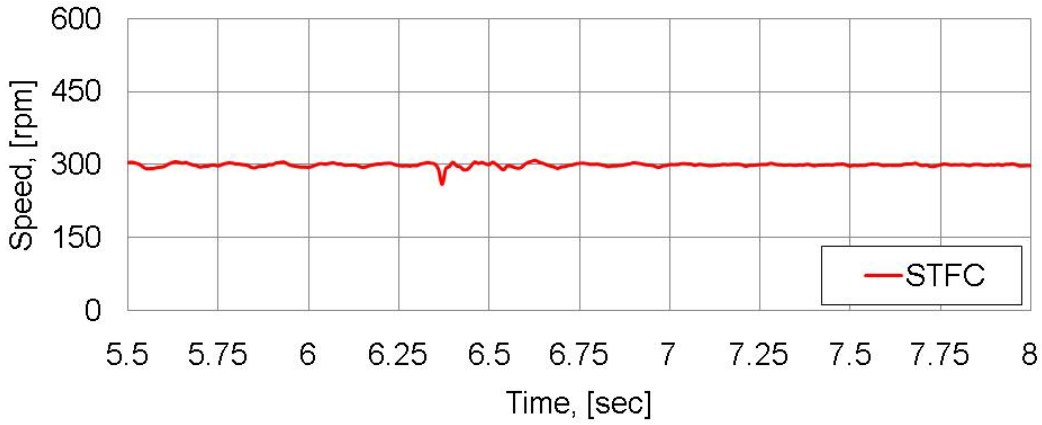

Figure 4-52: Experimental speed response of STFC to application of load at constant speed of 300rpm

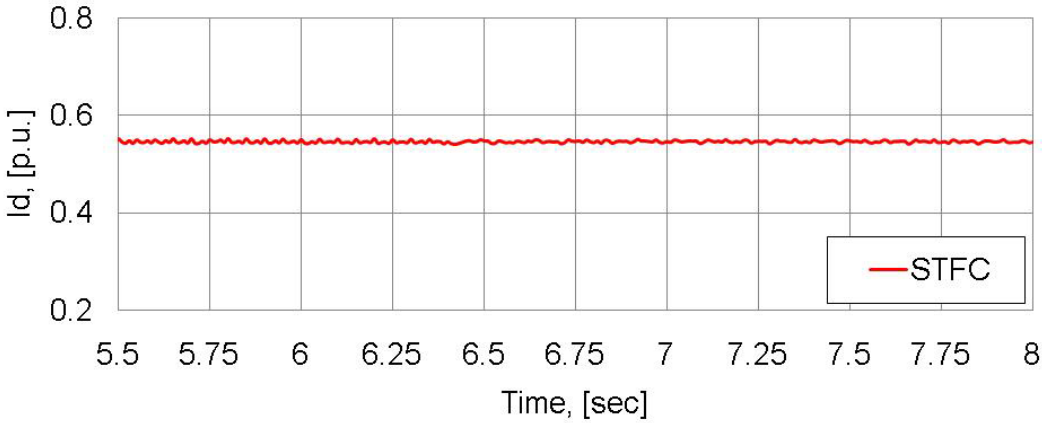

Figure 4-53: Experimental flux component current response of STFC to application of load at constant speed of 300rpm

This test (Figs 4.55 & 4.56) also indicates that the STFC has the ability to compensate for IM parameter (electrical and mechanical) disturbances. On the other hand, note that the torque-component current command (Figure 4-56) approaches 1.0p.u., even though the load is only 30% of rated. As one would expect, one could not expect to maintain *stability*

under all conditions in the case of such a severe error (without some sort of slip gain online estimation mechanism). Fortunately, a sudden 50% change of slip gain is not a practical occurrence. It was included in this thesis to allow comparison with the results published by other authors and to identify the current limit problem.

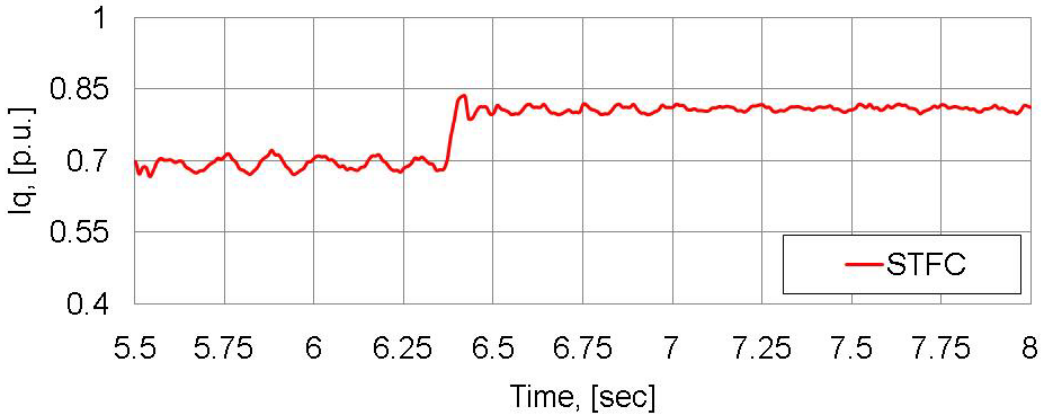

Figure 4-54: Experimental torque component current response of STFC to application of load at constant speed of 300rpm

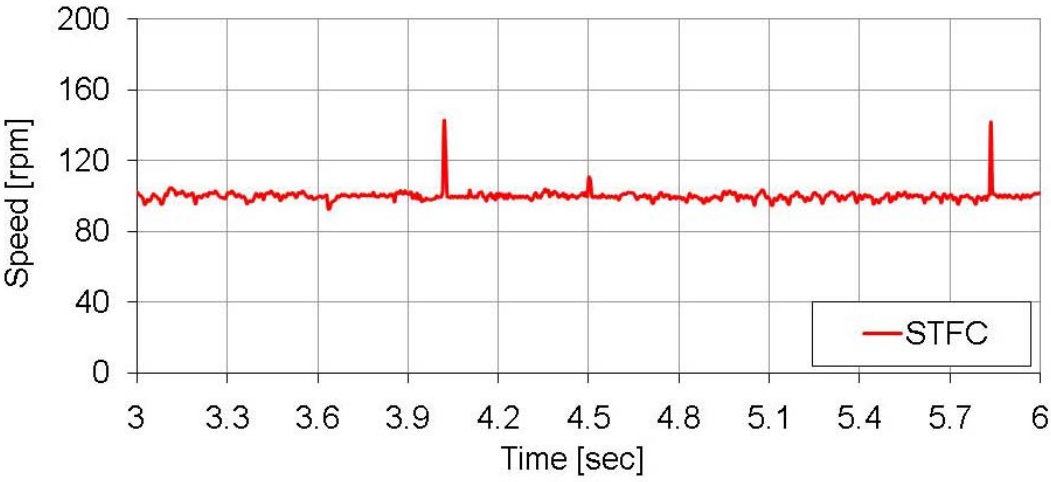

Figure 4-55: Experimental speed response of STFC to an increase and decrease of rotor time constant at 100rpm and low load

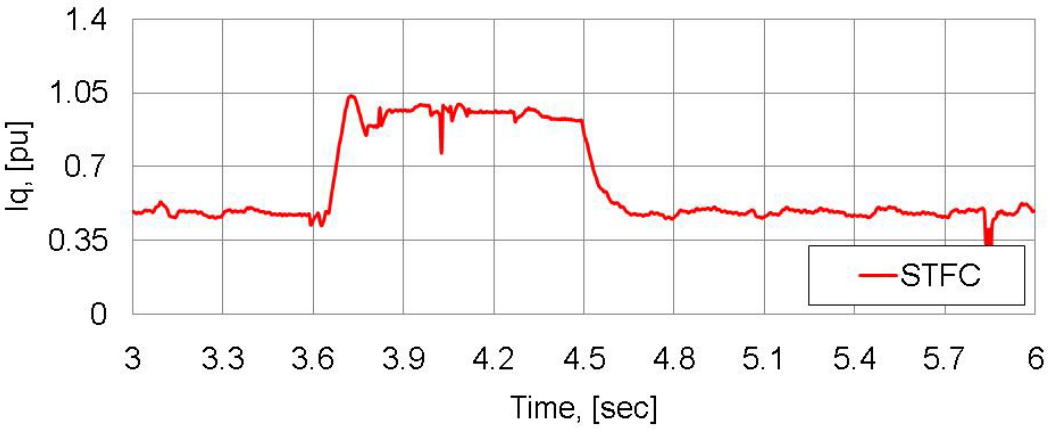

Figure 4-56: Experimental torque component current response of STFC to an increase and decrease of rotor time constant at 100rpm and low load

4.5. Stability Analysis

Stability analysis is one of the most controversial issues of FLCs. The main reason for that is the strong coupling between the parameters of the controller and the uncertainty in the process model. In many applications, FLCs are designed by heuristic approaches based on the knowledge of the operator and control engineers. This model-free approach is often presented as an attractive feature of FLCs. Unfortunately the lack of model for the process makes it difficult to obtain theoretical results on stability and performance of FLCs [149].

Different approaches to stability analysis of FLCs have been proposed in the past; including the Lyapunov stability [42][44][47][148], Hyper-Stability [149][150], Describing Function [152], and Circle Criteria [151]. Due to the lack of a model, it seems more natural to study stability for a class of FLCs rather than investigating the stability of one FLC, where the class of control laws must cover different possible implementation of the same human control rules. This is the approach used in this thesis to prove the stability of the proposed Non-adaptive FLC and that of the

STFC. Since the STFC is derived from the proposed Non-adaptive FLC, its stability analysis is also derived from that of the standard FLC.

From descriptions in the literature, many FLCs can be viewed as nonlinear controllers characterized by a bounded continuous input-output mapping with some symmetry properties. Hence, a promising approach to stability analysis of such FLCs appears to be the *Passivity* framework [149[150]. This is because passivity approaches lead to general conclusions on the absolute stability of a broad class of nonlinear systems, using only some general characteristics of the input-output dynamics of the controlled system and the input-output mapping of the controller. The lack of models for FLCs makes the approach very attractive. The class of FLCs considered in this thesis is referred to as Sectorial Fuzzy Controllers (SFCs).

4.5.1 Sectorial Fuzzy Controller (SFC)

Many FLCs considered in literature, including the proposed Non-adaptive FLC, share the same distinguished input-output characteristics [23][27][105]. This general class of FLCs has been established as SFCs [150]. They are characterized by the following:

(a) Their rule bases are symmetric about the off-diagonal of the table (odd symmetry)
(b) The numeric values of their control decision gradually increase (or decrease) from left to right within a row, and gradually increase (or decrease) from top to bottom (monotony).
(c) Their control decision corresponding to the central area of the fuzzy look-up table is usually zero (i.e., the output is zero for zero inputs).

Let's the input and output scaling gains of an FLC be represented by n_{e_1}, n_{e_2}, and n_u. Using the Mamdani minimum inference and the CAV defuzzification, the control law of the FLC can be written as:

$$u_i = \frac{\sum_{i,j}\left(\left(\mu_{E_i}(n_{e_1}\cdot e_1)\cap\mu_{E_j}(n_{e_2}\cdot e_2)\right)\cdot U_{n(i,j)}(n_u\cdot u)\right)}{\sum_{i,j}\left(\mu_{E_i}(n_{e_1}\cdot e_1)\cap\mu_{E_j}(n_{e_2}\cdot e_2)\right)} = \Phi(e_1,e_2) \tag{4.20}$$

where $e_1 = e(k)$, $e_2 = ce(k)$, $u_1 = \Delta u(k) = \Delta i_{qs}^*$ at time instant k, and E_i, E_j, and $U_{n(i,j)}$ are the linguistic variables of e_1, e_2, and u_1, respectively, and $\cap$ is the fuzzy "AND" operator. The scalar output $\Phi(e_1, e_2)$ represents the nonlinear static mapping of the inputs and output.

SFCs have specific input-output mapping properties described as follows. Let's assume that the FLC described in equation (4.19) is defined by $u_1 = \Phi(e_1, e_2)$. Let's also assume that its inputs variables are normalized in interval [-L, +L], with ($2N$ + 1) input fuzzy sets, with linguistic variables E_i (where i = -N, …, -1, 0, +1, …, +N). The properties of the inputs MFs are:

(1) The sum of MF values is one at all time: $\sum_i \mu_{E_i}(e) = 1$

(2) For input values outside the range of [-L, +L]: $\mu_{E_N}(e) = 1$ and $\mu_{E_{-N}}(e) = 1$

(3) E_i and E_{-i} cover intervals that are symmetric with respect to zero

(4) The input fuzzy sets must be convex [Wang 1997]: $\forall e \neq e'$ and $\forall\lambda \in [0,1]$:
$\mu_{E_i}(\lambda e + (1-\lambda)e') \geq \mu_{E_i}(e) \cap \mu_{E_i}(e')$.

(5) For E_0 the fuzzy set must be strictly convex in order to guarantee the uniqueness of the 0-state equilibrium state of the FLC. This does not allow, for example, the use of trapezoidal MF for E_0.

For rule bases designed for 2 inputs (e_1,e_2) and one output (u_1), such as the proposed FLC and STFC, the fuzzy statements (rules) can be written as

$$\text{IF } \{e_1 \text{ is } E_i \text{ AND } e_2 \text{ is } E_j\} \text{ THEN } u_1 \text{ is } OUT_{f(i,j)} \tag{4.21}$$

where $f(i,j)$ is the function that relates the indices i and j of the input sets to the index of the output fuzzy set $OUT_{f(i,j)}$ with the center value $U_{f(i,j)}$. Function $f(i,j)$ has the following properties:

(6) $f(0,0) = 0$

(7) $f(i,j) = -f(-i,-j), \ \forall i,j$

(8) $j\left[f(i,j) - f(i,0)\right] \geq 0 \quad \forall i,j \geq 0$

$i\left[f(i,j) - f(0,j)\right] \geq 0 \quad \forall i,j \geq 0$

(9) $U_0 = 0$, $U_i = -U_{-i}$, and $U_i > U_j$ for $i > j$

A FLC satisfying the characteristics (a)–(c) and the properties (1)–(9) is called SFC [150]. Based on this characterization, it is clear that the proposed Non-adaptive FLC satisfies the conditions of an SFC. If the proposed FLC is an SFC, then the STFC is also an SFC at all time, since it carries the properties and characteristics of an SFC at each step time or every time its scaling gains are updated [33].

For all SFCs the real input-output mapping $\Phi(.,.)$ relating the inputs with the output has the following properties:

(a) $\Phi(e_1,e_2)$ is globally Lipchitz continuous and bounded [42]:
$\Phi(e_1,e_2) \leq \mu_M$, where $M = max_{i,j} U_{f(i,j)}$

(b) $\Phi(0,0) = 0$: steady-state condition.

(c) $\Phi(e_1,e_2) = -\Phi(-e_1,-e_2)$: odd symmetry

(d) $\forall(e_1,e_2): 0 \leq e_1 \leq \left(\Phi(e_1,e_2) - \Phi(0,e_2)\right) \leq \lambda' e_1^2$

(e) $\forall(e_1,e_2): 0 \leq e_2 \leq \left(\Phi(e_1,e_2) - \Phi(e_1,0)\right) \leq \gamma' e_2^2$

4.5.2 Stability of a Continuous Time System

A state-space description of a nonlinear (stable) time-varying SISO control system can be written as:

$$\dot{x} = f(x,u) \tag{4.22}$$

$$y = h(x,u) \tag{4.23}$$

where $x \in R^n$ is a state vector, $u \in R^m$ is a control input, and $y \in R^m$ is the output. If the input and output variables are measurable, an approximate linear description of the system can be obtained by using any of the relevant off-line identification methods in a selected operating point. A very large number of servo systems can be satisfactorily approximated by linear 2nd-order systems (refer to Figure 4-1).

Let's assuming that the system described by equations (4.22)-(4.23) is driven by the FLC described in (4.20), the objective of the passivity approach for stability analysis consists of finding sufficient conditions for stability of zero solution of fuzzy controlled system (4.22)-(4.23), where the controller is SFC:

A continuous time SISO (4.22)-(4.23) is said to be passive if there exists a positive-definite storage function, $V(x)$, with $V(0) = 0$ and a supply rate $s(u,y) = u^T y$, such that the following dissipation inequality hold $\forall t > 0, u \in U$, and $x(0) \in X$ [149][150]:

$$V\big(x(t)\big) - V\big(x(0)\big) \leq \int_0^t s\big(u(\tau), y(\tau)\big) \quad \forall x,u \tag{4.24}$$

The system is strictly input passive if there exists a constant $\varepsilon > 0$ such that

$$s(u,y) = u^T y - \varepsilon u^T u \tag{4.25}$$

The system is strictly output passive if there exists a constant $\varepsilon > 0$ such that

$$s(u,y) = u^T y - \varepsilon y^T y \tag{4.26}$$

Finally, the system is input-output passive if

$$s(u,y) = u^T y - \varepsilon_1 u^T u - \varepsilon_2 y^T y \qquad \forall \varepsilon_1, \varepsilon_2 > 0 \tag{4.27}$$

By taking the input $u = 0$, passivity systems having positive storage functions V have a Lyapunov stable zero dynamics [153].

A sufficient condition for asymptotic stability of FLC closed-loop systems is the input-output passivity of the plant itself. For the proposed controllers, this is proven as follows. The FLC mapping described in (4.20) can take the following form:

$$\dot{e}_1 = e_2 \tag{4.28}$$

$$u_1 = \Phi(e_1, e_2) \tag{4.29}$$

Equations (4.28)-(4.29) show that an FLC can be considered a SISO nonlinear system with internal dynamics. Therefore, if $\Phi(.,.)$ is SFC, then the system should have $u_1 = 0$ as an equilibrium point.

To show that the SFC described by (4.28)-(4.29) is input-output passive: From input-output mapping $\Phi(.,.)$ properties (a)-(e) described above, it can be seen that:

$$0 \le e_1 \Phi(e_1, 0) \le \lambda' e_1^2 \tag{4.30}$$

Let

$$\Delta_{e_1}(e_1, e_2) = \Phi(e_1, e_2) - \Phi(0, e_2) \tag{4.31}$$

$$\Delta_{e_2}(e_1, e_2) = \Phi(e_1, e_2) - \Phi(e_1, 0) \tag{4.32}$$

It follows that

$$0 \le e_2 \cdot \Delta_{e_2}(e_1, e_2) \le \gamma' e_2^2 \tag{4.33}$$

$$0 \le e_1 \cdot \Delta_{e_1}(e_1, e_2) \le \lambda' e_1^2 \tag{4.34}$$

Applying the definition of passivity of SFC results in [149][153]:

$$\int_0^t e_2(\tau) \cdot \Phi\big(e_1(\tau), e_2(\tau)\big) \cdot dt \geq V_1\big(e_1(t)\big) - V_1\big(e_1(0)\big) \tag{4.35}$$

Omitting "τ" in equation (4.34), it results in

$$\begin{aligned} \int_0^t \dot{e}_1 \, \Phi(e_1, 0) \cdot d\tau + \int_0^t e_2 \, \Delta_{e_2}(e_1, e_2) \cdot d\tau &= \int_0^t \dot{e}_1 \Phi(e_1, 0) \cdot d\tau \\ &= \int_{e_1(0)}^{e_1(t)} \Phi(e_1, 0) \cdot de_1 \end{aligned} \tag{4.36}$$

This shows that the right-hand-side of equation (4.35) is a storage function with $V(0) = 0$. It is also evident that the left-hand-side of (4.35) is superior or equal to the right-hand-side. This ends the stability proof of the proposed Non-adaptive FLC and STFC closed-loop systems.

4.6. Conclusions

This chapter has described the design, simulation, and experimental tests of two new controllers: a Non-adaptive FLC and a Self-Tuning FLC (STFC). Both controllers are designed for speed control of FOC IM drives. Through a series of simulations and experimental tests, the speed tracking and disturbance rejection capabilities of the controllers were successfully validated.

A new systematic design methodology is proposed for initial calibration of Non-adaptive FLCs operated in FOC schemes. It was shown that under severe conditions of parameter and operating condition changes, the performances of the Non-adaptive FLC are insufficient to effectively control the drive; especially for high-performance applications. Under

these conditions, a self-tuning mechanism (STFC) was designed to update the scaling gains of the FLC in real time. Keeping in mind the requirement to minimize cost for industrial uses, the compromise between performance and computation burden was included in the design and implementation of both controllers, especially in the STFC.

The key feature of the proposed STFC is the fact that the knowledge of accurate motor (nominal) parameters is not strictly required at start-up. The controller is designed to self-tune its parameters based on the available information of the drive system. When necessary, the motor parameters can be included in the scaling gains computations to reduce the transient responses of the drive at start-up.

The ability of the system to indirectly respond to parameter and load changes, without the need for computationally expensive parameter estimators, makes the approach very attractive for a wide range of industrial applications. Implementing the proposed STFC and the standard PI controller, the STFC is shown to offer a number of performance advantages over the PI controller. These advantages include smaller overshoot and faster responses, even though the sampling time for current and speed control inputs is on the order of magnitude longer than that of the PI system.

Conclusions

The interplay of technical, economical, and environmental constraints in today's commercialized industry requires advanced approaches to control and design of electric machines. Hence, the ability to effectively control the speed and torque of electric machines to achieve the requirements of the system will continue to be a major stimulus to growth; particularly in the Servo and Variable Speed Drive market. This thesis followed the same line of target. It is a contribution to the ongoing research on effective methods to operate IM drives for high-performance applications with FOC schemes.

IFOC is one of the best approaches for high-performance IM drives. However, as discussed throughout this thesis, the implementation of this technique is faced with two major challenges: the estimation of the IM slip gain in real time and the compensation of sensitivity of the close-loop control system to parameter and operating condition. In order to solve these problems, two control systems were introduced and implemented.

The first controller dealt with the problem related to the estimation of slip gain for the purpose of maintaining decoupled control of flux and torque at all time. It was designed to operate in a very wide range of operating torque and speed. The second controller was designed to improve the (dynamic and steady-state) responses of the drive's speed, torque, and flux under severe internal and external disturbances. To validate the approaches, a 2HP 3–phase IM was used, along with an ADMC21992 160-MHz DSP.

The design of the first controller was carried out following a systematic procedure. First, a thorough review and comparative study of the relevant approaches for IM slip gain estimation were conducted. This

study revealed that none of the existing schemes can solve the tuning problem in the entire torque-speed plane. In many cases, if the drive system is required to operate in low-speed or low-torque regions, additional transducers or dynamic methods are used to expand the torque-speed operating region of the algorithm. It is well known that the addition of sensors often creates problems of reliability and cost; especially if the physical topology of the actual motor must be modified to accommodate the sensors. Dynamic methods on the other hand, require powerful DSPs due to their very complex algorithms (high computation burden). This also contributes to the overall cost and complexity of the drive.

The approach proposed and described in chapter 3 for IM slip gain estimation took into account the issues of reliability and cost. It is based on the combination of three distinctive and very simple MRAS schemes in a single controller. The three schemes (modified reactive power, *q*-axis voltage, and *d*-axis voltage) were selected based on their operating capabilities at low-speed and low-torque regions, as well as on their sensitivity to motor saturation and inductances. A FLC was used to generate the so-called Distribution Factor that decides which scheme (among the three) is best for slip gain estimation based on the current drive operating condition in terms of speed and load torque.

The results of the analysis, plotted in chapter 3, validated the applicability of the proposed slip gain estimation algorithm at rated conditions and at low-speed and low-torque regions: it was possible to maintain constant rotor flux operation and excellent control of torque despite the so-called detuned slip gain condition. The contribution of the approach can be summarized as follow:

(1) The proposed method can estimate the slip gain of an IM in low-speed and low-torque regions (in high- & medium-speed/torque as well), where the majority of schemes fail to operate adequately.

- The torque responses are not slowed down as a result of detuned FOC thanks to estimation capability of the algorithm. The rotor flux responses are also well controlled under the same condition. Hence, there is a good independent (decoupled) control of torque and speed.
- No over-excitation and/or under-excitation effects were observed in the stator phase voltage waveform: a good indication that stator losses can be also controlled under detuned conditions.

(2) The use of singleton MFs in the FLCs significantly reduces the computation burden of the algorithm. The use of MRAS schemes also contributes to reduction of computation burden (compared to dynamic methods such as the EKF method).

(3) The implementation of IFOC IM drive with the proposed slip gain algorithm is straightforward. It required only the hardware used for standard IFOC IM drives:

- Three current and voltage sensors for the IM terminal signals;
- A speed sensor to measure the rotor speed of the IM;
- A 3–phase Inverter to interface the IM with the controller;
- A DSP to process the measured signals, perform the online slip gain estimation (including the reference frame transformations), and generate the gate signals for the Inverter.

The investigation of parameter and operating condition disturbances on the drive led to the design of the second controller (STFC) in chapter 4. The key feature of the STFC is its ability to regulate the speed, torque, and flux despite internal and external perturbations. In order to obtain this performance, it was important to design not only a controller that is less sensitive to parameter changes of the drive but also one with special

abilities to self-tune its gains according to the actual trend of the system. These features of the controller were incorporated into the STFC using the approaches of FLC and MRAS.

The procedure for designing the STFC is relatively similar to the slip gain estimation controller. Initially a review of relevant systematic design methodologies for Non-adaptive FLCs for AC and DC motor drives was conducted. From this review, a novel systematic design methodology for speed control of FOC IM drives was introduced.
The proposed systematic methodology showed that the selection of the parameters of an FLC is not totally subjective but rather dictated by common sense relating design requirements, control resolution & specification, and a range of process variables. These characteristics were successfully incorporated into the proposed Non-adaptive FLC. Simulation and experimental tests were conducted to validate this design methodology. The contributions of this design approach are:

(1) Significant reduction of design time and effort is achieved by utilizing the proposed methodology.
(2) An FLC designed according to this method does not strictly rely on the designer experience (subjectivity) but rather on common sense relating design requirement(s), control resolution & specification, and range of process variables.
(3) The method is applicable or extendable to any size of IM operated in FOC schemes. The parameters of a Non-adaptive FLC of a different IM can be easily calibrated based on its nameplate information and its responses in FOC schemes, as demonstrated in chapter 4.
(4) The stability of the Non-adaptive FLC in a close-loop system is proven using the Passivity approach

When the IFOC IM drive with the proposed Non-adaptive FLC was (mechanically) disturbed severely, it was shown that its performances

were also affected severely. This is undesirable for high-performance applications, where very tight control of speed and torque is expected at all time. To deal with the issue, a Self-Tuning mechanism was added to the Non-adaptive FLC to form the STFC. The purpose of this mechanism was to reduce the influence of the IM parameters and operating conditions on the controller and to maintain excellent (steady-state and dynamic) performances of the drive at all time. The validity of the STFC was also verified by a series of simulation and experimental tests in a very wide range of operating conditions and parameter changes.

The key features of the STFC can be summarized as follow:

(1) Keeping in mind the requirement to minimize cost for industrial uses, the compromise between performance and computation burden was considered through the use of MRAS, and simplest forms of MFs and inference mechanism in the FLC. This is a topic of ongoing research.
(2) Accurate knowledge of IM parameters is not strictly required at start-up. The STFC can be started with unity scaling gains. However, when shorter transient responses are required at start-up, the nominal parameters of the IM can be used to set the initial scaling gains of the Non-adaptive FLC according to the procedure described in the proposed design methodology.
(3) The ability of the system to indirectly respond to parameter, load, and operating condition disturbances without the need for computationally expensive parameter estimations makes the approach attractive for a wide range of drive applications.
(4) Implementing both the STFC and a traditional (fixed-gain parameter) PI controller, the proposed approach offered a number of performance advantages over its counterpart PI controller. These advantages include smaller overshoot and faster response (of speed, torque, and flux), even though the sampling time for the

current and speed control inputs is on the order of magnitude longer for the PI system.

(5) Although the STFC is not designed to directly cope with the IFOC detuning effect problem, a partial compensation is performed since variations of the slip gain are seen as changes of torque constant.

(6) The stability of the STFC is also available and proven using the Passivity approach.

(7) The implementation of an IFOC IM drive with the proposed STFC is also straightforward. It only uses the hardware required in traditional FOC schemes:

- Three current sensors to measure the IM terminal currents
- A speed sensor to measure the rotor speed of the IM;
- A 3–phase Inverter to interface the motor;
- A DSP to process the measured signals, program the STFC mechanism (including the reference frame transformations), and generate the gate signals for the Inverter.

Possible improvements to the approaches will include:

(1) The use of a wound-round IM to be able to change the actual value of the slip gain in the motor and validate the proposed approach experimentally. This is not possible with a squirrel-cage type IM.

(2) Investigation of the approaches in sensorless mode in order to increase the drive reliability (especially in hostile environments): eliminate the speed sensor, estimate rotor speed from the measured currents and/or speed (using some available sensorless schemes), and validate the STFC and slip gain algorithms under this condition.

(3) Development of an effective method to determine the weight factors (α, β, γ) used in equations (4.13)–(4.15) in order to generalize the STFC approach to any size of IM in FOC schemed.

These factors were determined by trial-and-error during simulation tests.

References

[1] M. Barnes, *Practical Variable Speed Drives and Power Electronics*. Newness, Burlington, MA, 2003.

[2] R.D. Lorenz, T.A. Lipo, and D.W. Novotny, "Motion control with induction motors," *Proceedings of the IEEE*, vol. 82, no. 8, pp. 1215-1240, August 1994.

[3] D.F. Warne, *Electric Power Engineer's Handbook*. 2nd Edition, Elsevier, Burlington, MA, 2005.

[4] M.H. Rashid, *Power Electronics: circuits, devices, and applications*. Upper Saddle River, NJ: Prentice-Hall, 2004.

[5] B.K. Bose, *Modern Power Electronics and AC Drives*. Upper Saddle River, NJ: Prentice-Hall, 2002.

[6] D.W. Novotny and T.A. Lipo, *Vector Control and Dynamics of AC Drives*. Oxford, U.K.: Oxford Univ. Press, 1996.

[7] W. Leonhard, *Control of Electrical Drives*. 3rd Edition, Springer, 2001.

[8] R. Krishnan, *Electric Motor Drives: modeling, analysis, and control*. Upper Saddle River, NJ: Prentice-Hall, 2002.

[9] F. Blaschke, "*A new method for the structural decoupling of A.C. induction machines*," in Conf. Rec. IFAC, Duesseldorf, October 1971, pp.1-15.

[10] I. Takahashi and T. Noguchi, "A new quick-response and high efficiency control strategy of an induction machine," *IEEE Trans Industry Applications*, vol. 22, pp. 820-827, September/October 1986.

[11] I. Takahashi and Y. Ohmori, "High-performance direct torque control of an induction motor," *IEEE Trans Industry Applications*, vol. 25, pp. 257-264, March/April 1989.

[12] D. Casadei, F. Profumo, G. Serra, and A. Tani, "FOC and DTC: Two viable schemes for induction motors torque control," *IEEE Trans Power Electronics*, vol. 17, no. 5, pp. 779-787, September 2002.

[13] G.F. Franklin, J.D. Powel, and A. Emami-Naeini, *Feedback Control of Dynamic Systems*. Reading, MA: Addison-Wesley, 1994.

[14] R. Krishnan and A.S. Bharadwaj, "A review of parameter sensitivity and adaptation in indirect vector controlled induction motor drive systems," *IEEE Trans Power Electronics*, vol. 6, no. 4, pp. 695-703, October 1991.

[15] H. Toliyat, "Overcoming vector control challenges," *Motion System Design*, vol. 47, pp. 20-24, March 2005.

[16] H.A. Toliyat, E. Levi, and M. Raina, "A review of RFO induction motor parameter estimation techniques," *IEEE Trans Energy Conversion*, vol. 18, no. 2, pp. 271-283, June 2003.

[17] M. Masiala and A. Knight, "Self-tuning speed control of indirect field-oriented induction machine drives," in *Proc. XVII International Conf. on Electrical Machines*, Greece, sep. 2-5, 2006, pp. 563-568.

[18] T.M. Rowan, R.J. Kerkman, and D. Leggate, "A simple on-line adaptation for indirect field orientation of an induction machine," *IEEE Trans Industry Applications*, vol. 27, no. 4, pp. 720-727, July/August 1991.

[19] G.C.D. Sousa, B.K. Bose, and K.S. Kim, "Fuzzy logic based on-line MRAC tuning of slip gain for an indirect vector-controlled induction motor drive," *IEEE International Conference on industrial Electronics, Control, and Instrumentation*, 15-19 November, 1993, vol. 2, pp. 1002-1008.

[20] R.-J. Wai and K.-H. Su, "Adaptive enhanced fuzzy sliding-mode control for electrical servo drives," *IEEE Trans Industrial Electronics*, vol. 53, no. 2, pp. 569-580, April 2006.

[21] E. Cerruto, A. Consoli, A. Raciti, and A. Tesla, "Fuzzy adaptive vector control of induction motor drives," *IEEE Trans Power Electronics*, vol. 12, no. 6, pp. 1028-1040, November 1997.

[22] K.H. Chao and C.M. Liaw, "Fuzzy robust speed controller for detuned field-oriented induction motor drives," *Proc. IEE–Electric Power Applications*, vol. 147, no. 1, pp. 27-36, January 2000.

[23] B. Heber, L. Xu, and Y. Tang, "Fuzzy logic enhanced speed control of an indirect field-oriented induction machine drive," *IEEE Trans Power Electronics*, vol. 12, no. 5, pp. 772-778, September 1997.

[24] F. Cupertino, A. Lattanzi, and S. Salvatoire, "A new fuzzy logic-based controller design method for dc and ac impressed-voltage drives," *IEEE Trans Power Electronics*, vol. 15, no. 6, pp. 974-982, November 2000.

[25] M.N. Uddin, T.S. Radwan, and A. Rahman, "Performances of fuzzy-logic-based indirect vector control for induction motor drive," *IEEE Trans Industry Applications*, vol. 38, no. 5, pp. 1219-1225, September/October 2002.

[26] C.M. Liaw and F.J. Lin, "Position control with fuzzy adaptation for induction servomotor drive," *Proc. Inst. Elect. Eng. – Electrical Power Applications*, vol. 142, no. 6, pp. 397-404, November 1995.

[27] L. Zhen and L. Xu, "Fuzzy learning enhanced speed control of an indirect field-oriented induction machine drive," *IEEE Trans Control System Technology*, vol. 8, no. 2, pp. 270-278, March 2000.

[28] A. El-Dessouky and M. Tarbouchi, "Fuzzy model reference self-tuning controller," *in Proc. VII International Workshop on Advanced Motion Control*, July 3-5, 2002, pp. 153-158.

[29] M.A. Fnaiech, *et al.*, "Comparison between fuzzy logic and sliding mode control applied to six phase induction machine positioning," in *Proc. XVIII International Conference on Electrical Machines*, September 6-9, 2008, pp. 1-6

[30] R.-J. Wai, C.-M. Kim and C.-F. Hsu, "Hybrid control for induction servomotor drive," *Proc. Inst. Electr. Eng. - Control Theory Applications*, vol. 149, no. 6, pp. 555-562, November 2002.

[31] R.-J. Wai, C.-M. Kim and C.-F. Hsu, "Adaptive fuzzy sliding-mode control for electric servo drive," *Fuzzy Sets and Systems*, vol. 143, no. 2, pp. 295-310, April 2004.

[32] R.-J. Wai, "Fuzzy sliding-mode control using adaptive tuning technique," *IEEE Trans Industrial Electronics*, vol. 54, no. 1, pp. 586-594, February 2007.

[33] M. Masiala, B. Vafakhah, J. Salmon, and A.M. Knight, "Fuzzy self-tuning speed control of an indirect field-oriented control induction motor drive," *IEEE Trans Industry Applications*, vol. 44, no. 6, pp. 1732-1740, November/December 2008.

[34] Stephen J. Chapman, *Electric Machinery Fundamentals*. 4th Edition, McGraw-Hill, New York, NY, 2005.

[35] P.C. Sen, *Principles of Electric Machines and Power Electronics*. 2nd Edition, John Wiley & Sons, 1997.

[36] J. Holtz, "Pulsewidth modulation – A survey," *IEEE Trans Industrial Electronics*, vol. 39, no. 5, pp. 410-420, October 1992.

[37] R. Ueda, T. Sonada, K. Koga, and M. Ichikawa, "Stability analysis in induction motor driven by V/f controlled general-purpose

inverter," *IEEE Trans. Industry Applications*, vol. 28, no. 2, pp. 472-481, March/April 1992.

[38] H.A. Toliyat and S. Campbell, *DSP-Based Electromechanical Motion Control*. Boca Raton, FL: CRC Press, 2004.

[39] P. Krause, O. Wasynczuk, S.D. Sudhoff, *Analysis of Electric Machinery*. IEEE Press, New York, 1995.

[40] M. Summer and G.M. Asher, "Autocommissioning for voltage-referenced voltage-fed vector-controlled induction motor drives," *IEE Proceedings-B*, vol. 140, no. 3, pp. 187-200, May 1993.

[41] H. Schierling, "Self-commissioning- A novel feature of modern inverted-fed induction motor drives," in *Proc. Inst. Elect. Eng. Conf. Power Electronics and Variable Speed Drives*, 13-15 July 1988, pp. 287-290.

[42] L.-X. Wang, *A Course in Fuzzy Systems and Control*. Upper Saddle River, NJ: Prentice Hall, 1997.

[43] P.P. Bonisson, at all, "Industrial applications of fuzzy logic at general electric," *Proceedings of the IEEE*, vol. 83, no. 3, pp. 450-465, March 1995.

[44] K.M. Passino and S. Yurkovich, *Fuzzy Control*. Menlo Park, CA: Addison Wesley, 1998.

[45] C.C. Lee, "Fuzzy logic in control systems: Fuzzy logic controller," Parts I&II, *IEEE Trans Systems, Man, and Cybernetics*, vol. 20, no. 2, pp. 404-435, April 1990.

[46] F. Betin, D. Pinchon, and G.A. Capolino, "Fuzzy logic applied to speed control of a stepping motor drive," *IEEE Trans Industrial Electronics*, vol. 47, no. 3, pp. 610-622, June 2000.

[47] Z. Kovacic and S. Bogdan, *Fuzzy controller design: theory and applications*. Boca Raton, FL: Taylor & Francis Group, 2006.

[48] S.H. Zak, *Systems and Control*. Oxford, NY: Oxford University Press, 2003.

[49] I. Eker and Y. Torun, "Fuzzy logic control to be conventional method," *Energy Conversion and Management*, vol. 47, pp. 377-394, 2006.

[50] L.A. Zadeh, "The concept of linguistic variable and its application to approximate reasoning I, II, III," *Information Sciences*, vol. 8. pp. 199-251, pp. 301-357, pp. 43-80, 1975.

[51] M. Mizumoto, “Fuzzy controls under various fuzzy reasoning methods,” *Information Sciences*, vol. 15, pp. 129-151, 1988.

[52] F.S. Smith and Q. Shen, “Selecting inference and defuzzification techniques for fuzzy logic control,” in *Proc. of UKACC Inter. Conference on Control*, vol. 1, 1-4 Sept. 1998, pp. 54-59.

[53] A.V. Patela and B.M. Mohanb, “Analytical structures and analysis of the simplest PI controllers,” *Automatica*, vol. 38, pp. 981-993, 2002.

[54] T. Takagi and M. Sugeno, “Fuzzy identification of fuzzy systems and its applications to modeling and control,” *IEEE Trans Systems, Man, and Cybernetics*, vol. 15, no. 1, pp. 116-132, 1985.

[55] M. Sugeno and G.T. Kang, “Structure identification of fuzzy model,” *Fuzzy Sets and Systems*, vol. 28, no. 1, pp. 15-33, 1988.

[56] E.H. Mamdani and S. Assilian, “An experiment in linguistic synthesis with a fuzzy logic controller,” *International Journal of Man-Machine Studies*, vol. 7, no. 1, pp. 1-13, 1975.

[57] J. Yan, M. Ryan, and J. Power, *Using fuzzy logic*. Hemel Hempstead, UK: Prentice-Hall, 1994.

[58] P.J. King and E.H Mamdani, “The application of fuzzy control systems to industrial processes,” in *IFAC Word Congress*, MIT, Boston, 1975.

[59] T.A. Runkler, “Selection of appropriate defuzzification methods using application specific properties,” *IEEE Trans Fuzzy Systems*, vol. 5, no. 1, pp. 72-79, February 1997.

[60] R. Gabriel and W. Leonhard, “Microprocessor control of induction motor,” in *Proc. International Conference on Semiconductor Power Converter*, May 1982, pp. 385-396.

[61] H. Sugimoto and S. Tamai, “Secondary resistance identification of an induction-motor applied model reference adaptive system and its characteristics,” *IEEE Trans. Industry Applications*, vol. IA-23, no. 2, pp. 296-303, March/April 1987.

[62] R. Schmidt, “On line identification of the secondary resistance of an induction motor in the low frequency range using a test vector,” in *Proc. International Conference in Electrical Machines*, 1988, pp. 221-225.

[63] T. Matsuo and T.A. Lipo, "Rotor parameter identification scheme for vector-controlled induction motor drives," *IEEE Trans. Industry Applications*, vol. IA-21, no. 3, pp. 624-632, May/June 1985.

[64] L.C. Zai, C.L. DeMarco, and T.A. Lipo, "An extended Kalman filter approach to rotor time constant measurement in PWM induction motor drives," *IEEE Trans. Industry Applications*, vol. 28, no. 1, pp. 96-104, January/February 1992.

[65] J.W. Finch, D.J. Atkinson, and P.P. Acarnely, "Full-order estimator for induction motor states and parameters," *IEE Proc.–Electric Power Applications*, vol. 145, no. 3, pp.169-179, 1998.

[66] G.G. Soto, E. Mendes, and A. Razek, "Reduced-order observers for rotor flux, rotor resistance and speed estimation for vector controlled induction motor drives using the extended Kalman filter techniques," *IEE Proc.–Electric Power Applications*, vol. 146, no. 3, pp. 282-288, 1999.

[67] T. Du, P. Vas, and F. Stronach, "Design and application of extended observers for joint state and parameter estimation in high-performance ac drives," *IEE Proc.–Electric Power Applications*, vol. 142, no. 2, pp. 71-78, 1995.

[68] Y. Dote and K. Anbo, "Combined parameter and state estimation of controlled current induction motor drive system via stochastic nonlinear filtering technique," in *Proc. IEEE Industry Applications Annual Meetings, Conf. Rec.*, 1979, pp. 838-842.

[69] F. Hillenbrand, "A method for determining the speed and rotor flux of the asynchronous machine by measuring the terminal quantities," in *Proc. 3rd IFAC Symposium on Control, Power Electronics, and Electric Drives*, September 1983, pp. 55-62.

[70] T. Du and A. Brdys, "Algorithms for joint state and parameter estimation in induction motor drives systems," in *Proc. Inst. Elect. Eng. Conf. Contr.*, 1991, pp. 915-920.

[71] S. Wade, M.W. Dunnigan, and B.W. Williams, "Improvements for induction machine vector control," in *Proc. European Conference on Power Electronics Applications*, 1995, vol. 1, pp. 542-546.

[72] L.J. Garces, "Parameter adaptation for the speed-controlled static AC drive with a squirrel-cage induction motor," *IEEE Trans. Industry Applications*, vol. IA-16, no. 2, pp. 173-178, March/April 1980.

[73] M. Koyama, at al, “Microprocessor-based vector control system for induction motor drives with rotor time constant identification function,” in *Proc. IEEE Industry Applications Society Annual Meeting*, 1985, pp. 564-569.

[74] D. Dalal and R. Krishnan, “Parameter compensation of indirect vector controlled induction motor drive using estimated airgap power,” in *Proc. IEEE Industry Applications Society Annual Meeting*, 1987, pp. 170-176.

[75] R.D. Lorenz and D.B. Lawson, “A simplified approach to continuous on-line tuning of field-oriented induction machine drives,” *IEEE Trans. Industry Applications*, vol. 26, no. 3, pp. 420-424, May/June 1990.

[76] R. Lessmeier, W. Schumacher, and W. Leonhard, “Microprocessor-controlled AC-servo drives with synchronous or induction motors: which is preferable?” *IEEE Trans. Industry Applications*, vol. IA-22, pp. 812-819, September/October 1986.

[77] A. Dittrich, “Parameter sensitivity of procedures for on-line adaptation of the rotor time constant of induction machines with field oriented control,” *IEE Proc.–Electric Power Applications*, vol. 141, no. 6, pp. 353-359, November 1994.

[78] M. Sumner, G.M. Asher, and R. Pena, “The experimental investigation of rotor time constant identification for vector controlled induction motor drives during transient operating conditions,” in *Proc. European Conference on Power Electronics Applications*, vol. 5, 1993, pp. 51-56.

[79] S.N. Vukosavic and M.R. Stojic, “On-line tuning of the rotor time constant for vector-controlled induction motor in position control applications,” *IEEE Trans. Industrial Electronics*, vol. 40, no. 1, pp. 130-138, February 1993.

[80] S.K. Sul, “A novel technique of rotor resistance estimation considering variation of mutual inductance,” *IEEE Trans. Industry Applications*, vol. 25, no. 4, pp. 578-587, July/August 1989.

[81] S. Sivakumar, A.M. Sharaf, and K. Natarajan, “Improving the performance of indirect field orientation schemes for induction motor drives,” in *Proc. IEEE Industry Applications Annual Meeting*, 1986, pp. 147-154.

[82] M. Akamatsu, et all, "High performance IM drive by coordinate control using a controlled current inverter," *IEEE Trans Industry Applications*, vol. IA-18, no. 4, pp. 382-392, July/August 1982.

[83] H. Toliyat, M.S. Arefeen, K.M. Rahman, and D. Figoli, "Rotor time constant updating scheme for a rotor flux oriented induction motor drive," *IEEE Trans. Power Electronics*, vol. 14, no. 5, pp. 850-857, September 1999.

[84] H.T. Yang, K.Y. Huang, and C.L. Huang, "An artificial neural network based identification and control approach for the field-oriented induction motor," *Electric Power Systems Research*, vol. 30, pp. 35-45, 1994.

[85] E. Bim, "Fuzzy optimization for rotor constant identification of an indirect FOC induction motor drive," *IEEE Trans. Industrial Electronics*, vol. 48, no. 6, pp. 1293-1295, December 2001.

[86] F. Alonge and F.M. Raimond, "Model reference adaptive control of motion control systems with induction motor," *IEEE International Symposium on Industrial Electronics*, vol. 2, 10-14 July 1995, pp. 803-808.

[87] A. Sabanovic and D.B. Izosimof, "Application of sliding modes to induction motor control," *IEEE Trans. Industry Applications*, vol. IA-17, no. 1, pp. 41-49, January 1981.

[88] F. Alonge, "MRAC and sliding motion control techniques to design a new robust controller for induction motor drives," *IEEE Power Conversion Conference*, 19-21 April, 1993, pp. 290-296.

[89] E.E.Y. Ho and P.C. Sen, "Control dynamics of speed drive systems using sliding mode controllers with integral compensation," *IEEE Trans. Industry Applications*, vol. 27, no. 5, pp. 883-892, September/October 1991.

[90] E.E.Y. Ho and P.C. Sen, "A high-performance parameter-insensitive drive using a series-connected wound rotor induction motor," *IEEE Trans. Industry Applications*, vol. 25, no. 6, pp. 1132-1138, November/December 1989.

[91] V.S.C. Raviraj and P.C. Sen, "Comparative study of proportional-integral, sliding mode, and fuzzy logic controllers for power converters," *IEEE Trans Industry Applications*, vol. 33, no. 2, pp. 518-524, March/April 1997.

[92] L. Mokrani and R. Abdessemed, "A fuzzy self-tuning PI controller for speed control of induction motor drive," in *Proc IEEE Conference on Control Applications*, June 2003, vol. 2, pp. 785-790.

[93] P. Vas, A.F. Stronach, and M. Neuroth, "Fully fuzzy control of a DSP-based high performance induction motor drive," *IEE Proc. Control Theory Applications*, vol. 144, no. 5, pp. 361-368, Sep 1997.

[94] J. Sun, P. Su, Y. Li, and L. Li, "Application of self-adjusting fuzzy controller in a vector-controlled induction motor drive," in *Proc. III IEEE International Conference on Power Electronics and Motion Control*, Aug. 15-18, 2000, vol. 3, pp. 1197-1201.

[95] J.B. Wang and C.M. Liaw, "Indirect field-oriented induction motor drive with fuzzy detuning correction and efficiency optimization controls," *IEE Proc.–Electric Power Applications*, vol. 144, no. 1, pp. 37-45, January 1997.

[96] M. Masiala, B. Vafakhah, A. Knight, and J. Salmon, "Performance of PI and fuzzy-logic speed control of field-oriented induction machine drives," *IEEE Canadian Conference on Electrical and Computer Engineering,* 22-26 April, 2007, pp. 397-400.

[97] F. Betin, at all, "Determination of scaling factors for fuzzy logic control using the sliding-mode approach: application to control of a dc machine drive," *IEEE Trans. Industrial Electronics*, vol. 54, no. 1, pp. 296-309, February 2007.

[98] Z. Ibrahim and E. Levi, "A comparative analysis of fuzzy logic and PI speed control in high-performance ac drives using experimental approach," *IEEE Trans Industry Applications*, vol. 38, no. 5, pp. 1210-1218, September/October 2002.

[99] Y.L. Li and C.C. Lau, "Development of fuzzy algorithms for servo systems," *IEEE Control Magazine*, vol. 9, no. 3, pp. 65-72, April 1989.

[100] F. Alonge, et al, "Method for designing PI-type fuzzy controllers for induction motor drives," *IEE Proc.-Control Theory Applications*, vol. 148, no. 1, pp. 61-69, January 2001.

[101] J.X. Shen, *et al.*, "Fuzzy logic speed control and current-harmonic reduction in permanent-magnet brushless ac drives," *IEE Proc.-Electrical Power Applications*, Vol. 152, no. 3, pp. 437–446, May 2005.

[102] J.-S. Yu, et al, "Fuzzy-logic-based vector control scheme for permanent-magnet synchronous motors in elevator drive applications, " *IEEE Trans. Industrial Electronics*, vol. 54, no. 4, pp. 2190–2200, August 2007.

[103] M.N. Uddin and M.A. Rahman, "High–speed control of IPMSM drives using improved fuzzy logic algorithms," *IEEE Trans Industrial Electronics*, vol. 54, no. 1, pp. 190-199, February 2007.

[104] R.K. Mudi and N.R. Pal, "A robust self-tuning scheme for PI- and PD-type fuzzy controllers," *IEEE Trans Fussy Systems*, vol. 7, no. 1, pp. 2-17, Feb. 1999.

[105] Y. Miloud, A. Miloudi, M. Mostefai, and A. Draou, "Self-tuning fuzzy logic speed controller for induction motor drives," in *Proc. IEEE International Conf. on Industrial Technologies*, Dec. 8-10, 2004, pp. 454-459.

[106] E.-C. Shin, T.-S. Park, and J.-Y Yoo, "A design method of PI controller for an induction motor with parameter variation," *IEEE Industrial Electronics Conference-IECON*, Nov. 2-6, 2003, vol. 1, pp. 408-413.

[107] Y.-Y. Tzou, "DSP-based robust control of an AC induction servo drive for motion control," *IEEE Trans Control Systems Technology*, vol. 4, no. 6, pp. 614-626, November 1996.

[108] R. Ortega and D. Taoutaou, "Indirect field oriented speed regulation of induction motors is globally stable," *IEEE Trans Industrial Electronics*, vol. 43, pp. 340-341, April 1996.

[109] F.-J. Lin, "Robust speed-controlled induction-motor drive using EKF and RLS estimators," *IEE Proc. Electrical Power Applications*, vol. 143, no. 3, pp. 186-192, May 1996.

[110] G.-W. Chang, at All, "Tuning rules for the PI gains of field-oriented controllers of induction motors," *IEEE Trans Industrial Electronics*, vol. 47, no. 3, pp. 592-602, June 2000.

[111] C.C. Hang, K.J. Astrom, and W.K. Ho, "Refinements of the Ziegler-Nichols tuning formula," *IEE Proceedings-D*, vol. 138, no. 2, pp. 111-118, March 1991.

[112] J.G Zieglier and N.B. Nichols, "Optimum settings for automatic controllers," *Trans ASME*, vol. 65, pp. 433-444, 1942.

[113] H.-X. Li, "Approximate model reference adaptive mechanism for nominal gain design of fuzzy control system," *IEEE Trans Systems, Man, and Cybernetics*, vol. 29, no. 1, pp. 41-46, February 1999.

[114] W. Pedrycz, "Fuzzy control engineering: reality and challenges," in *Proc. 4th International Conference on Fuzzy Systems*, 20-24 March 1995, vol. 2, pp. 437-446.

[115] I. Miki, at all, "Vector control of induction motor with fuzzy PI controller," in *IEEE Industry Applications Annual Meetings*, 28 September - 4 October 1991, vol. 1, pp. 341-346.

[116] C.-M. Liaw and J.-B. Wang, "Design and implementation of a fuzzy controller for a high performance induction motor drive," *IEEE Trans Systems, Man, and Cybernetics*, vol. 21, no. 4, pp. 921-929, July/August 1991.

[117] F.-F. Cheng and S.-N. Yeh, "Application of fuzzy logic in the speed control of ac servo system and an intelligent inverter," *IEEE Trans Energy Conversion*, vol. 8, no. 2, pp. 312-318, June 1993.

[118] G.C.D. Sousa and B.K. Bose, "Fuzzy set theory based control of a phase-controlled converter dc machine drive," *IEEE Trans Industry Applications*, vol. 30, no. 1, pp. 34-44, January/February 1994.

[119] V. Donescu, at all, "A systematic design method for fuzzy logic speed controller for brushless dc motor drives," in *Proc. 27th IEEE Power Electronics Specialists Conference*, 23-27 June 1996, vol. 1, pp. 689-694.

[120] H.-X. Li, "A comparative design and tuning for conventional fuzzy control," *IEEE Trans Systems, Man, and Cybernetics*, vol. 27, no. 5, pp. 884–889, October 1997.

[121] T.O. Kowalska, K. Szabat and K. Jaszczak, "The influence of parameters and structure of PI-type fuzzy-logic controller on dc drive system dynamics," *Fuzzy Sets and Systems*, vol. 131, pp. 251–264, 2002.

[122] D. Fodor, J. Vass, and Z. Katona, "DSP-based fuzzy logic controller for VSI-fed vector controlled ac motors," in *Proc. 21st IEEE Industrial Electronics, Control, and Instrumentation Conference*, 6-10 November 1995, pp. 1478-1483.

[123] V.C. Altrock and S. Beierke, "Fuzzy logic enhanced control of an ac induction motor with a DSP," in *Proc. 5th IEEE International Conference on Fuzzy Systems*, 8-11 September 1996, vol. 2, pp. 806-810.

[124] D. Fodor, J. Vass, and Z. Katona, "Embedded controller board for field-oriented ac drives," in *Proc. 23rd IEEE Industrial Electronics, Control, and Instrumentation Conference*, 9-14 November 1997, pp. 1022-1027.

[125] J. Fonseca, at all, "Fuzzy logic speed control of an induction motor," *Microprocessors and Microsystems*, vol. 22, pp. 523-534, 1999.

[126] H. Marzi, "Using ac motors in robotics," *International Journal of Advanced Robotic Systems*, vol. 4, no. 3, pp. 365–370, 2007.

[127] P. Guillemin, "Fuzzy logic applied to motor control," *IEEE Trans Industry Applications*, vol. 32, no. 1, pp. 51–56, January/February 1996.

[128] F. Mrad and G. Deeb, "Experimental comparative analysis of conventional, fuzzy logic, and adaptive fuzzy logic controllers," in

Proc. 34th IEEE Industry Applications Annual Meeting, 3-4 October, 1999, vol. 1, pp. 664–673.

[129] A. Rubaai, D. Ricketts and M.D. Kankam, "Laboratory implementation of a microprocessor-based fuzzy logic tracking controller for motion controls and drives," *IEEE Trans Industry Applications*, vol. 38, no. 2, pp. 448–456, March/April 2002.

[130] H.L. Tan, N.A. Rahim and W.P. Hew, "A dynamic input membership scheme for a fuzzy logic dc motor controller," in *Proc. 12th IEEE International Conference on Fuzzy Systems*, 25-28 May 2003, vol. 1, pp. 426–429.

[131] I. Eminoglu and I.H. Altas, "The effects of the number of rules on the output of a fuzzy logic controller employed to a PM D.C motor," *Computers & Electrical Engineering*, vol. 24, pp. 245-261, 1998.

[132] I. Eminoglu and I.H. Altas, "A method to form fuzzy logic control rules for a PMDC motor drive system," *Electric Power Systems Research*, vol. 39, pp. 81-87, 1996.

[133] C.M. Lim and T. Hiyama, "Experimental implementation of a fuzzy logic control scheme for a servomotor," *Mechatronics*, vol. 3, no. 1, pp. 39-47, 1993.

[134] B.K. Bose, "Expert system, fuzzy logic, and neural network applications in power electronics and motion control," *Proceedings of the IEEE*, vol. 82, no. 8, pp. 1303–1323, August 1994.

[135] M. Giles and S. Rahman, "Using neural–fuzzy in control applications, " *IEEE WESCON/94, Conference record*, 27–29 September 1994, pp. 337–341.

[136] M.N. Uddin and H. Wen, "Development of a self-tuned neuro-fuzzy controller for induction motor drives," *IEEE Trans Industry Applications*, vol. 43, no. 4, pp. 1108-1116, July/August 2007.

[137] T.S. Radwan, M.N. Uddin and M.A. Rahman, "A new and simple structure of fuzzy logic based indirect field oriented control of induction motor drives," in Proc. *35th IEEE Power Electronics Specialists Conference*, 20-25 June 2004, vol. 5, pp. 3290-3294.

[138] F. Cheong and R. Lai, "On simplifying the automatic design of fuzzy logic controller," *IEEE Proceedings on Fuzzy Information Processing Society*, 27-28 June 2002, pp. 481-487.

[139] H.-X. Li and H.B. Gatland, "A new methodology for designing a fuzzy logic controller," *IEEE Trans Systems, Man, and Cybernetics*, vol. 25, no. 3, pp. 505-512, March 1995.

[140] P.J. MacVicar-Whelan, "Fuzzy sets for man-machine interaction," *International Journal of Man-Machine Studies*, vol. 8, pp. 687-697, 1976.

[141] J. Zhao and B.K. Bose, "Evaluation of membership functions for fuzzy logic controlled induction motor drive," in *Proc. 28th IEEE Industrial Electronics Society Annual Conference*, 5-8 November 2002, vol. 1, pp. 229-234.

[142] M. Braae and D.A. Rutherford, "Selection of parameters for a fuzzy logic controller," *Fuzzy Sets and Systems*, vol. 2, pp. 185-199, 1979.

[143] R. Palm, "Sliding mode fuzzy control, in *Proc. IEEE International Conference on Fuzzy Systems*," 8-12 March 1992, pp. 519-526.

[144] J. Zhao and B.K. Bose, "Membership function distribution effect on fuzzy logic controlled induction motor drive," in *Proc. 29th IEEE Industrial Electronics Society Annual Conference*, 2-6 November 2003, vol. 1, pp. 214-219.

[145] C.-L. Chen and C.-T. Hsieh, "User-friendly design method for fuzzy logic controller," *IEE Proc.-Control Theory Applications*, vol. 143, no. 4, pp. 358-366, July 1996.

[146] Z. Kovacic and S. Bogdan, "Model reference adaptive fuzzy control of high-order systems," *Engng Applic. Artif. Intell.*, vol. 7, no. 5, pp. 501-511, 1994.

[147] F.J. Lin and C.M. Liaw, "Reference model selection and adaptive control induction motor drives," *IEEE Trans Automatic Control*, vol. 38, no. 10, pp. 1594-1600, October 1993.

[148] C. Melin, "Stability analysis of fuzzy control systems: some frequency criteria," *in Proc. 3rd European Control Conference*, August 1995, pp. 815-819.

[149] G. Calcev, R. Gorez, and M. De Neyer, "Passivity approach to fuzzy control systems," *Automatica*, vol. 34, no. 3, pp. 339-344, 1998.

[150] G. Calcev, "Some remark on stability of Mamdani fuzzy control systems," *IEEE Trans Systems*, vol. 6, no. 3, pp. 436-442, August 1998.

[151] K. Ray and D.D. Majumder, "Application of circle criteria for stability analysis of linear SISO and MIMO systems associated with fuzzy logic controller," *IEEE Trans. Systems, Man, and Cybernetics*, vol. SMC-14, pp. 345-349, 1984.

[152] D.P. Atherton, "A describing function approach for the evaluation of fuzzy logic control," *in Proc. American Control Conference*, 1993, vol. 3, pp. 765-766.

[153] R.E. Haber and J.R. Alique, "Fuzzy logic-based torque control system for milling process optimization," *IEEE Trans Systems, Man, and Cybernetics*, vol. 37, no. 5, pp. 941-950, Sept ember 2007.